Insulin signalling and functional characterisation of human microvascular endothelial cells in heart failure and diabetes

Sunti Limumpornpetch, MD

Submitted in accordance with the requirements for the degree of
Doctor of Philosophy

The University of Leeds

School of Medicine and Health
Leeds Institute of Cardiovascular and Molecular Medicine
2022

Acknowledgements

My journey started with my decision to leave my hometown in Thailand and travel to the United Kingdom to pursue new experiences. I was well aware of the challenging nature of my Ph.D. program and the length of time it would take me to complete it. I was warned that pursuing a Ph.D. would be difficult and frustrating when I agreed to do so. I found the transition from the comforting familiarity of clinical medicine to the unfamiliar territory of basic science to be more difficult than I had anticipated. To have reached the point of being able to author and submit a thesis is something that I am very proud of and something for which I owe a huge debt of gratitude to a great many people.

To begin, I would like to express my gratitude to Dr. Piruthivi Sukumar, Dr. Klaus Witte, and Professor Mark Kearney, who served as my supervisors. Their guidance, encouragement, and unwavering support have all contributed to my achievements. Additionally, I would like to express my gratitude to the Songkhlanakarin hospital for their financial assistance.

I am extremely appreciative of all my laboratory colleagues for their guidance, wisdom, and cooperation over the last 3 years. I am unable to thank everyone individually, but the following individuals deserve special recognition: Dr. Hema Viswambharan, for her input with Western blotting; Dr. Romana Mughal, for her patience in teaching me so many laboratory techniques; and Dr. Jason Scragg, for his input on endothelial cell isolation.

A special mention must be made for Dr. Richard Cubbon, Dr. John Huntriss, Dr. Vijayalakshmi Deivasikamani, Dr. Andrew Walker, Dr. Nicole Watt, Dr. Laeticia Lichtenstein, Dr. Euan Baxter, Dr. Chew Cheng, Dr. Jack Garnham, Dr. Katherine Taylor, Mrs. Jane Brown, Mrs. Jessica Smith, Mrs. Kay White, Mr. David Balcer-Whittle, Mrs. Ping Jin, and Mr. Alan Burnett. The company they have provided has contributed to the last 3 years being the most social of my professional career.

Finally, I have reserved my most heartfelt gratitude for those who mean the most to me: my parents, whose sacrifice enabled me to pursue a career as a doctor, and my wife Padiporn and sons Theetawat and Gunthat, for bringing joy to my life.

Abstract

Endothelial cell dysfunction plays a key role in heart failure and diabetic cardiovascular disease. There is extensive heterogeneity among endothelial cells, the characteristics of which depend on the tissue in which they are located. The metabolic characteristics of microvascular endothelial cells from skeletal muscle and adipose tissue remain largely understudied.

Endothelial cells were isolated from the skeletal muscle and adipose tissue of four patient groups: those with either heart failure or type II diabetes, a group with both conditions, and a group with neither condition. After incubating the endothelial cells for 4–5 weeks, until passage 2, the identity of the cells was confirmed by their response to stimulation with vascular endothelial growth factor (VEGF). Flow cytometry confirmed further that >98% of the cells were endothelial in origin.

The insulin signalling pathway was then explored in these endothelial cells by real-time PCR and Western blotting. Insulin was used to increase the phosphorylation of some protein reacting. Phosphorylated proteins of Akt and eNOS were identified by using specific phospho-Akt (Ser473) and phospho-eNOS (Ser1177) antibodies. Simple qualification and comparative analysis of expression and signalling were investigated. Endothelial cell functional characterisation was explored. Our findings indicated that while diabetes conditions impaired adipose tissue angiogenesis, HF conditions produced the most superoxide generation.

A comprehensive understanding of the molecular mechanisms of endothelial cell function may aid in developing more effective therapeutic drugs to improve symptoms and survival rates in heart failure and diabetes patients. The overall aim of this research was to investigate downstream of the insulin signalling pathway of microvascular endothelial cells in these patients.

Table of contents

Abstract iii
Table of contents i
Table of figures v
Table of tables viii
List of abbreviations ix
1 Introduction 1
1.1 Endothelial cell function 3
1.1.1 Role of endothelial cells in vascular biology 3
1.1.2 Endothelial cell heterogeneity 6
1.1.3 The role of endothelial cells in adipose tissue 6
1.2 Endothelial cell function in heart failure and diabetes 8
1.2.1 Pathophysiology of heart failure and diabetes 8
1.2.2 Endothelial dysfunction in heart failure and diabetes 8
1.3 Insulin signalling in endothelial cells in heart failure and diabetes 10
1.3.1 Insulin signalling in the normal state 10
1.3.2 Insulin receptor 14
1.3.3 Insulin-like growth factor 1 receptor 16
1.3.4 Insulin receptor substrate (IRS) 17
1.3.5 Phosphatidylinositol 3-kinase 17
1.3.6 Akt/Protein kinase B 18
1.3.7 Endothelial NOS 19
1.3.8 Insulin signalling in the insulin-resistant state 20
1.4 Reactive oxygen species in endothelial cells 22
1.4.1 ROS generation and regulation 23
1.4.2 NADPH oxidases 24

1.4.3 ROS and antioxidants in endothelial cells 28
1.4.4 Oxidative stress in endothelial dysfunction in heart failure and diabetes 31
1.4.5 Antioxidative stress in endothelial dysfunction in heart failure and diabetes 32
1.5 Angiogenesis 32
1.5.1 Nitric oxide and new blood vessel formation 33
1.5.2 ROS and angiogenesis 34
1.5.3 Angiogenesis in heart failure and diabetes 35
2 Objectives 38
3 Materials 39
3.1 Endothelial cell isolation 39
3.2 Cell culture 39
3.3 Fluorescence-based method for calcium measurement 40
3.4 Flow cytometry 40
3.5 Real time quantitative PCR 41
3.6 Western blotting 41
3.7 Lucigenin enhanced chemiluminescent 43
3.8 Angiogenesis assay 43
4 Methods 45
4.1 Endothelial cell isolation 45
4.1.1 Tissue harvesting 45
4.1.2 ATEC isolation 46
4.2 Cell culture 47
4.3 Identity confirmation 47
4.3.1 Fluorescence-based method for calcium measurement 47
4.3.2 Flow cytometry 49
4.4 Real-time quantitative PCR 50

4.4.1 RNA isolation 50
4.4.2 DNase treatment 51
4.4.3 RNA measurement 51
4.4.4 Reverse transcription of RNA 52
4.4.5 Real-time quantitative PCR 52
4.5 Insulin signalling by Western blot technique 55
4.5.1 Preparing endothelial cell samples 55
4.5.2 Protein measurement 55
4.5.3 Gel electrophoresis 55
4.5.4 Membrane transfer 56
4.5.5 Immunostaining 56
4.5.6 Densitometry (band quantification) 57
4.6 Superoxide measurement 57
4.7 Angiogenesis assay 58
4.8 Statistical analysis 59
5 Results 60
5.1 Endothelial cell isolation 63
5.2 Confirmation of the identity of endothelial cells 65
5.2.1 Intracellular calcium measurement induced by VEGF 65
5.2.2 Flow cytometric analysis of isolated endothelial cells 66
5.3 Gene expression analysis 67
5.4 Protein expression analysis 73
5.5 Superoxide production in endothelial cells 82
5.6 Angiogenic capacity of adipose tissue 85
6 Discussion 90
6.1 Summary of key findings 92
6.1.1 Isolation and confirmation of identity of the endothelial cells 92

6.1.2 Insulin signalling in human microvascular endothelial cells 94
6.1.3 Functional characterisation of human microvascular endothelial cells . 98
6.2 Limitations 99
6.2.1 Factors affecting insulin sensitivity and insulin signalling 99
6.2.2 Contamination of HSkMECs 100
6.2.3 Small sample size 101
6.2.4 Model of angiogenesis 101
6.3 Future directions 101
6.3.1 Insulin signalling in HMVECs 101
6.3.2 HMVECs in other functional assays 102
6.3.3 The translational value of HMVEC research 102
6.4 Conclusion 103
7 References 105

Table of figures

Figure 1: Mechanism of endothelial cell control vascular tone under physiological and pathological conditions. 5
Figure 2: Schematic of the insulin signalling pathway. When the insulin receptor is activated, it primarily recruits and phosphorylates two adaptor proteins: IRS and Shc. PI3K/Akt is an IRS-mediated pathway that is crucial for activation of eNOS activity and regulation of a variety of metabolic events, including glucose transport and glycogen, protein, and lipid synthesis. Shc is involved in the activation of the mitogen-activated protein kinase (MAPK) pathway, which regulates growth and differentiation. 12
Figure 3: Balancing two major insulin signalling pathways to regulate vascular tone. 14
Figure 4: Insulin receptor. The insulin receptor is a disulphide-linked, α/β heterodimer glycoprotein that is predominantly found on the cell surface. Once activated by insulin, the receptor kinase can phosphorylate exogenous substrates that act as adaptors: IRS 1–4, Shc at the juxtamembrane region via their PTB domains, and SH2B2 at the kinase region via its SH2 domain, serving as an adaptor protein for the substrate Cbl. 16
Figure 5: The structure of the Akt1, Akt2, and Akt3 proteins consists of the pleckstrin homology (PH) domain, helical domain (Helix), kinase domain, and regulatory domain. Although all three isoforms are formed by genes on different chromosomes, they have similar locations for the addition of the phosphate group. 19
Figure 6: Insulin signalling in the PI3K/Akt/eNOS pathway under physiological conditions and in insulin resistance. 21
Figure 7: Insulin signalling in the early and late stages of heart failure. 22
Figure 8: The NOX family includes seven isoforms that are distinguished by their catalytic core component, including five NOX homologues (NOX1–5) and two dual oxidases (DUOX1–2), all of which have different tissue distributions (84). 25
Figure 9: Oxidative enzymes, reactive molecules, and their conversion to other species by antioxidative enzymes. 30
Figure 10: Schematic illustrating the process of isolating endothelial cells from skeletal muscle and adipose tissue. 47
Figure 11: Phase separation process 51

Figure 12: Stack preparation for the protein from SDS-PAGE gel transfer to PVDF membrane. 56
Figure 13: Average time to confluence of the isolated cells in each group from P0–P1 and P1–P2. 64
Figure 14: Morphology of the isolated cells showed a ‘cobblestone’ monolayer pattern, which is compatible with endothelial cells. A. Cells isolated from skeletal muscle. B. Cells isolated from adipose tissue. 64
Figure 15: Cells isolated from a skeletal muscle sample that had been contaminated with skeletal muscle cells. 65
Figure 16: Intracellular calcium flux of isolated cells from skeletal muscle (sk.msl EC) and adipose tissue (adipose tissue EC) increased significantly in response to 50 ng/ml VEGF stimulation. 65
Figure 17: Flow cytometry of human skeletal muscle endothelial cells fully stained with CD31+ and CD144+ demonstrated a high-purity population of endothelial cells (98.22%). The axes in the lower panel dot plot depict both the fluorescence intensity and the fluorescence channel wavelength of CD144-PE (x-axis) and CD31-PerCP (y-axis). 66
Figure 18: Flow cytometry of human adipose tissue endothelial cells fully stained with CD31+ and CD144+ demonstrated a high-purity population of endothelial cells (99.59%). The axes in the lower panel dot plot depict both the fluorescence intensity and the fluorescence channel-wavelength of CD144-PE (x-axis) and CD31-PerCP (y-axis). 67
Figure 19: Relative gene expression of IR, IGF1R, Akt1, Akt2, Akt3, eNOS, NOX4, SOD1, SOD2, and catalase between the normal, DM, HF, and DM/HF groups (asterisks denote statistical significance with p-value less than 0.05). 70
Figure 20: Relative gene expression of IR, IGF1R, Akt1, Akt2, Akt3, eNOS, NOX4, SOD1, SOD2, and catalase between the non-DM and DM groups (asterisks denote statistical significance with p-value less than 0.05). 72
Figure 21: Relative gene expression of IR, IGF1R, Akt1, Akt2, Akt3, eNOS, NOX4, SOD1, SOD2, and catalase between the non-HF and HF groups. 73
Figure 22: Protein expression of basal phospho-IR, total IR, IGF1R, phospho-Akt, total Akt, phospho-eNOS, total eNOS, phospho-p47phox, total p47phox, NOX2, and NOX4 from human ATECs between the non-diabetic and diabetic groups. 76

Figure 23: Insulin-stimulated phosphorylation of IR, Akt, eNOS, and p47phox from human ATECs between the non-diabetic and diabetic groups. Values (means ± SE) are expressed relative to no insulin (asterisks denote statistical significance with p-value less than 0.05). 78
Figure 24: Protein expression of basal phospho-IR, total IR, IGF1R, phospho-Akt, total Akt, phospho-eNOS, total eNOS, phospho-p47phox, total p47phox, NOX2, and NOX4 from human ATECs between the non-HF and HF groups. 80
Figure 25: Insulin-stimulated phosphorylation of IR, Akt, eNOS, and p47phox from human ATECs between the non-HF and HF groups. Values (means ± SE) are expressed relative to no insulin (asterisks denote statistical significance with p-value less than 0.05)..... 82
Figure 26: Lucigenin-enhanced chemiluminescence of HCAECs (Lonza cells) between the normal (n = 3) and DM (n = 4) groups..... 83
Figure 27: Lucigenin-enhanced chemiluminescence of ATECs between the normal (n = 11), DM (n = 3), HF (n = 10), and DM/HF (n = 5) groups. 83
Figure 28: Lucigenin-enhanced chemiluminescence of ATECs between the non-DM (n = 21) and DM (n = 8) groups..... 84
Figure 29: Lucigenin-enhanced chemiluminescence of ATECs between the non-HF (n = 14) and HF (n = 15) groups..... 84
Figure 30: Insulin stimulated the production of superoxide in ATECs under normal, HF, and DM/HF conditions. 85
Figure 31: Angiogenesis assay of human white adipose tissue. On day 7, when adipose tissue was assessed, the number of sprouts was difficult to count. 86
Figure 32: Average sprout number and length on day 4 in human white adipose tissue between the normal (n = 9), DM (n = 5), HF (n = 21), and DM/HF (n = 11) groups. 89
Figure 33: Average sprout number and length on day 4 in human white adipose tissue between the non-DM (n = 30) and DM (n = 16) groups. 89
Figure 34: Average sprout number and length on day 4 in human white adipose tissue between the non-HF (n = 14) and HF (n = 32) groups. 89

Table of tables

Table 1: Staining cocktail with the proportion of fluorochrome-labelled antibodies. . 49
Table 2: Components of the mixture for one reaction of the extension step..... 52
Table 3: Components of the mixture for real-time quantitative PCR..... 53
Table 4: Sequence of each target gene. 54
Table 5: Sequences of NOX2 primers..... 54
Table 7: Demographic and clinical characteristics of the patients, with comparison between normal, DM, HF, and DM/HF patients..... 60
Table 8: Demographic and clinical characteristics of non-diabetic and diabetic patients..... 61
Table 9: Demographic and clinical characteristics of the patients with and without heart failure. 62
Table 10: Medications taken by each cohort of patients: Normal, DM, HF, and DM/HF..... 63
Table 11: Gene expression of GAPDH was compared between the first (real-time PCR performed 1 week after cDNA samples were prepared) and second (real-time PCR performed >8 weeks after the cDNA samples were prepared and stored in 4 ^{o}C) results..... 68
Table 12: Patient characteristics and results of the angiogenesis assay on fresh adipose tissue. 87
Table 13: Patient characteristics and results of the angiogenesis assay on adipose tissue stored overnight in tissue storage solution (preserved)..... 88

List of abbreviations

AGEs	Advanced glycation end products
Akt/PKB	Protein kinase B
ATECs	Adipose tissue endothelial cells
BCA	Bicinchoninic Acid
BH_4	Tetrahydrobiopterin
BMI	Body mass index
Bp	Base pair
BSA	Bovine serum albumin
CAD	Coronary artery disease
CD	Cluster of differentiation
cDNA	Complementary deoxyribonucleic acid
cGMP	Cyclic guanosine monophosphate
CHF	Congestive heart failure
Ct	Cycle threshold
CV	Co-efficient of variation
CVD	Cardiovascular disease
DM	Diabetes mellitus
DMSO	Dimethylsulfoxide
DNA	Deoxyribonucleic acid
dNTP	Deoxynucleotide phosphate
ECs	Endothelial cells
EDHF	Endothelium-derived hyperpolarizing factor
EGM	Endothelial growth medium
eNOS	Endothelial nitric oxide synthase
ERK	Extracellular signal-regulated kinases
ET-1	Endothelin-1
FACS	Fluorescence activated cell sorting
FBS or FCS	Fetal bovine serum or fetal calf serum
FFA	Free fatty acid
FITC	Fluorescein isothiocyanate
FMD	Flow mediated dilatation
GLUT-4	Glucose transporter type 4

Grb2	Cytosolic growth factor receptor-bound protein 2
GTP	Guanosine triphosphate
HBSS	Hank's balanced salt solution
HIFs	Hypoxia-inducible factors
HMVEC	Human microvascular endothelial cell
H_2O_2	Hydrogen peroxide
HUVEC	Human umbilical vein endothelial cell
ICAM-1	Intercellular adhesion molecule 1
IGF	Insulin-like growth factor
IGF1R	Insulin-like growth factor 1 receptor
IGF2/M6PR	Insulin-like growth factor 2/mannose 6-phosphate receptor
IGFBPs	Insulin-like growth factor binding proteins
IHD	Ischemic heart disease
IR	Insulin receptor
IRS	Insulin receptor substrate
LDL	Low density lipoprotein
MAPK	Mitogen active protein kinase
MEK	MAPK/ERK kinases
$MgCl_2$	Magnesium chloride
MI	Myocardial infarction
mRNA	Messenger ribonucleic acid
mTORC2	Mammalian target of rapamycin complex 2
NADPH	Nicotinamide adenine dinucleotide phosphate
NFκB	Nuclear factor kappa B
NO	Nitric oxide
NOS	Nitric oxide synthase
NOX	Nicotinamide adenine dinucleotide phosphate oxidase
O_2^-	Superoxide anion
$ONOO^-$	Peroxynitrite
PAI-1	Plasminogen activator inhibitor 1
PBS	Phosphate-buffered saline
PCR	Polymerase chain reaction

PDGF	Platelet derived growth factor
PE	R-phycoerythrin
PECAM-1	Platelet endothelial cell adhesion molecule 1
PI3K	Phosphoinositide 3-kinase
PIP	Phosphatidyl inositol phosphate
PPAR	Peroxisome proliferator activated receptor
Raf	Serine/threonine specific protein kinases
Ras	Family of related proteins
RNA	Ribonucleic acid
ROS	Reactive oxygen species
RT	Reverse transcriptase
SAT	Subcutaneous adipose tissue
SATEC	Subcutaneous adipose tissue endothelial cell
SEM	Standard error of mean
Shc	Src homology and collagen protein
siRNA	Small interfering ribonucleic acid
SOD	Superoxide dismutase
SOS	Proline-rich domain of the son of sevenless
Taq	Thermophillus aquaticus
TNF	Tumor necrosis factor
VAT	Visceral adipose tissue
VATEC	Visceral adipose tissue endothelial cell
VCAM-1	Vascular cell adhesion molecule 1
VEGF	Vascular endothelial growth factor
VSMC	Vascular smooth muscle cell
vWF	von Willibrand’s factor
WT	Wild type

Chapter 1: **Introduction**

1 Introduction

Type 2 diabetes mellitus (DM) and heart failure (HF) both have a high risk of morbidity and mortality. The global prevalence of each condition has been expanding over recent years. The global prevalence of diabetes is estimated to have been 463 million people in 2019 and will rise to 700 million people in 2045 (1). This rise in prevalence is attributable to various factors, including increasing population growth, aging, urbanisation, the prevalence of obesity, and physical inactivity. According to global estimates, 4.2 million people aged 20 to 79 years died from diabetes in 2019 (2). In 2017, the global prevalence of HF was estimated to be 64.3 million people (3). HF prevalence has a linear relationship with the socio-demographic index (SDI), and it continues to represent a healthcare burden in low-to-middle SDI regions (4). Despite advances in cardiovascular care, the mortality rate of HF remains high at 22% in the first year, and approximately 42% within 5 years of diagnosis (5).

Having one of DM or HF independently increases the risk of developing the other, and both conditions often occur simultaneously, with a synergistic adverse effect on sufferer's physical condition and quality of life. The prevalence of diabetes in patients with congestive HF (CHF) is dependent on several factors, including race. Whereas the prevalence of diabetes in white CHF patients is 24%, in Asian CHF patients it is 57% (6). A recent study found that CHF patients with type 2 DM had double the risk of all-cause mortality, cardiovascular mortality, and progressive heart failure, and the risk of sudden death was nearly three times higher than in patients without diabetes (7).

The aetiology of progressive HF in diabetes can be ascribed to an amplification of the neurohumoral response to CHF, especially the aggravation of the renin-angiotensin-aldosterone system (RAAS) and sympathetic nervous system (SNS). In addition, the production of advanced glycation end-products (AGEs) and reactive oxygen species (ROS) in hyperglycaemic conditions encourages cardiac fibrosis, which drives progressive HF and the development of cardiac arrhythmia (8).

In type 2 DM, CHF can manifest as either HF with a reduced ejection fraction (HFrEF) or HF with a preserved ejection fraction (HFpEF). HFrEF is classically defined by a left ventricular ejection fraction (LVEF) less than 40% and HFpEF by an LVEF greater than 50%. There exists a group with an LVEF between 40 and 49% labelled HF with a mid-range EF (HFmrEF) (9). In general, the pathogenesis of HFrEF in patients with diabetic is derived from the risk of coronary artery disease (CAD). Moreover, diabetes can cause a HFpEF known as ‘diabetic cardiomyopathy’, which initially manifests as a diastolic relaxation abnormality and progresses to clinical HF. This type of cardiomyopathy is not associated with CAD or hypertension; rather, it is thought to be driven primarily by insulin resistance and hyperglycaemia (10).

Both DM and HF have known links in their pathophysiology, which include insulin resistance and endothelial dysfunction. Insulin resistance is the primary pathological process underlying the development of cardiovascular disease (CVD) through the initiation and progression of atherosclerosis. Insulin resistance occurs in type 2 diabetes due to ectopic lipid accumulation in muscle and liver, adipose tissue dysfunction (e.g., altered adipokines, inflammation), mitochondrial dysfunction, oxidative stress, and incomplete fatty acid oxidation (FAO). Insulin resistance occurs in HF for a variety of reasons, including ectopic lipid accumulation in skeletal muscle and liver, inflammation in skeletal muscle and adipose tissue, and growth hormone resistance. Furthermore, insulin resistance can cause hyperinsulinaemia, which results in increased lipolysis in adipose tissue and decreased glucose uptake in skeletal muscle (11). This phenomenon is known as selective insulin resistance. This can occur through several mechanisms, including changes in the expression or localization of insulin receptors, alterations in downstream signaling pathways, and increased levels of inhibitory signaling molecules. Additionally, factors such as inflammation, oxidative stress, and nutrient excess can contribute to the development of selective insulin resistance.

Insulin resistance is a characteristic of HF and type 2 DM that can contribute mechanistically to the disorder’s development by inflammation, hyperglycaemia, hypertension, bone marrow dysfunction, visceral obesity, and atherogenic hyperlipidaemia. In addition, there is a strong correlation between insulin resistance

and endothelial dysfunction. Insulin resistance has been demonstrated to disrupt the insulin signalling pathway, resulting in decreased endothelial nitric oxide (NO) production (12) and increased ROS generation, which are crucial pathogenic processes in endothelial dysfunction (13).

Regarding endothelial dysfunction, this pathological process plays a significant role in HF and diabetic cardiovascular disease. However, endothelial cells exhibit enormous heterogeneity depending on the tissue in which they are found (14). The metabolic characteristics of microvascular endothelial cells from skeletal muscle and adipose tissue remain largely understudied. Therefore, the purpose of this research was to investigate the downstream insulin signalling pathways of microvascular endothelial cells in HF and diabetes patients.

1.1 Endothelial cell function

Endothelial cells are squamous cells that line the inner surface of the blood vessel wall as a monolayer. They play a variety of essential roles, including barrier function, stimulating and managing the inflammatory response, encouraging angiogenesis (the formation of new vessels), controlling vascular tone, and regulating thrombosis (15).

1.1.1 Role of endothelial cells in vascular biology

1.1.1.1 Barrier function

Endothelial cell layers play a crucial role in selectively controlling the movement of fluids, solutes, and circulating cells between the bloodstream and various tissues. Molecules can cross the tight endothelial barrier via two routes: transcellular (through the endothelial cells) or intercellular (between the endothelial cells) (16). The permeability of these cell layers can be classified into either normal/physiological or pathological conditions. The effectiveness of the endothelial barrier depends on many factors, including shear stress, inflammation, pathogens, and disease states. These factors induce changes in endothelial permeability by altering the synthesis and expression of cell-cell junction proteins or cell-matrix adhesion molecules. Reduced shear stress in HF and metabolic/inflammatory disorders in DM result in endothelial

barrier dysfunction, allowing plasma proteins and lipids to flow excessively into the vascular wall and adjacent tissues (17).

1.1.1.2 Inflammation

Endothelial cells have a central role in regulating inflammatory reactions. They participate in both innate and adaptive immune responses, including cytokine secretion, phagocytic function, antigen presentation, and proinflammatory, immune-enhancing, anti-inflammatory, and immunosuppressive responses (18). Under physiological conditions, all endothelial cells contribute to the inhibition of inflammation; under pathological conditions, they stimulate an inflammatory response by interacting with white blood cells and producing adhesion molecules, including vascular cell adhesion molecule-1 (VCAM-1) and intercellular adhesion molecule-1 (ICAM-1), and proinflammatory cytokines like tumour necrosis factor-beta (TNF-β) and macrophage colony-stimulating factor (M-CSF) (19). These factors are an essential part of the development of atherosclerosis as they induce inflammation in the vascular wall (20).

1.1.1.3 New blood vessel formation and damage repair

Angiogenesis, or the sprouting of new vessels from pre-existing vessels, is another critical function of endothelial cells. Key to normal vessel growth and development, is a balance between endothelial cell migration and proliferation which are regulated by chemotactic, haptotactic, and mechanotactic stimuli (21). When this process is inappropriately activated, abnormal vessel formation occurs, as seen in diabetic retinopathy and tumour growth. Typically, endothelial cells respond to vascular endothelial growth factor (VEGF), which is the central mediator of angiogenesis. Other angiogenic stimuli include hypoxia-inducible factors (HIFs) and insulin-like growth factors (IGFs) (22).

1.1.1.4 Control of vascular tone

Endothelial cells regulate vascular tone by releasing vasodilators, such as nitric oxide (NO), endothelium-derived hyperpolarising factor (EDHF), and prostacyclin, in

addition to vasoconstrictors, such as endothelin-1 (ET-1) and angiotensin II. These vasodilators and vasoconstrictors diffuse to adjacent smooth muscle cells and cause relaxation or constriction, respectively. NO is thought to play a critical role in the regulation of vascular dilation. We now know that endothelial NO is produced from endothelial nitric oxide synthase (eNOS), L-arginine, O_2, and the cofactors tetrahydrobiopterin (BH_4), haem, nicotinamide adenine dinucleotide diphosphate (NADPH), flavin mononucleotide (FMN), and flavin adenine dinucleotide (FAD) to L-citrulline and NO. Diffusion of the NO to adjacent vascular smooth muscle cells (VSMCs), is followed by binding to soluble guanylyl cyclase (sGC), resulting in an increase in cyclic guanosine monophosphate (cGMP) levels, which activates protein kinase G (PKG) and decreases calcium concentrations, resulting in vascular dilation (23).

While eNOS plays a pivotal role in controlling vascular function by producing NO, eNOS uncoupling is associated with pathological conditions by leading to the production of superoxide. Superoxide can combine with NO to form peroxynitrite ($ONOO^-$), a highly reactive oxidant that can cause endothelial cell dysfunction (Figure 1) (23) and thereby playing a key role in a vicious cycle.

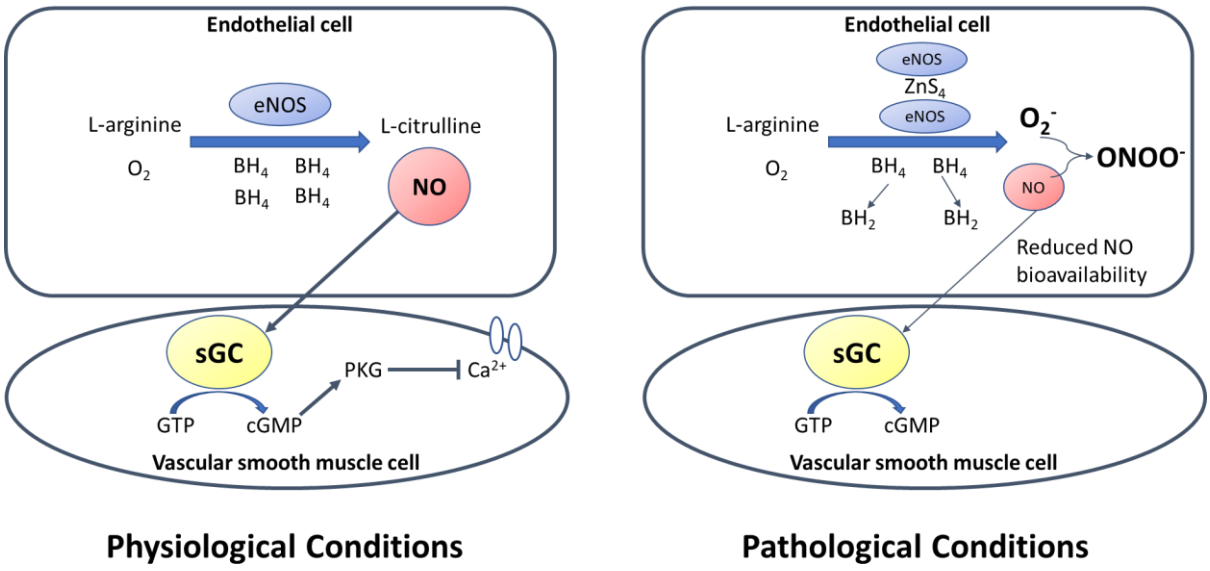

Figure 1: Mechanism of endothelial cell control vascular tone under physiological and pathological conditions.

1.1.1.5 Thrombosis and fibrinolysis

In addition to controlling vascular tone, all endothelial cells play a role in inhibiting blood coagulation under physiological conditions by binding tissue factor pathway inhibitors (TFPIs), activating protein C, and synthesising heparan sulphate (HS) proteoglycans, which have cell-surface anti-coagulant properties. Furthermore, vascular endothelial cells regulate thrombosis through their interaction with platelets by producing pro-thrombotic molecules, such as thromboxane, plasminogen activator inhibitor-1 (PAI-1), von Willebrand's factor (vWF), and tissue factor (24).

As a result of these diverse functions of endothelial cells, they have been implicated in the development, persistence and progression of a variety of diseases, including atherosclerosis, hypertension, primary pulmonary hypertension, systemic inflammatory response syndrome, CHF, and cancer (25).

1.1.2 Endothelial cell heterogeneity

In addition to the various functions described, endothelial cell also exhibit extensive heterogeneity across cell lines derived from different tissues (26). This heterogeneity exists at the level of cell morphology, function, gene expression, and antigen composition. As a result, studying endothelial cell function requires consideration of the endothelial cells' origin. For example, while endothelial cells derived from large vessels, such as the umbilical vein (human umbilical vein endothelial cell [HUVEC]) and aorta (human aortic endothelial cell [HAEC]) are suitable for atherosclerosis research, endothelial cells derived from small vessels (human microvascular endothelial cell [HMVEC]), skeletal muscle (human skeletal muscle endothelial cell [HSkMEC]), and fat tissue (human adipose tissue endothelial cell [HATEC]) are better suited for angiogenesis research. Therefore, understanding the molecular basis of endothelial heterogeneity may provide valuable insights into vascular bed-specific therapies (14).

1.1.3 The role of endothelial cells in adipose tissue

Adipose tissue is composed of stromal vascular cells, immune factors, stem cells, endothelial cells, lymphocytes, adipocytes, preadipocytes, connective tissue matrix, and nerve tissue. New perspectives have emerged on adipose tissue being

not just a tissue for storing energy in the form of lipids, but also as an endocrine tissue. Adipose tissue produces several adipokines, such as adiponectin, leptin, resistin, and adipsin. Furthermore, adipose tissue is now known to be a critical regulator of cardiovascular health by producing various bioactive molecules, including adipocytokines, microvesicles, and ROS, which act as autocrine, paracrine, and endocrine effectors of the cardiovascular system (27). Consequently, adipose tissue dysfunction contributes to the development of CVD by stimulating inflammation, hyperlipidaemia, and insulin resistance.

One unique feature of adipose tissue is that it has the capacity to expand many-fold, and vascularisation is essential for this growth; therefore, the angiogenesis function of endothelial cells in adipose tissue is critical. This process comprises endothelial cell proliferation, directed migration through the extracellular matrix, formation of intercellular junctions and a lumen, organisation of perivascular supporting cells, anastomosis with pre-existing vessels, and establishment of circulation (28). There are two possible models for the stimulation of angiogenesis during the growth of adipose tissue: A) in response to increased caloric consumption, adipocyte hypertrophy and hyperplasia occur, resulting in the formation of areas of tissue hypoxia that stimulate angiogenesis; and B) increased caloric intake alters systemic levels of trophic factors like insulin, which directly encourages adipose tissue angiogenesis. Increased angiogenesis promotes hyperplasia and lipid storage in adipocytes. Simultaneous expansion of adipocytes and vasculature prevents hypoxia and metabolic stress.

In addition to their barrier, inflammatory, and angiogenesis functions, adipose tissue endothelial cells (ATECs) also play a role in fat metabolism by regulating fatty acid transport and storage. The exchange of fatty acids between ATECs and adipocytes is bidirectional, and fatty acids activate peroxisome proliferator-activated receptor-γ (PPARγ) in ATECs. PPARγ, also known as the glitazone receptor, is a master regulator of adipocyte differentiation and plays a critical role in regulating adipogenesis. This fat metabolism-related function is unique to ATECs and does not exist in HUVECs (29).

A previous study on adipogenesis suggested that both brown adipocytes (BAs) and white adipocytes (WAs) had a common origin from endothelial cells in adipose tissue capillaries. After treatment with a PPARγ agonist, cells within capillary sprouts produced lipid droplets and exhibited molecular and morphological characteristics consistent with adipocytes. This development of adipocytes from endothelial cells appeared to follow the transdifferentiation pathway (conversion from one cell type to another) rather than differentiation from a poorly differentiated stem cell (30).

1.2 Endothelial cell function in heart failure and diabetes

1.2.1 Pathophysiology of heart failure and diabetes

HF and DM are both common diseases that, when combined, exacerbate one another. HF is a chronic clinical syndrome characterised by the inability of the heart to maintain adequate circulation to meet the needs of the body, which manifests as the symptoms of shortness of breath and fatigue, as well as an increased risk of hospitalisation and early death. DM is caused by impaired glucose tolerance due to decreased insulin levels or resistance to their effect, eventually leading to hyperglycaemia, which manifests as nocturia, polyuria, unexplained weight loss, and extreme tiredness. Although often considered distinct entities, HF and DM have a closely related pathophysiology; both conditions are characterised by neurohumoral activation, specifically overactivation of the RAAS and SNS. Furthermore, both HF and DM result in functional defects in the endothelial cell response to insulin, which accelerates the progression of atherosclerosis and other cardiovascular pathologies (31, 32).

1.2.2 Endothelial dysfunction in heart failure and diabetes

Both HF and DM are associated with endothelial cell dysfunction, which contributes to an increased risk of atherosclerotic events. As a result of this atherosclerotic complication, diabetic patients develop microcirculatory disturbances and subsequent multiple end-organ diseases, such as retinopathy, nephropathy, neuropathy, cardiomyopathy, peripheral vascular disease, and foot disease. Endothelial dysfunction in DM is caused by several mechanisms, including altered cell

signalling in endothelial cells, which results in decreased NO production, augmented oxidative stress, increased mitochondrial dysfunction, and is activated by proinflammatory factors such as tumour necrosis factor-alpha (TNF-α) and enabled by protein kinase C beta (PKCβ) (33, 34).

In HFrEF, a key cause of endothelial dysfunction is decreased shear stress on the luminal endothelial surface, resulting in decreased production of endothelium-derived NO and decreased endothelium-dependent dilation (35). Lower NO production in the vascular wall is also contributed by neurohumoral activation in HF which increases angiotensin II production, resulting in increased superoxide anion (O_2^-) formation. The superoxide anion reacts with NO to form peroxynitrite ($ONOO^-$), a potent oxidant that can damage molecules in endothelial cells.

HF with preserved left ventricular systolic function (HFpEF) is also associated with endothelial dysfunction. The factors causing endothelial dysfunction include increased oxidative stress, eNOS uncoupling, reduced NO production, and impaired GMP-PKG signalling. Impaired nitric oxide-cyclic guanosine monophosphate (NO-cGMP) pathway and endothelial dysfunction contribute to the pathophysiology of HF with both reduced and preserved left ventricular systolic function (36-38).

Endothelial dysfunction in HF and DM is associated with decreased NO generation. NO is a colourless free radical gas that is synthesised by various nitric oxide synthase (NOS) enzymes from NADPH, oxygen, and L-arginine. Existing data strongly suggest that NO production by endothelial cells has an essential role in preventing complications of atherosclerosis in several ways, including endothelium-dependent vasodilation, inhibiting platelet aggregation, and preventing smooth muscle proliferation (39). Therefore, decreased NO production resulting in endothelial dysfunction is a systemic process that occurs early in atherosclerosis and could represent a treatment target in both HF and DM.

1.3 Insulin signalling in endothelial cells in heart failure and diabetes

1.3.1 Insulin signalling in the normal state

Insulin and the IGF system are essential for the growth and development of living organisms. These systems include insulin, IGF1, IGF2, IGF-binding proteins (IGFBPs), and their receptors, insulin receptor (IR), IGF1 receptor (IGF1R) and IGF2/mannose 6-phosphate receptor (IGF2/M6PR). While insulin is an anabolic hormone protein produced exclusively by the beta cells of the pancreas, IGF1 is a hormone with a molecular structure similar to that of insulin and is produced by the liver under the control of growth hormone, and IGF2 and IGFBP are proteins produced by brain, muscle, and kidney (Figure 2). The insulin-related receptor family consists of three receptors: IR, IGF1R, and IGF2/M6PR (40). The receptors are all tyrosine kinase based with two identical units. Each unit contains an alpha chain localised on the outer membrane and linked to the other units via disulphide bonds, and a beta chain that spans the membrane and extends to the inner surface of the cell membrane. Tyrosine kinase domains are found in the beta chain, and they play a role in the process of autophosphorylation (41).

As a potent anabolic hormone, insulin promotes cellular nutrient uptake, storage, and synthesis while simultaneously inhibiting nutrient breakdown and release into the circulation. The basal concentration of insulin in the blood ranges between 0.01 nM and 0.2 nM, and it can be increased up to tenfold following a meal, causing cells to take up more glucose (42). Insulin also stimulates protein synthesis, free fatty acid uptake and synthesis, and inhibits lipolysis in adipocytes. In addition, insulin regulates adipose tissue growth and adipocyte differentiation via gene transcription, various adipokines, and fat-specific transcription factors, such as PPARγ (43). In physiological concentrations, insulin exerts anti-inflammatory and anti-atherosclerotic effects on the cardiovascular system through endothelial cell function whilst the degree of insulin resistance is correlated with endothelial dysfunction, which is directly linked to cardiovascular complications. Most of the actions of insulin occur through IR. However, both insulin and IGF1 can bind to and activate the IGF1R, leading to similar downstream signaling pathways (44).

The IGF system has a critical role in endothelial cells. IGF1 promotes vital cellular processes necessary for normal growth and development, such as proliferation, differentiation, survival, and metabolism. IGF1 activation through the IGF1R, IGF2/M6PR, and IR promotes proliferation, migration, survival, and tube formation in endothelial cells, although the greatest response occurs through IGF1R (40). IGF2 exerts some of its actions through IGF2/M6PR, which acts as a clearance receptor. The activity of IGF is also regulated by six IGFBPs: IGFBP1, IGFBP2, IGFBP3, IGFBP4, IGFBP5, and IGFBP6. These IGFBPs can either enhance or inhibit the activities of IGF. Recent animal studies have indicated that IGF1R serves a variety of physiological functions, including promoting cell proliferation, inhibiting apoptosis, and stimulating growth and development (45). In addition, IGF1R has been shown to protect endothelial cells by inhibiting apoptosis induced by hydrogen peroxide (H_2O_2) (46). According to a recent study, decreased IGF1R expression was associated with the development of diabetes and cardiovascular disease (47). The mechanism by which IGF1R acts on endothelial cells under these conditions is complex and requires further investigation.

Intracellular signalling involves the addition and breakdown of phosphate groups on proteins, called ‘phosphorylation’ and ‘dephosphorylation’, respectively. These essential processes can stimulate or reduce the activity of proteins. The enzyme responsible for the addition of the phosphate group is called a ‘kinase’; it takes the γ-phosphate group from adenosine triphosphate (ATP) and adds it to the target protein at specific locations, such as at serine/threonine or tyrosine. Therefore, protein kinases can be classified according to the location of the phosphate group addition, e.g., serine (Ser or S)/threonine (Thr or T) kinase and tyrosine (Tyr or Y) kinase. The enzyme responsible for the breakdown of phosphate groups from proteins is called a ‘phosphatase’ (48).

Once insulin and IGF1 bind to their receptors, the alpha and beta chains in the receptors move closer together and undergo autophosphorylation, increasing their tyrosine kinase activity. The phosphorylated tyrosine residues of the insulin receptor attract and activate the insulin receptor substrate 1 and 2 (IRS 1/2) protein. As a result, phosphoinositide 3-kinase (PI3K) is translocated to the plasma membrane, where the

SH2 domain of the PI3K adaptor subunit binds to the tyrosine residues of IRS, leading to PI3K activation, which generates phosphatidylinositol (3,4,5)-triphosphate (PIP3) from phosphatidylinositol (3,4)-biphosphate (PIP2). The phosphoinositide-dependent protein kinase 1 (PDPK1) then binds to PIP3 and phosphorylates protein kinase B (also known as Akt) (49). Akt is phosphorylated at Thr 308 by PDPK1, and at Ser 473 by mTORC2 (mechanistic target of rapamycin complex 2). Once Akt is phosphorylated, it activates multiple cellular proteins, including forkhead box O (FOXO), B-cell leukaemia/lymphoma 2 (BCL-2), mTOR, and eNOS (50). Phosphorylation of these Akt signalling proteins induces pleiotropic cellular responses, increasing cell survival and proliferation through negative regulation of FOXO proteins, increasing protein synthesis through activation of mTOR complex 1, and inducing vasodilation through enhanced eNOS activity (Figure 2). The present study focuses on the PI3K/Akt and eNOS pathways. eNOS is an essential enzyme in the cardiovascular system since it produces NO, which is a crucial regulator of blood pressure control, and is associated with the pathogenesis of atherosclerosis (51).

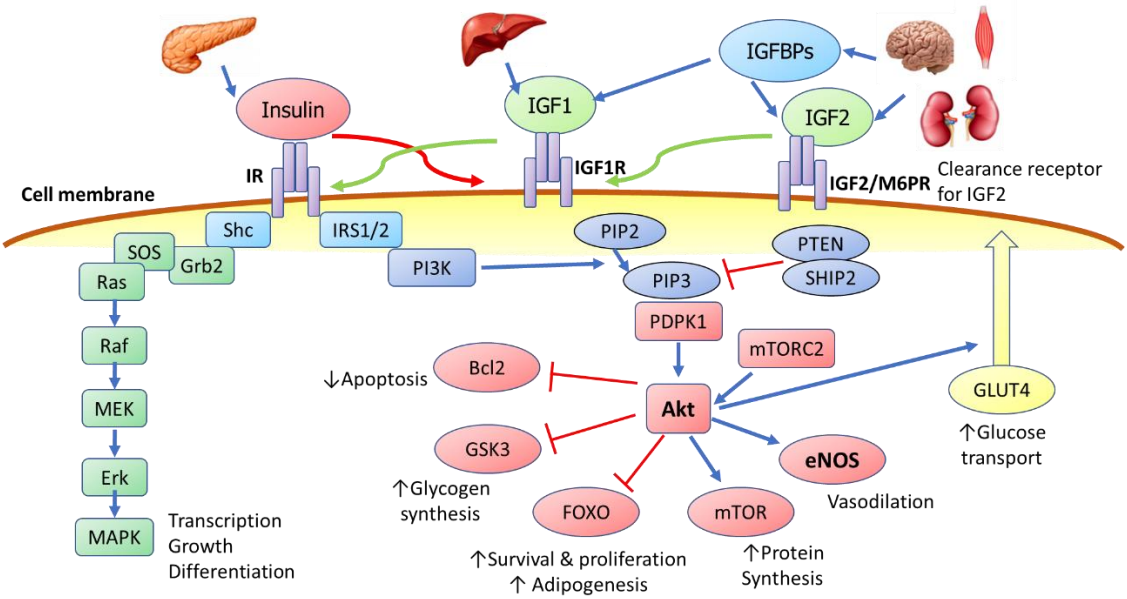

Figure 2: Schematic of the insulin signalling pathway. When the insulin receptor is activated, it primarily recruits and phosphorylates two adaptor proteins: IRS and Shc. PI3K/Akt is an IRS-mediated pathway that is crucial for activation of eNOS activity and regulation of a variety of metabolic events, including glucose transport and glycogen, protein, and lipid synthesis. Shc is involved in the activation of the mitogen-activated protein kinase (MAPK) pathway, which regulates growth and differentiation.

In endothelial cells, insulin action stimulates two major signalling pathways: the PI3K pathway and the MAPK pathway (Figure 3) (52). In the PI3K pathway, also known as the 'metabolic signalling pathway', activation of PI3K is required for insulin-mediated glucose transport into insulin-dependent target tissues, such as skeletal muscle and adipose tissue. Furthermore, this pathway has been shown to play a role in the regulation of insulin-dependent endothelial NO production. It was demonstrated that when insulin-mediated glucose uptake was impaired, insulin-stimulated endothelial vasodilation was also impaired. Therefore, a systemic defect in the PI3K pathway, which most likely characterises insulin resistance, causes both insulin-mediated glucose transport and insulin-stimulated endothelial vasodilation to be impaired.

Previous work has shown that activation of the PI3K/Akt pathway was terminated when phosphatase and tensin homolog deleted on chromosome 10 (PTEN) extracted the phosphate group from PIP3 at the 3'-OH group in the inositol ring (53). Alternatively, the SH2 domain-containing inositol polyphosphate 5-phosphatase (SHIP) enzyme removed phosphate groups at the 5'-OH group, resulting in dephosphorylation of PIP3 to PIP2 (54). Furthermore, it was found that the PH domain and leucine-rich repeat protein phosphatase (PHLPP) inhibited Akt by removing the phosphate group from Akt at Ser 473 and/or Thr 308 (55). Therefore, PTEN, SHIP, and PHLPP act as negative regulators of this pathway.

The MAPK pathway is also known as the 'mitogenic signalling pathway'. This pathway begins when Src homology and collagen (Shc) isoforms bind to IR via their phosphotyrosine binding (PTB) domain and undergo tyrosine phosphorylation. Shc then interacts with growth factor receptor-bound protein 2 (Grb2), which acts as the adaptor protein. Grb2 is also linked to the proline-rich domain of the son of sevenless (SOS), which can activate the Ras pathway (56). This pathway involves the activation of a cascade including Ras, Raf, MAPK/ERK kinases (MEKs), and extracellular signal-regulated kinases (ERKs), which lead to nuclear translocation of ERK and phosphorylation of transcription factors (Elk1, $p62^{TCF}$, etc.), resulting in the initiation of a transcriptional process that mediates cellular proliferation and differentiation (57). This pathway also regulates endothelial cell, vascular smooth muscle cell, and monocyte migration in the vasculature. In addition, it appears to mediate expression

of the prothrombotic and profibrotic factor, plasminogen activator inhibitor 1, by a variety of stimuli.

Endothelial balance is maintained by vasodilatory substances via the PI3K pathway and vasoconstriction via the MAPK pathway (Figure 3) (58). Previous data clearly demonstrate that insulin resistance and the associated defects accompanying metabolic syndrome are dependent on a defect in the PI3K pathway, whereas functions mediated by the MAPK pathway remain active (59). As a result, this may cause an imbalance between decreased endothelial production of NO and enhanced production of ET-1, leading to decreased blood flow due to vasoconstriction and subsequent endothelial dysfunction.

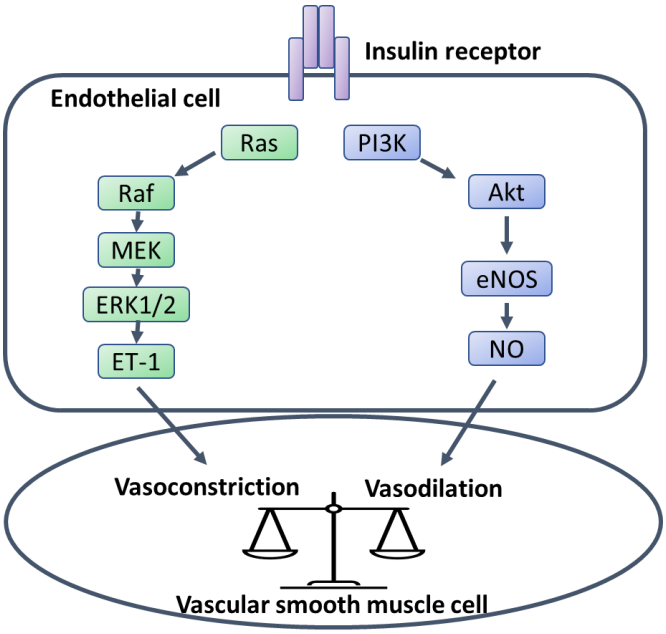

Figure 3: Balancing two major insulin signalling pathways to regulate vascular tone.

1.3.2 Insulin receptor

The IR is a heterotetramer made up of two extracellular and two transmembrane subunits, extracellular subunit (IRα) and transmembrane subunit (IRβ), which are connected by disulphide bridges (60). The extracellular subunit of the IR consists of two isoforms, IR-A and IR-B, due to alternate splicing during transcription, resulting in the absence (IR-A) or presence (IR-B) of a 12-amino acid

segment encoded by exon 11 (61). Relative expression of the two isoforms varies depending on the tissue. IR-A promotes cell growth and is mostly found in foetal and tumour tissues, although it can also be found in most adult tissues. IR-B regulates glucose homeostasis and is primarily expressed in insulin target tissues, such as the liver, muscle, adipose tissue, and kidney in adults.

During adulthood, increased IR-A expression may play a role in a variety of pathological processes and cancers, including lung, colon, ovarian, thyroid, and muscle cancers (62), while increased IR-B expression is associated with a predominance of insulin metabolic actions. The IR-A/IR-B ratio was found to be increased in diabetic patients, and was linked to decreased glucose uptake, decreased insulin signalling in insulin target tissues such as the liver and white adipose tissue, and increased growth of atherosclerotic plaques in aorta. Furthermore, weight loss from a very low-calorie diet or bariatric surgery has been shown to cause an increase in IR-B levels in adipose tissue, which improves insulin resistance (63).

The transmembrane subunit of IR contains seven tyrosine phosphorylation sites: two in the juxtamembrane domain (Tyr 965 and Tyr 972), three in the tyrosine kinase domain (Tyr 1158, Tyr 1162, and Tyr 1163), and two in the carboxy-terminal tail (Tyr 1328 and Tyr 1334) (Figure 4). When an insulin receptor tyrosine kinase is activated, it promotes autophosphorylation of the β subunit, with phosphorylation of three crucial tyrosine residues (Tyr 1158, Tyr 1162, and Tyr 1163), leading to full activation of the receptor kinase (64).

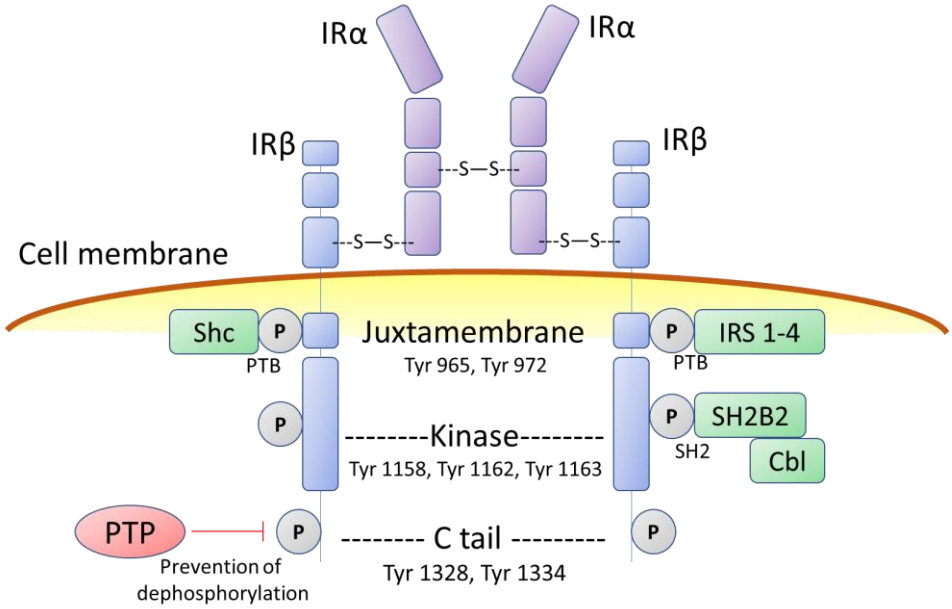

Figure 4: Insulin receptor. The insulin receptor is a disulphide-linked, α/β heterodimer glycoprotein that is predominantly found on the cell surface. Once activated by insulin, the receptor kinase can phosphorylate exogenous substrates that act as adaptors: IRS 1–4, Shc at the juxtamembrane region via their PTB domains, and SH2B2 at the kinase region via its SH2 domain, serving as an adaptor protein for the substrate Cbl.

1.3.3 Insulin-like growth factor 1 receptor

IGF1R is a transmembrane receptor that is activated by the hormones IGF1 and IGF2. It is a member of the large family of tyrosine kinase receptors. This receptor mediates the effects of IGF1, which is critical for growth, and its anabolic effects persist in adulthood. IGF1R may contribute to progression in early atherosclerosis by mediating the proatherogenic effects of IGFs. mRNA IGF1R expression was shown to be increased in VSMCs from asymptomatic patients' atherosclerotic plaques when compared with those of symptomatic patients (65). Because IGF1 is a potent mitogen for VSMCs, numerous studies in experimental atherosclerosis models have suggested that IGF1 promotes vascular hyperplasia by stimulating neointimal growth.

When the kinase domain of IGF1R is activated, specific tyrosine residues are autophosphorylated. The subsequent recruitment and phosphorylation of IRS allows PI3K to be recruited and the Akt-mTOR pathway to be activated. This signalling pathway promotes cell survival, growth, and proliferation by regulating metabolism and transcription. IGF1R activation may also recruit Shc adaptor proteins, and IGF1-induced Shc phosphorylation activates the RAS and MAPK pathways, which are

involved in the transmission of mitogenic, differentiation, and migratory signals (66). Furthermore, IGF1R activity has been shown to promote tumorigenesis, maintenance of the transformed phenotype, and progression of cancer (67).

While IGF1R shares structural similarities with IR, most notably in the kinase and juxtamembrane domains (84% and 61% sequence identity, respectively), the C-terminal tails are distinct (44% sequence identity) (68). In IGF1R, sequential autophosphorylation of three tyrosines (Tyr 1135, Tyr 1131, and Tyr 1136) facilitates stabilisation of the kinase activation loop (A-loop) in a position that promotes catalysis and subsequent phosphorylation of substrates (69).

1.3.4 Insulin receptor substrate (IRS)

The IRS protein family consists of nine members, which are found in the cytosol and bound to intracellular membranes. Isoforms IRS1–4 are required for complete insulin signal transduction in various tissues and species. Among all isoforms, IRS1 plays a critical role in activating the PI3K/Akt pathway. IRS3 is not encoded by a gene in the human genome. Studies in mice with tissue-specific knockout of IRS1 or IRS2 have found that IRS1 plays a significant role in insulin resistance in muscle and adipose tissue (70, 71), whereas IRS2 play a role in liver and the pancreatic β-cells (72). At the amino terminal of IRS1, a pleckstrin homology (PH) domain aids in the protein's anchoring to the membrane near the IR. IRS1 sequences are highly conserved across species, and motifs potentially involved in IRS1 function in mice and human are conserved (73). Multiple tyrosine phosphorylation sites are located at the C-terminal of IRS proteins. When phosphorylated, these sites act as docking sites for other signalling proteins with SH2 domains, such as the PI3K p85 regulatory subunit, Grb2, and SHP-2, which further propagate and regulate insulin signalling inside the cell (74).

1.3.5 Phosphatidylinositol 3-kinase

PI3K is classified as a lipid kinase, due to its ability to add phosphate groups to the inositol ring at the 3'-OH group position in phosphatidylinositol (PI) and phosphoinositide (PIP, PIP2) molecules by using ATP as a phosphate group donor.

As a result, molecules of phosphatidylinositol-3-monophosphate (PIP), phosphatidylinositol-4,5-bisphosphate (PIP2), and phosphatidylinositol-3,4,5-trisphosphate (PIP3) are formed. PIP3 is a second messenger that controls a variety of cellular processes, including cell division, cell multiplication, and cell survival. In mammals, PI3K is classified into three classes, each of which is composed of distinct genes: class I, class II, and class III. These three groups are classified according to their properties, specificity, substrates, structure, expression in various tissues, activation mechanism, and function. Class I PI3Ks primarily phosphorylate PIP2 to generate the lipid second messenger PIP3 (75).

1.3.6 Akt/Protein kinase B

Akt/PKB is a serine/threonine kinase that is classified as a downstream effector of PI3K. It was found that the Akt1 and Akt2 gene were similar to viral oncogene (v-akt), which was first discovered in mice with T-cell lymphoma. Further studies were conducted to determine that the kinase domain of Akt was similar to that of protein kinase A (PKA) and protein kinase C (PKC), so it was called protein kinase B (PKB). Akt is currently classified into three isoforms in mammals: Akt1/PKBα, Akt2/PKBβ, and Akt3/PKBγ (Figure 5) (76). Although the three isoforms are derived from different genes, amino acid homology accounts for approximately 80% of their structural components.

Akt expression studies revealed that Akt1 and Akt2 were found in common tissues, with Akt1 playing a role in embryonic development, cell growth, and survival. Akt2 is more common in insulin-targeted tissues, and it plays a role in the control of blood sugar levels (glucose homeostasis). Akt3 has been reported in the brain and has been linked to brain cell proliferation. When human retinal endothelial cells (HRECs) were exposed to high concentrations of glucose, the relative expression levels of AKT3 mRNA and protein were significantly increased; furthermore, VEGF mRNA and protein expression levels were significantly decreased in high glucose-treated HRECs transfected with AKT3 siRNA (77). There is evidence that increasing Akt3 inhibits adipogenesis and prevents mice from developing obesity (78). Although the three isoforms of Akt perform different functions, their structures are highly preserved across each, especially Akt1 and Akt2.

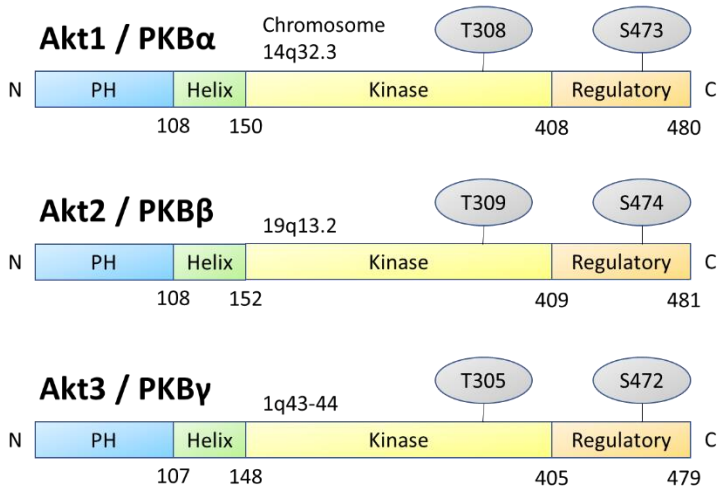

Figure 5: The structure of the Akt1, Akt2, and Akt3 proteins consists of the pleckstrin homology (PH) domain, helical domain (Helix), kinase domain, and regulatory domain. Although all three isoforms are formed by genes on different chromosomes, they have similar locations for the addition of the phosphate group.

1.3.7 Endothelial NOS

eNOS, also known as nitric oxide synthase 3 (NOS3), is one of three enzyme isoforms responsible for NO synthesis; the other isoforms are neuronal nitric oxide synthase (nNOS) and inducible nitric oxide synthase (iNOS). While nNOS expression is localised in specific neurons of the brain, iNOS expression is typically induced in inflammatory diseases. All three isoforms have 50–60% amino acid sequence homology and have an N-terminal oxygenase domain with haem, L-arginine, BH_4-binding domains, a central calmodulin (CaM)-binding region, and a C-terminal reductase domain with NADPH-, FAD-, and FMN-binding sites (79). eNOS is primarily responsible for production of NO in the vascular endothelium, which plays a vital role in promoting vasorelaxation, and activates anti-inflammatory and anti-atherosclerotic pathways. As a result, eNOS function is essential for keeping the cardiovascular system healthy.

Multiple phosphorylation sites on tyrosine (Tyr or Y), serine (Ser or S), and threonine (Thr or T) residues can regulate eNOS. The currently identified tyrosine sites localise to Tyr 83 and Tyr 567, the serine sites localise to Ser 114, Ser 615, Ser 633, and Ser 1177, and the threonine site localises to T495 (using the human sequence nomenclature). The phosphorylation of tyrosine residues has been shown to regulate

the NO-producing capability of eNOS (80). It has been noted that tyrosine phosphorylation appears to be most prominent in primary EC and may be lost when cells are cultured. eNOS becomes rapidly serine phosphorylated when EC are exposed to fluid shear stress (FSS), leading to phosphorylation of Ser 1177 that is mediated by AKT1 (81) and other kinases, such as PKA and AMP-activated protein kinase (AMPK) (82). PKC signalling inhibits eNOS activity in endothelial cells by phosphorylating Thr 495 and dephosphorylating Ser 1177, whereas PKA signalling activates eNOS by increasing phosphorylation of Ser 1177 and dephosphorylation of Thr 495 (83).

Akt phosphorylation of Ser 1177 significantly increases (>50%) the maximal superoxide generated by eNOS. In endothelial cells, VEGF-induced phosphorylation of Ser 1177 increases superoxide production via eNOS. Therefore, phosphorylation of eNOS at Ser 1177 is required for the direct control of superoxide and NO generation (84).

1.3.8 Insulin signalling in the insulin-resistant state

Both HF and DM are characterised by generalised insulin resistance, which leads to a cascade of effects on insulin signalling in endothelial cells (32). Insulin resistance is a condition in which normal concentrations of insulin cannot influence metabolism at important sites, such as skeletal muscle and adipose tissue. Insulin resistance in skeletal muscle significantly decreases glucose uptake, thereby encouraging hyperglycaemia and possibly local maladaptive effects, whilst insulin resistance in adipose tissue promotes lipolysis, resulting in increased fatty acids and hypertriglyceridaemia. Moreover, peripheral insulin resistance leads to a chronic adaptation of beta cells, resulting in a several-fold increase in insulin production and hyperinsulinaemia. This combination of metabolic abnormalities has an effect on insulin signalling.

Hyperglycaemia in patients with insulin resistance can induce the formation of AGEs because high blood sugar levels promote the non-enzymatic glycation of proteins, lipids and nucleic acids. In this process, sugar molecules bind to and modify

the structure of these biomolecules, leading to the formation of AGEs. AGEs, such as pyrraline, pentosidine, and N-carboxy-methyl lysine (CML), stimulate the production of ROS (Figure 6), inhibit tyrosine phosphorylation of IRS1 and IRS2 and decrease activation of the PI3K/Akt pathway by activating PKC (85).

Lipotoxicity, caused by an increase in free fatty acids, inhibits the PI3K/Akt signalling pathway and activates the MAPK/ERK signalling pathway. Free fatty acids also stimulate PKC, impairing Akt function via IRS1/2 inactivation and increasing NOX-mediated ROS generation (86). Furthermore, ROS can stimulate NF-κB, which promotes the formation of adhesion molecules and ET-1. Adhesion molecules facilitate monocyte contact with endothelial cells, resulting in the formation of foam cells that produce IL-6 and TNF-α. This contributes to the development of atherosclerosis and increases the risk of cardiovascular disease (87).

Initially, hyperinsulinaemia in the early stage stimulates insulin signalling, resulting in increased expression of IRS1, PI3K, and Akt (88). However, longer-standing hyperinsulinaemia desensitises the insulin signalling pathways, resulting in decreased expression of IRS1, PI3K and Akt (89). This reduction in insulin action via the IRS1/PI3K/Akt pathway results in a decrease in antiatherosclerotic activity and contributes to the acceleration of atherosclerosis and other cardiovascular diseases.

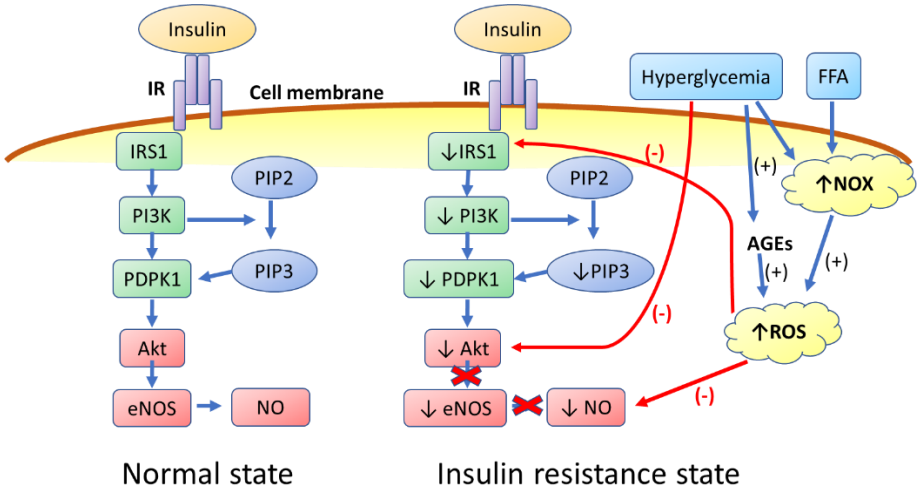

Figure 6: Insulin signalling in the PI3K/Akt/eNOS pathway under physiological conditions and in insulin resistance.

In early stages of HF caused by pressure overload or in the early stages of metabolic syndrome, hyperinsulinaemia leads to activation of IRS1 and Akt1 to promote pathological hypertrophy, mitochondrial dysfunction, and decreased autophagy, all of which contribute to accelerated left ventricular (LV) remodelling. As HF progresses, insulin signalling pathways may become desensitised, resulting in loss of the cytoprotective effects of Akt signalling and persistent nuclear localisation of FOXO proteins, which accelerates HF through a variety of mechanisms that include increased apoptosis and exacerbation of lipotoxicity (Figure 7) (11).

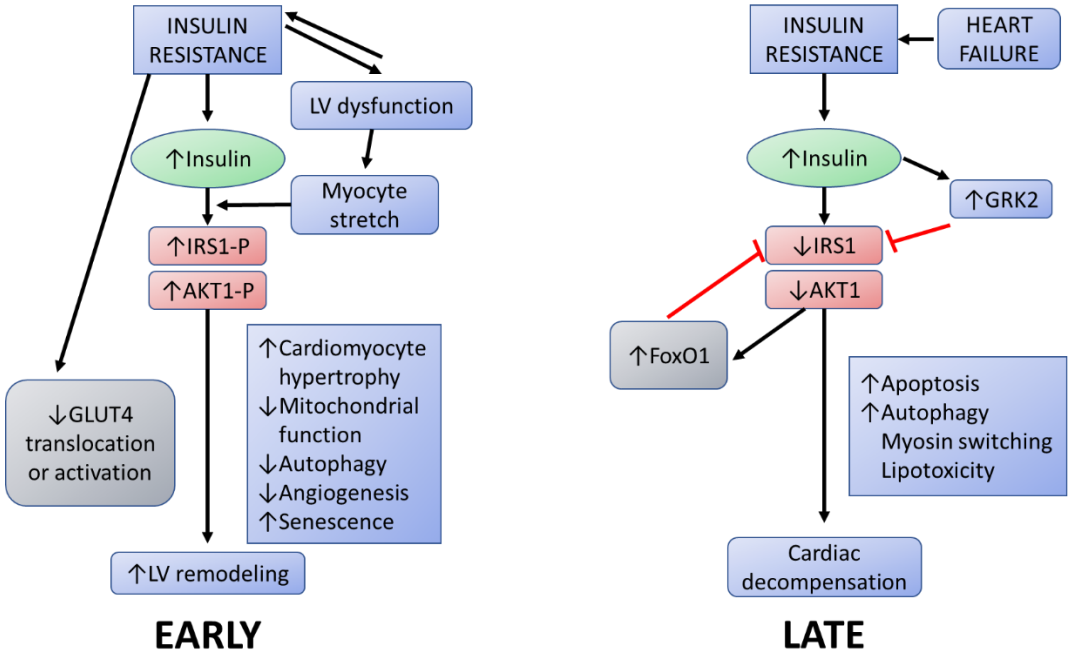

Figure 7: Insulin signalling in the early and late stages of heart failure.

1.4 Reactive oxygen species in endothelial cells

ROS are a group of highly reactive intermediate molecules derived from oxygen obtaining an electron from another molecule during an oxidation reaction. ROS can be classified into two types: non-radicals (ozone, hydrogen peroxide, peroxynitrite) and free radicals (superoxide anion, hydroxyl radicals, peroxyl radicals). ROS, such as hydrogen peroxide and the superoxide anion, play a key role as messengers in normal cell signal transduction and are involved in a variety of physiological processes known as ‘redox signalling’ (90). ROS are also a known component of the immune cells' killing response, causing cell differentiation, apoptosis, and damage to lipids,

proteins, and nucleic acids. Therefore, ROS contribute to the natural aging process and play a role in the development of a variety of diseases, including atherosclerosis, obesity, hepatitis, pancreatitis, neurodegenerative diseases, inflammatory conditions, heart failure, and diabetes, in addition to being involved in gene mutations causing cancer (91).

1.4.1 ROS generation and regulation

The production of ROS is influenced by both endogenous and exogenous factors. Endogenous sources of ROS are produced mainly in the mitochondrial electron transport chain and by several enzymes, including NADPH oxidases (NOXs), uncoupled eNOS, flavoprotein oxidases, xanthine oxidase (XO), myeloperoxidase (MPO), cytochrome P450 oxidase, microsomal cyclooxygenase (COX), lipoxygenase, and catalysed metal reactions. Exogenous sources of ROS include various sources, such as chemicals, drugs, pollutants, nutrient overdose, mutagens, xenobiotics, and ionising radiation (92).

Under physiological conditions, low levels of ROS are involved in signalling termed ‘oxidative eustress’, which initiates a protective response in the form of cellular defence mechanisms, cell proliferation, differentiation, migration, and angiogenesis. However, excessive ROS production, termed ‘oxidative stress’, can result in inflammation, fibrogenesis, tumour growth, metastasis, growth arrest, and cell damage (93). Balancing homeostasis between these processes through the breakdown of ROS is critical for normal cell function. While superoxide anion is dismuted into hydrogen peroxide and oxygen by superoxide dismutase (SOD), hydrogen peroxide is broken down into water and oxygen by catalase, glutathione peroxidase, and peroxiredoxins (94). Within the ROS group, superoxide anion is the primary cause of oxidative stress in diabetes and HF, and it is primarily produced by NOXs.

1.4.2 NADPH oxidases

NOXs are membrane-bound enzyme complexes that produce ROS in phagocytic cells, skeletal muscle cells, and endothelial cells. All NOXs transfer electrons from NADPH to molecular oxygen, resulting in the formation of superoxide anions and other downstream ROS with $NADP^+$ as a by-product. In humans, the NOX family consists of seven isoforms distinguished by their catalytic core component, including five NOX homologues (NOX1–5) and two dual oxidases (DUOX1/2), each of which vary in their tissue distribution (Figure 8) (95). The predominant NOX isoforms present in endothelial cells are NOX1, 2, 4, and 5 (96). NOX1, 2, 3, and 5 produce mainly superoxide anion and are associated with endothelial dysfunction, whereas NOX4 produces mainly hydrogen peroxide and is associated with protective effects on the vessel wall; DUOX1 and DUOX2 produce both superoxide anion and hydrogen peroxide (97). Each NOX isoform contains two membrane-bound subunits, including one catalytic subunit and one $p22^{phox}$ subunit (for stability and activation), and various cytosolic subunits; NOX5 contains only one catalytic subunit (98), and NOX4 requires only the $p22^{phox}$ subunit, without a cytosolic subunit (99). NOX2 and NOX4 promote the proliferation of endothelial cells, whereas NOX1 promotes mitogenesis and proliferation in smooth muscle cells. Furthermore, NOXs regulate vascular contractility and are involved in the pathogenesis of vascular dysfunction and disease.

Despite their similar structure and enzymatic functions, the NOX family of enzymes have distinct activation mechanisms. NOX1 activity requires the presence of $p22^{phox}$, NOXO1, NOXA1, and the small GTPase Rac. NOX2 activity requires the presence of $p22^{phox}$, $p47^{phox}$, $p67^{phox}$, and Rac. NOX3 requires $p22^{phox}$ and NOXO1, and may also require NOXA1, depending on the species; Rac can participate but its necessity for activity is not clearly established. NOX4 requires $p22^{phox}$ in vivo and is constitutively active. NOX5, DUOX1, and DUOX2 are activated by Ca^{2+} ions, and DUOX1 and DUOX2 require association with the maturation factors DUOXA1/DUOXA2 for activation (96).

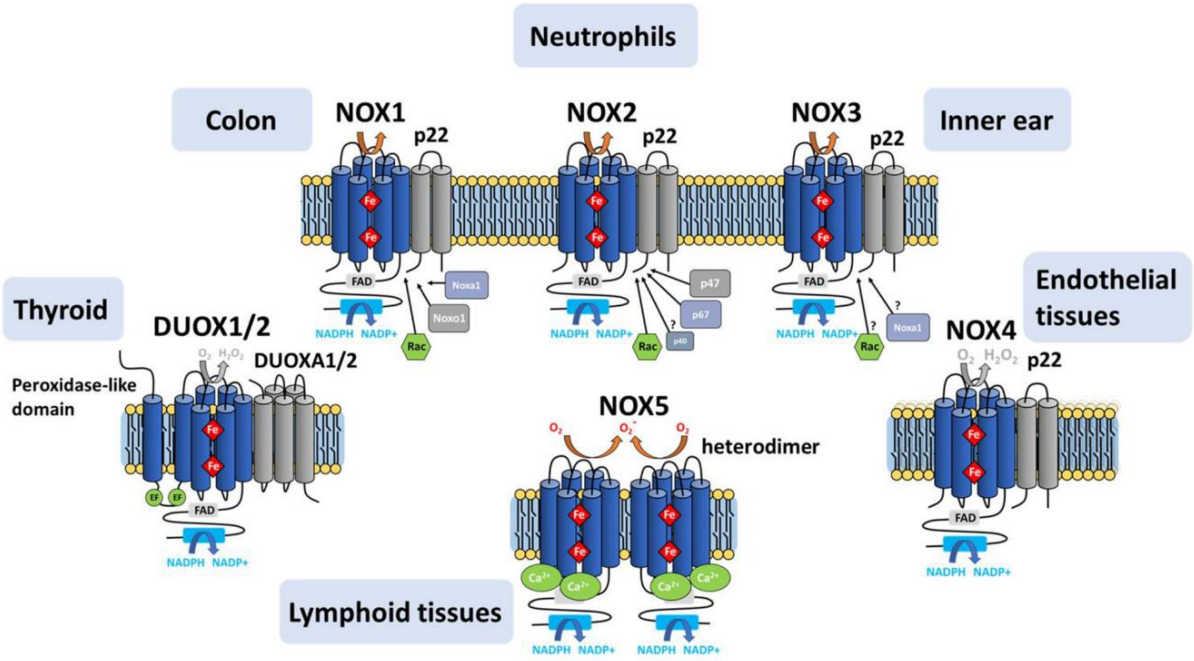

Figure 8: The NOX family includes seven isoforms that are distinguished by their catalytic core component, including five NOX homologues (NOX1–5) and two dual oxidases (DUOX1–2), all of which have different tissue distributions (95).

1.4.2.1 NOX1

NOX1, the first NOX2 homologue, plays a role in host defence, cell growth (proliferation and mitogenesis), and malignant transformation. NOX1 is expressed at high levels in colon epithelial cells (100), smooth muscle cells, and in endothelial cells. In a recent study, it was discovered that high levels of NOX1 were associated with human gastrointestinal malignancies (101). Due to the fact that NOX1 is expressed in both endothelial cells and VSMCs, global NOX1 KO-mediated improvements in endothelium-dependent (acetylcholine-induced dilation) and smooth muscle-dependent (NO donor-induced dilation and myogenic tone) responses suggest that NOX1 is likely involved in metabolic vascular pathology in both cell types (102). In the endothelium, NOX1 is expressed at low levels; its expression is increased in cardiovascular diseases, including hypertension, atherosclerosis, diabetes, and hypercholesterolaemia (103). NOX1 also contributes to diabetes-associated endothelial dysfunction and is the predominant NOX isoform underlying eNOS uncoupling in diabetes (104).

1.4.2.2 NOX2

NOX2, also known as gp91phox-containing NOX, is the prototype NOX and is typically highly expressed in phagocytic cells and found in all vascular wall cells, especially the endothelial cells of large arteries. The two major NOX isoforms expressed in cardiac cells are NOX2 and NOX4 (105). NOX2 is highly expressed in myeloid leukaemia cells (106). NOX2 is an important source of superoxide anion (107), and also plays a role in endothelial dysfunction. Sukumar and colleagues generated transgenic mice with endothelial-specific insulin resistance and demonstrated that deletion of NOX2 decreased superoxide generation and improved endothelial cell function (108).

NOX2 activation in the endothelium can be mediated by a variety of metabolic factors, including glucose, palmitate, and oxidised low-density lipoprotein (LDL) (109). Furthermore, hyperinsulinaemia can lead to NOX2-mediated superoxide production in microvascular endothelial cells, resulting in a decrease in NO and an increase in peroxynitrite formation (110). Evidence suggests that NOX2-mediated endothelial dysfunction is mediated in part by activation of ERK1/2. ERK1/2 signalling also downregulates IR and eNOS signalling. In middle-aged mice, it was demonstrated that NOX2-knockout prevented high-fat diet-induced ROS production and ERK1/2 activation, and reduced weight gain and improved insulin sensitivity and endothelial function (111). In clinical studies, obese patients (irrespective of gender) were shown to have increased expression of endothelial $p47^{phox}$ (required for canonical NOX2 activation), implying that NOX2 contributes to increased vascular superoxide production and oxidative stress in these patients. Furthermore, endothelial NOX2 has been shown to induce cardiac fibrosis and diastolic dysfunction (112), and the NOX2-selective inhibitor NOX2ds-tat effectively reduced oxidative stress and vascular dysfunction caused by insulin resistance (108).

1.4.2.3 NOX4

NOX4 is highly expressed in the kidney (distal and proximal tubules) and blood vessels. It is overexpressed in various types of cancer, such as breast cancer and prostate cancer (113). In contrast to NOX1, 2, and 5, NOX4 is the isoform with the

highest expression in HUVECs, with 100-fold higher levels than NOX2 (114, 115) and is the only isoform with mitochondrial localisation (116). Ninety per cent of NOX4 is involved in the production of hydrogen peroxide, which is thought to be an endothelium-derived relaxing factor, and ten per cent produces superoxide anion (117). This NOX4 activity is generally considered protective of vascular function and promotes endothelial angiogenic responses (99, 118). It is also involved in the physiological functions of cell survival, apoptosis, senescence, insulin signalling, differentiation, and migration (96). Importantly, NOX4-derived H_2O_2 does not react with NO. Another study demonstrated that laminar shear stress may facilitate eNOS activation in the endothelium via NOX4-induced sulphenylation of SHP2 (tyrosine-protein phosphatase non-receptor type 11) (119). Moreover, endothelial NOX4 contributes significantly to the prevention of arterial stiffness and progression of atherosclerosis (120). Previous research established that NOX4-mediated downregulation of NOX2 is a critical aspect of the vasoprotective effects of NOX4 (121). Therefore, altered or decreased NOX4 expression in obesity may be an early event triggering endothelial dysfunction and vascular stiffness. Furthermore, excessive production of mitochondrial ROS plays an important role in the development of diabetes and diabetic complications (122, 123) and in the development of cardiac fibrosis and remodelling via the NOX4 signalling pathway (124).

1.4.2.4 NOX5

NOX5 is highly expressed in the testes and lymph nodes and is involved in the motility and viability of sperm (125). It is overexpressed in a number of cancers, including prostate cancer (126), malignant melanomas, breast cancer (127), and oesophageal cancer (128). NOX5 is an isoform that is expressed at the plasma membrane and is responsible for the production of superoxide anion (129). A recent study established that NOX5 can induce eNOS uncoupling and can cause age-related hypertension (130). Furthermore, elevated expression of NOX5 in the kidneys of diabetic patients has been linked to diabetic nephropathy (131), atherosclerosis (132), pulmonary hypertension, and diabetes-related cardiovascular complications.

1.4.3 ROS and antioxidants in endothelial cells

As previously stated, oxidative stress is defined as an imbalance between ROS production and antioxidant defence that results in a change in the cellular redox status.

1.4.3.1 Superoxide anion

Superoxide anion (O_2^-) is a compound formed by one-electron reduction of dioxygen. Superoxide anion is a highly reactive molecule with a charge that prevents it from readily crossing membranes; it is short-lived, and its effect is mostly local. In the vasculature, superoxide anion promotes contraction and hypertrophy of VSMCs through Ca^{2+} signalling and activation of a variety of kinases, including Src, Rho, and ERKs (133). Superoxide anion also promotes macromolecular extravasation and leucocyte adhesion at the vascular wall (134).

1.4.3.2 Hydrogen peroxide

Hydrogen peroxide (H_2O_2) is an important oxidising molecule that is produced by NOXs and the mitochondrial respiratory chain. Superoxide anion produced by the NOX family (except for NOX4, which mainly releases hydrogen peroxide) can be converted to hydrogen peroxide via SOD (99). Hydrogen peroxide can react with transition metals like Fe^{2+} and Cu^{2+} in the extracellular environment, resulting in the formation of a highly reactive hydroxyl radical that cause damage to macromolecules. However, within cells and tissues, hydrogen peroxide acts as a signalling modulator and initiated cellular responses, such as proliferation, immune cell recruitment, and cell shape alterations. For example, in murine models, hydrogen peroxide has been shown to aid in the prevention of atherosclerosis (121) by maintaining eNOS and haem oxygenase 1 expression during vascular stress, inhibition of vascular smooth muscle cell proliferation, and prevention of vascular inflammation and remodelling (99, 135). In addition, hydrogen peroxide produced by NOX4 promotes endothelial angiogenesis via eNOS activation (136).

1.4.3.3 Superoxide dismutase

This protein family of metalloprotein antioxidant enzymes can catalyse the dismutation of two superoxide radicals into hydrogen peroxide and oxygen (Figure 9). It is the most powerful antioxidant enzyme in humans to counteract superoxide anion (137). SOD exists in three isoforms, SOD1–3, each with specific cofactors and subcellular localisation that places it close to the source of ROS production.

SOD1 (Cu/ZnSOD or cytosolic SOD) is found in the cytoplasm and the mitochondrial intermembrane space. The highest SOD1 activity has been reported in the human liver. Excess hydrogen peroxide produced by overexpression of SOD1 results in the formation of proatherogenic molecules, such as hydroxyl radicals and metal-associated reactive species (138). SOD2 (MnSOD or mitochondrial SOD) is expressed in the mitochondrial matrix and plays a role in the protection of superoxide anion from the mitochondrial electron transport chain. SOD2 activity is found at high levels in the renal cortex. Lack of SOD2 leads to mitochondrial dysfunction and an increased risk of developing atherosclerosis (139). SOD3 (ecSOD or extracellular SOD) is found in the extracellular matrix, on the cell surface, and in the vascular wall (140, 141). SOD3 is present in human lymphocytes and plasma, and its deficiency increases the risk of developing ischemic heart disease and HF (142).

1.4.3.4 Catalase

Catalase, a tetrameric haem protein, is a common and critical enzyme found exclusively in peroxisomes, where it catalyses hydrogen peroxide to water and oxygen (Figure 9) (143). Catalase plays a vital role in protecting cells from the toxic effects of hydrogen peroxide. It has also been associated with the pathophysiology of various diseases, as evidenced by the increased oxidative stress and decreased catalase activity observed in patients with type 1 and type 2 diabetes (144, 145). Catalase also prevents progressive remodelling of the myocardium, leading to HF (146). Furthermore, decreased catalase activity has been observed in a variety of different cancers, including lymphoma, breast cancer, gynaecological cancer, urological cancer, head and neck cancer, prostate cancer, and pancreatic cancer (147-149).

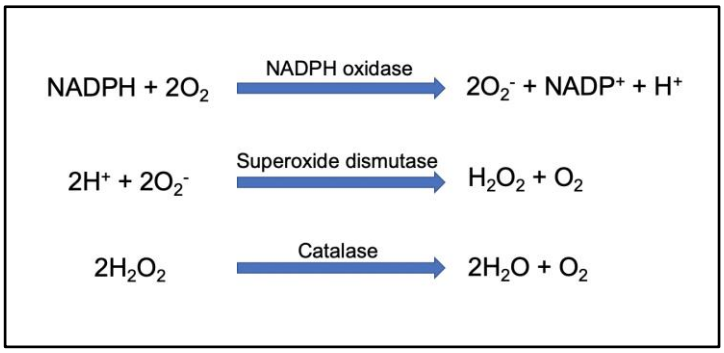

Figure 9: Oxidative enzymes, reactive molecules, and their conversion to other species by antioxidative enzymes.

1.4.3.5 Peroxiredoxin

Peroxiredoxins (Prxs) are enzymes that protect endothelial cells from peroxide damage caused by hydrogen peroxide and peroxynitrite. Peroxiredoxin exists in six different isoforms, each with a different subcellular localisation. While Prx1 contributes to the reduction of pressure overload-induced cardiac hypertrophy and HF (150), Prx2 and Prx4 are significantly upregulated and involved in cardiomyopathy and HF (151, 152).

1.4.3.6 Glutathione peroxidase

Glutathione peroxidase (Gpx) is a tetrameric selenoprotein that is found in the cytoplasm, nucleus, and mitochondria. The main biological function of Gpx is to detoxify free hydrogen peroxide to water and to reduce lipid hydroperoxides by using the reducing capacity of coupled glutathione/glutathione disulphide (GSH/GSSG). Lipid hydroperoxides, such as cholesterol, free fatty acids, cholesterol esters, and phospholipids are neutralised by phospholipases, Prx, and glutathione S-transferase (GST). There is a positive correlation between increased Gpx concentration and anti-inflammatory activity of the cardiovascular system. To date, eight different isoforms of Gpx have been identified in humans. Gpx1 (cytosolic or classical Gpx [cGpx]) is localised in the cytoplasm and its preferred substrate is hydrogen peroxide (153). The preferred substrate of Gpx4 (phospholipid Gpx or PHGpx) is lipid hydroperoxides and its expression is downregulated in the early and middle stages of myocardial infarction (154).

1.4.3.7 Non-enzymatic antioxidants

Non-enzymatic antioxidants are critical for human health because they protect cells from free radicals, which can be classified as either exogenous or endogenous (155). Examples of non-enzymatic antioxidants are vitamin C, E, A, flavonoids, carotenoids, glutathione, plant polyphenols, uric acid, theaflavin, allyl sulphides, curcumin, melatonin, bilirubin, and polyamines. Vitamin C (ascorbic acid) is the most potent water-soluble antioxidant found in human plasma, with evidence supporting its ability to improve vascular endothelial function (156). Vitamin E, which is lipophilic and is found on the cell membrane, is a potent antioxidant that prevents lipid peroxidation. Vitamin E treatment neutralises circulating free radicals and enhances endothelium-dependent vasodilation (157).

1.4.4 Oxidative stress in endothelial dysfunction in heart failure and diabetes

Oxidative stress refers to an imbalance in the antioxidant response caused by an excess of ROS or oxidants, which results in endothelial cell damage. Superoxide anion, hydrogen peroxide, and NO are required under physiological conditions to maintain vascular function, structure, and angiogenesis (158). ROS play a major role in cellular signalling and function; this process is referred to as redox signalling. Hydrogen peroxide encourages calcium-dependent eNOS activity, allowing for adequate production of NO (159).

Several studies suggest that oxidative stress plays a role in the pathophysiology of a variety of diseases, including atherosclerosis, hypertension, diabetes, and HF, in which the levels of superoxide anion in the vascular wall is increased (160). Excess superoxide anion can inactivate NO, resulting in the rapid formation of peroxynitrite ($ONOO^-$) in endothelial cells. Peroxynitrite then enhances the effect of eNOS uncoupling by oxidising the eNOS cofactor BH4 to inactive dihydrobiopterin (BH2). Uncoupling eNOS results in the formation of a toxic superoxide anion cycle, which decreases NO bioavailability and results in endothelial dysfunction (23). Furthermore, oxidative stress can induce cellular transformation under pathological conditions, such as in HF and diabetes. This process can transform

endothelial cells into myofibroblasts via TGF-β-induced endothelial-to-mesenchymal transition (161).

1.4.5 Antioxidative stress in endothelial dysfunction in heart failure and diabetes

In patients with endothelial dysfunction, antioxidants can help prevent oxidative damage and restore endothelial function (162, 163). Several antioxidants, including SOD (164), catalase (165), vitamin D (166), and vitamin E (167), have been shown to neutralise circulating free radicals and improve vascular cells in experimental conditions. However, most of the clinical research has been conducted on healthy and diseased humans, and there is inconsistent evidence for the benefit of exogenous antioxidants in preventing adverse cardiovascular complications (168-171). This finding could be explained by several factors, including the exogenous antioxidants' lack of site specificity. Furthermore, excessive dietary intake of exogenous antioxidants could interfere with the activation of the endogenous antioxidant defence system and can cause partial immune depression (172, 173). Further research is required to fully understand the role of antioxidants in the treatment of human disease states and in the promotion of health.

1.5 Angiogenesis

Angiogenesis is defined as the process of new capillary blood vessel formation from pre-existing vasculature and is vital to the growth and development of all organ systems. Numerous complex processes occur during angiogenesis, including vasodilation, increased endothelial permeability, basal membrane dissolution, endothelial cell proliferation, migration, tubule formation, replasticity, and endothelial cell differentiation and maturation. Angiogenesis is critical and occurs in both physiological and pathological processes, including wound healing, post-ischemic neovascularisation, adipose tissue expansion, diabetic retinopathy and nephropathy, and carcinogenesis. It is regulated by a balance of proangiogenic and antiangiogenic factors (174-179). Angiogenesis is classified into either 'sprouting' or 'intussusception' types and endothelial cells facilitate this process by proliferating, migrating, differentiating, and forming new capillaries (180).

Angiogenesis is activated by mechanical forces and a variety of chemical stimuli, such as VEGF, HIF-1α, FGF, and angiopoietin-2 (Ang-2). Among these proangiogenic factors, VEGF-A, acting through VEGF receptor 2 (VEGFR2, also known as KDR) is the most potent mitogenic and chemoattractant signal that is capable of activating quiescent endothelial cells into tip and stalk cells. Tip cells have numerous long and mobile filopodia that release proteases to degrade the basement membrane, allowing the stalk cells to proliferate and migrate, following behind the tip cells along the proangiogenic factor gradient (181). Following angiogenesis, a balance is established between pro- and anti-angiogenic factors, such as angiopoietin-1 (Ang-1) and pigment epithelium derived factor (PEDF), and vessels begin to regress through apoptosis in order to maintain a functional vascular network (182).

Adipose tissue has the highest angiogenic capacity and its remodeling in response to body weight changes is dependent upon angiogenesis. During weight gain, adipose tissue can overexpand manyfold. Adequate blood flow to this tissue is thus critical for growth and proper function; however, blood flow is insufficient during rapid adipose tissue expansion, resulting in tissue hypoxia. This hypoxic stress stimulates the production of VEGF, promoting inflammation and insulin resistance. Overexpression of VEGF results in enhanced vascularisation, decreased inflammation, and restored insulin resistance in adipose tissue (183). VEGF and other proangiogenic factors participate in angiogenesis by inducing endothelial cells to release NO (184).

1.5.1 Nitric oxide and new blood vessel formation

NO is produced by NOSs and is considered to be a critical mediator of the angiogenic response of endothelial cells. Within the NOS family, eNOS, nNOS, and iNOS are interchangeable; however, eNOS is the main source of NO and is selectively activated in response to VEGF. There is evidence in murine models that dietary supplementation with L-arginine, the eNOS substrate, increases NO production and improves vascularisation (185). In eNOS-deficient mice, the angiogenic response to hindlimb ischemia is impaired and cannot be reversed by VEGF, implying that eNOS acts downstream of VEGF (186). NO produced by eNOS has been shown to increase expression of HIF-1α, which can in turn induce the synthesis and release of VEGF via

a positive feedback mechanism (187). During angiogenesis, NO also acts as an endothelial survival factor, inhibiting apoptosis and promoting endothelial cell proliferation and migration (188). Furthermore, increased flow from NO-induced vasodilation promotes angiogenesis, which has been observed via increasing endothelial cell proliferation (189).

1.5.2 ROS and angiogenesis

In physiological concentrations, superoxide anion and hydrogen peroxide act as second messengers and influence cell signalling, proliferation, survival, migration, and angiogenesis. Several cytokines and growth factors are involved in the production of ROS and angiogenesis, including VEGF, protein tyrosine phosphatases (PTPs), FGFs, and TNFα. VEGF is the major contributor to angiogenesis; VEGF-A has the most angiogenic potential and can bind to three receptors, including VEGFR1, 2, and 3, of which VEGFR2 is the best characterised. The binding of VEGF-A to VEGFR2 promotes the production of ROS in endothelial cells via NOX enzymes (190). The downstream effectors of VEGFR2 include NOX4, p66Shc-Rac1, and PKC, all of which are capable of activating NOX1/2. The superoxide anion produced by NOX2 and the hydrogen peroxide produced by NOX4 have been shown to increase the activity of cellular sarcoma (c-Src) and MAPKs, which promote endothelial cell proliferation, survival, and migration (191-193). Hydrogen peroxide derived from NOX4 can induce and activate eNOS, and NOX4-deficient mice exhibit reduced angiogenesis, eNOS, and NO production (99). Hydrogen peroxide also induces reversible S-glutathionylation of the sarcoplasmic-endoplasmic reticulum calcium ATPase (SERCA), resulting in Ca^{2+} influx and endothelial cell migration (194). Furthermore, extracellular hydrogen peroxide produced by SOD3 was able to sustain VEGF signalling through oxidative inactivation of the membrane-bound phosphatases PTP1B and DEP1, which encourage angiogenesis (195).

Prolonged exposure to pathologically high levels of ROS is detrimental to vascular tissues. Among the types of ROS, superoxide anion appears to be more harmful than hydrogen peroxide. Superoxide anion can reduce the bioavailability of NO by forming peroxynitrite, and both superoxide anion and peroxynitrite have a high oxidative potential. It has been proposed that high concentrations of superoxide anion

and hydrogen peroxide inhibit angiogenesis, whereas low concentrations of superoxide anion and hydrogen peroxide stimulate angiogenesis (196, 197).

1.5.3 Angiogenesis in heart failure and diabetes

Insulin resistance occurs in both heart failure and diabetes, and this metabolic abnormality results in endothelial dysfunction and decreased angiogenesis. Insulin resistance has been shown to result in a significant reduce in endothelial NO bioavailability when insulin signalling is impaired. NO is a free radical gas produced by the NOS family that plays a role in physiological responses, such as vasodilation, anticoagulation, vascular permeability, and angiogenesis. As a result, angiogenesis tends to be reduced in HF and diabetes.

1.5.3.1 Angiogenesis in heart failure

In HFrEF, decreased shear stress affects endothelial function and angiogenesis by decreasing eNOS, decreasing endothelial repair, increasing ROS production, increasing leucocyte adhesion, and increasing inflammation (198). Reduced eNOS activity in HF results in decreased NO production, which promotes endothelial cell apoptosis while inhibiting angiogenesis (199). Reduced NO in HF typically coexists with increased superoxide anion synthesis, which is capable of oxidising BH4 to BH2 and biopterin, causing NOS to become uncoupled and produce superoxide instead of NO (200). The interaction of NO with superoxide anion in the form of peroxynitrite may have an additional effect on NO generation.

1.5.3.2 Angiogenesis in diabetes

Endothelial cells exposed to long-term elevated blood glucose become dysfunctional, resulting in loss of integrity and increased susceptibility to apoptosis, detachment, and circulation into the blood stream, ultimately becoming the source of micro- and macrovascular complications. Numerous complications of diabetes are characterised by vasculopathy related to abnormalities in angiogenesis, including diabetic retinopathy, diabetic nephropathy, impaired wound healing, and impaired formation of coronary collaterals.

Diabetes is unique. As a systemic disease, whether the chronic hyperglycaemia and the other dyscrasias, enhance or inhibit angiogenesis is determined by the balance of neurohumoral factors and tissue or organ involved. Excessive angiogenesis in diabetes occurs due to upregulation of VEGF, FGF, integrins, fibronectin and fibronectin fragments, non-enzymatic glycosylation, and activation of the polyol metabolic pathway. In diabetic retinopathy, pericyte coverage in the retinal capillary network is decreased, resulting in vascular oedema and leakage. Furthermore, hypoxia caused by capillary damage leads to increase expression of HIF-1 transcription factor and subsequent upregulation of VEGF-A. In diabetic nephropathy, expression of VEGF-A and its receptor VEGFR-2 are increased in the early stages, whereas abnormal receptors are observed during disease progression, resulting in increased circulating of VEGF-A but decreased VEGF-A sensing (201).

In contrast to diabetic retinopathy and nephropathy, angiogenesis is decreased in diabetic patients during wound healing and the formation of coronary collaterals. The deficient angiogenesis is caused by various mechanisms, including a decrease in proangiogenic factors, an increase in anti-angiogenic factors (202), insufficient extracellular matrix/basement membrane (ECM/BM) degradation, cytokine imbalance, signal transduction abnormalities (203), and a decrease in the population of endothelial progenitor cells (EPCs) from the bone marrow (204). In wound healing, it has been established that macrophages are the major source of VEGF and other proangiogenic factors. In diabetic wounds, impaired macrophage function switches them from a proinflammatory to pro-reparative phenotype, resulting in decreased VEGF-A and angiogenic function (205, 206).

As discussed in detail above, the present thesis deals with the role of insulin signalling and functional characterisation in human microvascular endothelial cells, with a particular emphasis on patients with HF and type 2 DM. A comprehensive understanding of insulin signalling may facilitate the development of more effective medications, improving the symptoms and survival rate of these patients.

Chapter 2: **Objectives**

2 Objectives

The overall aim of my Ph.D. research is:

1. Isolation and characterisation of human skeletal muscle and adipose tissue microvascular endothelial cells (isolation, confirmation of identity/purity using a multitude of techniques).
2. To understand insulin signalling in heart failure and diabetic patient endothelial cells (simple qualification and comparative analysis of expression and signalling).

Hypotheses

1. Impaired insulin signaling in microvascular endothelial cells of patients with heart failure and diabetes leads to decreased functional characteristics, such as increased ROS production and decreased new capillary blood vessels formation.
2. Insulin treatment may improve insulin signaling in microvascular endothelial cells, leading to improved functional characteristics such as decreased production of ROS.

Chapter 3: **Materials**

3 Materials

3.1 Endothelial cell isolation

MACS Tissue Storage Solution	Miltenyi Biotec
Hank's Balanced Salt Solution (H9269)	Sigma-Aldrich
Collagenase/Dispase (11097113001)	Roche
Scalpel blades size 22	Swann-Morton
Venflon Pro Safety IV Cannula with Injection Port 14G	BD Biosciences
Dulbeccos's Phosphate Buffered Saline (PBS)	Sigma-Aldrich
Bovine serum albumin 7.5%	Sigma-Aldrich
MACSmix™ tube rotator	Miltenyi Biotec
Dead Cell Removal Kit	Miltenyi Biotec
MidiMACS™ Separator	Miltenyi Biotec
MiniMACS™ Separator	Miltenyi Biotec
MACS LS cell separation columns	Miltenyi Biotec
MACS MS cell separation columns	Miltenyi Biotec
MACS 70 μm cell strainers and filters	Miltenyi Biotec
MACS 30 μm cell strainers and filters	Miltenyi Biotec
Red Blood Cell Lysis Solution (10x) – Removal reagents	Miltenyi Biotec
CD31 microbead, human #130-091-935	Miltenyi Biotec
EC growth medium MV + supplements	PromoCell
Antibiotic/antimycotic supplement	Invitrogen
Corning® Costar® cell culture plates 24 well, flat bottom	Sigma-Aldrich

3.2 Cell culture

Dulbeccos's Phosphate Buffered Saline (PBS)	Sigma-Aldrich
Trypsin-EDTA 0.25%	Sigma-Aldrich
EC growth medium MV + supplements	PromoCell
Antibiotic/antimycotic supplement	Invitrogen
Corning® Costar® cell culture plates 6 well, flat bottom	Sigma-Aldrich

ReagentPack Subculture Reagent, 100 ml	Lonza
EBM™-2 Endothelial Cell Growth Basal Medium-2, 500 mL	Lonza
Olympus Fluorescence Microscope	Olympus

3.3 Fluorescence-based method for calcium measurement

Fura-2AM (INV F1221)	Invitrogen
Pluronic acid (PA)	Sigma-Aldrich
Dimethyl sulfoxide (DMSO)	Sigma-Aldrich
Vascular endothelial growth factor (VEGF)	Sigma-Aldrich
Sodium Chloride (NaCl)	Sigma-Aldrich
Potassium Chloride (KCl)	Sigma-Aldrich
Calcium Chloride (CaCl2)	Sigma-Aldrich
Magnesium Chloride (MgCl2)	Sigma-Aldrich
Glucose	Sigma-Aldrich
HEPES sodium salt	Sigma-Aldrich
Sodium hydroxide (NaOH)	Sigma-Aldrich
FLEX Station 3 Multi-mode microplate reader	Molecular Devices
Costar® clear plates 96 well	Sigma-Aldrich
Costar® 96 Ubtm clear 0.3 ml	Sigma-Aldrich
Pipette Tips 96 clear	Molecular Devices

3.4 Flow cytometry

Dulbeccos's Phosphate Buffered Saline (PBS)	Sigma-Aldrich
Bovine serum albumin 7.5%	Sigma-Aldrich
Trypsin-EDTA 0.25%	Sigma-Aldrich
EC growth medium MV + supplements	PromoCell
Foetal bovine serum	Biosera
Antibiotic/antimycotic supplement	Invitrogen
CD45-FITC, human #130-113-679	Miltenyi Biotec
CD144-PE, human #130-118-495	Miltenyi Biotec
CD31-PerCP-Vio700, human #130-110-811	Miltenyi Biotec
Cytoflex 4-laser system	Life Sciences

3.5 Real time quantitative PCR

Dulbeccos's Phosphate Buffered Saline (PBS)	Sigma-Aldrich
TRIzol (Tri reagent)	Sigma-Aldrich
1-Bromo-3-chloropropane	Sigma-Aldrich
Isopropyl alcohol	Sigma-Aldrich
Ethyl alcohol	Sigma-Aldrich
DNA/RNA free water	BD Biosciences
Precision DNase kit	Primer design
Precision nanoScript™ 2 reverse transcription kit	Primer design
2X iTaq SYBR Green mastermix	Bio-RAD
NanoDrop ND1000 Spectrophotometer	Thermo Scientific
ND-1000 v3.1 software	Thermo Scientific
LightCycler 480 Real-Time PCR System	Roche
LightCycler Multiwell Plate 384, clear	Roche

3.6 Western blotting

Dulbeccos's Phosphate Buffered Saline (PBS)	Sigma-Aldrich
Bovine serum albumin 7.5%	Sigma-Aldrich
Trypsin-EDTA 0.25%	Sigma-Aldrich
EC growth medium MV + supplements	PromoCell
Foetal bovine serum	Biosera
Antibiotic/antimycotic supplement	Invitrogen
Insulin	Sigma-Aldrich
Cell extraction buffer (CEB)	Thermo Scientific
Cell scraper	Krackeler Scientific
Pierce® BCA protein assay kit	Thermo Scientific
96 well clear microplate	Greiner Bio-One
PowerWave HT microplate spectrophotometer	BioTek
XCell SureLock™ Mini-cell	Invitrogen
NuPAGE™ LDS sample buffer	Thermo Scientific

NuPAGE™ sample reducing agent	Thermo Scientific
NuPAGE™ MES SDS Running Buffer (20x)	Thermo Scientific
NuPAGE™ 4-12% Bis-Tris Protein Gels, 1.5 mm, 15-well	Thermo Scientific
NuPAGE™ 4-12% Bis-Tris Gel (1.5 mm x 10 well)	Thermo Scientific
Filter paper	Merck Millipore
Transfer membrane Immobilon®-P PVDF	Merck Millipore
Tris base	Sigma-Aldrich
Glycine	Sigma-Aldrich
20% Sodium dodecyl sulphate (SDS)	Sigma-Aldrich
Methanol	Sigma-Aldrich
Scalpel blades size 22	Swann-Morton
Magnetic stirrer	Thermo Scientific
Precision Plus Protein™ WesternC™ Blotting Standards	Bio-RAD
Precision Protein™ StrepTactin-AP Conjugate	Bio-RAD
Phosphate buffered saline tablets	Sigma-Aldrich
Tween®-20	Sigma-Aldrich
Skim milk	Sigma-Aldrich
Restore™ PLUS Western Blot Stripping Buffer	Thermo Scientific
Immobilon Western Chemiluminescent HRP Substrate	Merck Millipore
Syngene G-box imaging system	Syngene
Purified mouse Anti-eNOS/NOS Type III #610297	BD Biosciences
Phospho-eNOS (S1177) Rabbit Antibody #9571	Cell signaling technology
Phospho-Akt (Ser473) (D9E) XP® Rabbit mAb #4060	Cell signaling technology
Akt Rabbit Ab #9272	Cell signaling technology
Phospho-IR (Tyr1334) Polyclonal Antibody #44-809G	Invitrogen
Insulin Receptor β (4B8) Rabbit mAb #3025	Cell signaling technology
IGF-I Receptor β (D23H3) XP Rabbit mAb #9750	Cell signaling technology
IGF-IRβ Antibody (3G5C1) mouse mAb #sc-81167	Santa Cruz Biotechnology
Anti-NOX2/gp91phox antibody [EPR6991] #ab129068	Abcam
Anti-NADPH oxidase 4 antibody [UOTR1B492] #ab230322	Abcam
p47phox Polyclonal Antibody #PA1-9073	Invitrogen
Phospho-p47phox (Ser370) Polyclonal Antibody #PA5-36863	Invitrogen
CD38 Antibody (T16) #sc-51726	Santa Cruz Biotechnology

Polyclonal Goat Anti-Mouse Ig/HRP #P0447	DAKO
Polyclonal Goat Anti-Rabbit Ig/HRP #P0448	DAKO

3.7 Lucigenin enhanced chemiluminescent

Trypan blue	Sigma-Aldrich
Neubauer Counting Chamber	Hawksley
Microscope slide coverslip 22 mm x 22 mm	SLS
Sodium Chloride (NaCl)	Sigma-Aldrich
Potassium Chloride (KCl)	Sigma-Aldrich
Calcium Chloride (CaCl2)	Sigma-Aldrich
Magnesium Chloride (MgCl2)	Sigma-Aldrich
Glucose	Sigma-Aldrich
HEPES sodium salt	Sigma-Aldrich
Sodium hydroxide (NaOH)	Sigma-Aldrich
Lucigenin	Sigma-Aldrich
NADPH tetrasodium salt	Santa Cruz
Tiron	Sigma-Aldrich
GP91-ds tat RP21052	Genscript
GP91-ds tat scrambled peptide RP21051	Genscript
CLARIOstar® Plus Luminescence Plate Reader	BMG Labtech
Corning 96-Well Solid White Polystyrene Microplates	Thermo Scientific

3.8 Angiogenesis assay

Scalpel blades size 22	Swann-Morton
Sterile Syringe Filter	Sigma-Aldrich
Petri dishes, polystyrene 100 mm x 20 mm	Sigma-Aldrich
Dulbeccos's Phosphate Buffered Saline (PBS)	Sigma-Aldrich
Aprotinin from bovine lung (lyophilized powder, 3-8 TIU/mg solid)	Sigma-Aldrich
Fibrinogen type 1	Sigma-Aldrich
Thrombin from bovine plasma	Sigma-Aldrich
Corning® Costar® cell culture plates 24 well, flat bottom	Sigma-Aldrich
EC growth medium MV + supplements	PromoCell

Antibiotic/antimycotic supplement	Invitrogen
Olympus Fluorescence Microscope	Olympus
MACS Tissue Storage Solution	Miltenyi Biotec

Chapter 4: **Methods**

4 Methods

Several methods exist for studying the insulin signalling pathway and functional characterisation of human microvascular endothelial cells. All the experiments in this study were chosen for their reliability and validity. Ethical approval was obtained for work on patient tissue (11/YH/0291). The study recruited participants from Leeds General Infirmary and patients were allocated by the presence or absence of type 2 DM, HFrEF, neither or both. Classify these conditions based on medical history, blood test results, and echocardiography. All participants were over the age of 18 years, provided informed consent, and read the information sheet prior to tissue sampling. The participant or the participant's family was informed of any anticipated risks and benefits.

4.1 Endothelial cell isolation

4.1.1 Tissue harvesting

Approximately 250–500 mg of fresh human tissue (skeletal muscle from the pectoralis major and fat tissue from the subcutaneous adipose tissue of the pectoral region) was obtained from all eligible participants during the implantation of cardiac implantable electronic devices (CIEDs). Local anaesthesia was provided prior to a small incision by infiltrating the skin and subcutaneous tissue around the implant site with 1–2% lidocaine. A 1.5- to 2-inch incision and a subcutaneous pocket was created before a small tissue biopsy. The tissues were immediately placed in ice-cold Hank’s balanced salt solution (HBSS) or tissue-storage solution (Miltenyi Biotec) and transported to the laboratory. Tissues were stored overnight in a 1.5 ml microcentrifuge tube containing 1 ml MACS tissue storage solution prior to endothelial cell isolation the next morning.

4.1.2 ATEC isolation

Tissues were minced into 1 mm^2 pieces using a double scalpel blade technique and digested for 60 minutes at 37 °C in a MacsMix rotator with 1 mg/ml collagenase/dispase in HBSS containing 1 mM $CaCl_2$ and 1 mM $MgCl_2$ (Figure 10). Post-incubation, the digestion process was stopped by adding 10 ml of endothelial cell growth medium MV. The digested mix was triturated and passed through a 70-μm cell sieve. The suspension was collected and centrifuged to aspirate the supernatant, followed by removal of dead cells and red blood cells (RBCs) using a Dead Cell Removal Kit (Miltenyi Biotec) and RBC lysis buffer, respectively. To remove dead cells, the cell pellet was resuspended in 200 μl of Dead Cell Removal microbeads and incubated at room temperature for 15 minutes. After incubation, the cell suspension was passed through an LS cell separation column attached to a MidiMACS™ Separator and washed with 1x binding buffer. The cell suspension was collected and centrifuged to aspirate the supernatant. To lyse the RBCs, the cell pellet was resuspended in 400 μl of 0.5% PBS-BSA (phosphate-buffered saline–bovine serum albumin) and 3.6 ml of 1x RBC lysis solution was added and incubated at room temperature for 10 minutes. The cells were then pelleted and washed with 0.5% PBS-BSA buffer and incubated with CD31-coated magnetic beads (Miltenyi Biotec) for 20 minutes at 4 °C. After passing the mixture through an MS cell separation column attached to a MiniMACS ™ Separator, the bound CD31-positive cells were eluted, pelleted, and resuspended in the endothelial growth medium MV. The isolated cells were plated into two wells of a gelatine-coated 24-well plate (passage 0 or P0).

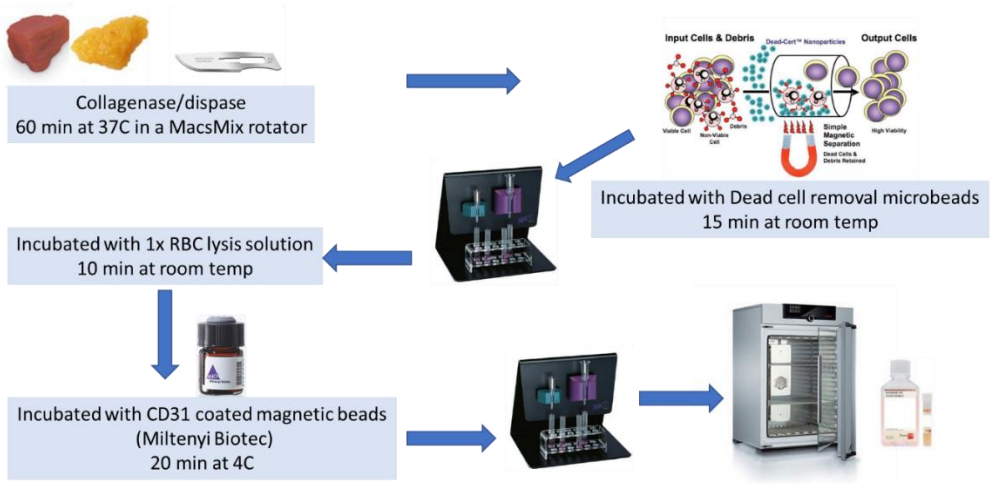

Figure 10: Schematic illustrating the process of isolating endothelial cells from skeletal muscle and adipose tissue.

4.2 Cell culture

The isolated cells were incubated at 37°C in the incubator and the endothelial growth media MV was changed every three days (the endothelial growth media MV already included antibiotics and supplement). Cells in each well of a 24-well plate were plated onto a single well of a 6-well plate once they reached 80% confluency, which typically took approximately 2–4 weeks (passage 1 or P1). Normally, it took approximately 1 week for the P1 cells to reach confluence and be ready for passage onto a six-well plate again (P2). Experiments were performed on P2–P4-generation cells. The endothelial cells could maintain their normal morphology until P5.

4.3 Identity confirmation

4.3.1 Fluorescence-based method for calcium measurement

The purpose of this method was to demonstrate the intracellular calcium flux of the endothelial cells in response to stimulation with VEGF. Cell plates and compound plates were prepared before starting calcium measurement at the FLEX station. For the cell plate, endothelial cells were cultured in 96-well plates (200 µl/well). These cells were transported to the darkroom, then incubated for 45 minutes at 37 °C with 50 µl of a mixture of standard bath solution (SBS: NaCl 135 mM, KCl 5 mM, MgCl2 1.2 mM, glucose 8 mM, HEPES 10 mM, and CaCl2 1.5 mM; osmolarity 290 mOsm, pH 7.2

adjusted with 4 M NaOH), Fura2 (aminopolycarboxylic acid), and pluronic acid (PA) in a ratio of 1000:2.5:1 μl, respectively. During the incubation period, the cell plate was covered in aluminium foil. After 45 minutes, cells were washed twice with 200 µl SBS added to each well. The cells were then incubated in 100 µl fresh SBS and left for 15 minutes at room temperature (the cell plate was again covered in aluminium foil). For the compound plate, VEGF was prepared at a concentration of 50 ng/ml to assess the calcium influx response. The FLEX station was set up, as shown below.

Setup:

a. Wavelengths
    i. Excitation 340/380 nm
    ii. Emission 510 nm
    iii. Emission cut-off 495 nm
b. Sensitivity
    i. Readings 6
    ii. PMT Medium
c. Timing
    i. Time 360 s, Reads: 73
    ii. Interval 5 s, Min int: 3.09 s, Min run time: 88 s
d. Assay plate type 96-well Costar clear
e. Wells to read Columns 1–4 (read area A1–F4)
f. Compound source Costar 96 Ubtm clear 0.3 ml
g. Compound transfer T1: 80, 1, 100@60
    i. Transfers 1
    ii. Pipettor height 80 µl
    iii. Sample volume 100 µl
    iv. Dispense speed (Rate) 1 (~16 µl/s)

v. Time Point 60 s

vi. Transfer times 20 s

The FLEX station added compounds and read the response column-by-column, so that if the experiment required four columns to be read at a time of 6 minutes each, the assay would be completed in 24 minutes.

4.3.2 Flow cytometry

Flow cytometry was used to determine the purity of the endothelial cells. To begin, cells were visually inspected to ensure they were healthy and morphologically representative. Cells in the confluent well were washed twice with PBS and then detached using a warm trypsin/EDTA solution. Then cells were placed in the incubator for 2 minutes and detachment was verified using a tissue culture microscope. Once detached, the trypsin was neutralised with endothelial cell growth media MV containing FCS (foetal calf serum). Then cell suspension was aspirated and dispensed into a 15 ml Falcon tube. The cell suspension was centrifuged at 400 g for 8 minutes and the supernatant was discarded without disturbing the pellet. The cell pellet was resuspended in 1 ml MACS buffer and 500 µl was transferred to two Eppendorf tubes and labelled as either ‘unstained control’ or ‘stained sample’. Then, 500 µl MACS buffer was added to each Eppendorf tube and centrifuged at 400 g for 8 minutes (MACS buffer was prepared using 500 mL PBS, 2.5 g BSA, and 2 mM EDTA [292 mg]). A staining cocktail was prepared in the manner described in Table 1.

Table 1: Staining cocktail with the proportion of fluorochrome-labelled antibodies.

Sample number	**CD45-FITC (µl)**	**CD144-PE (µl)**	**CD31-PerCP-Vio700 (µl)**	**MACS buffer (µl)**
1	2	10	2	100
2	4	20	4	200
3	6	30	6	300
4	8	40	8	400
5	10	50	10	500

FITC = fluorescein isothiocyanate, PE = phycoerythrin, PerCP = peridinin chlorophyll protein

The supernatant was discarded and the cells resuspended in 100 µl MACS buffer for the unstained control and 100 µl staining cocktail for the stained sample. The cells were vortexed and placed in the refrigerator for 10 minutes, and 1 ml MACS buffer was then added to each tube. The cells were centrifuged at 400 g for 8 minutes and the supernatant was discarded. Then, cells were resuspended in 500 µl MACS buffer and the Eppendorf tubes were stored in a covered icebox until analysis. Flow cytometry was performed using the template on the Cytoflex 4-laser system. Data were recorded for 10,000 cells per sample in singlet gate (P2), and the tube was labelled with the unique patient ID, tissue type, 'unstained' or 'stained', and date. P1 was inspected to ensure that it surrounded a major cell cluster and that most of these cells fell within the P2 singlet gate. The unstained control was inspected to ensure that it had minimal CD45- CD144+ CD31+ cells as a percentage of singlets. The CD45- CD144+ CD31+ cells in the stained sample were recorded as the percentage of singlets.

4.4 Real-time quantitative PCR

4.4.1 RNA isolation

Cells (P2) from one well of the six-well plate were used to isolate RNA. The endothelial cell growth medium MV was removed and washed with 2 ml PBS. Then, 1 ml Tri-Reagent was added to each well and left at room temperature for approximately 90 seconds (caution is warranted in this step due to phenol and chloroform in Tri-Reagent that may lead to serious chemical burns and permanent scarring). The sample was then transferred to a 1.5-ml Eppendorf tube. At this stage, the cells could be stored at -80 °C in a freezer, if necessary. Each sample of the cells in the Tri-Reagent was mixed with 100 µl of 1-bromo-3-chloropropane. The sample was vortexed and allowed to stand at room temperature for 15 minutes before centrifuging at 13,000 rpm for 15 minutes at 4 °C for the phase separation process (Figure 11). An upper aqueous phase (clear layer containing nucleic acids) was transferred to another Eppendorf tube and an equal volume of isopropanol was added for RNA precipitation. The sample was vortexed and left at room temperature for 10 minutes, then centrifuged at 13,000 rpm for 20 minutes at 4 °C. After centrifugation, the supernatant was removed without disturbing the pellet. Then, 1 ml 70% ethanol was added to the

sample, vortexed, and centrifuged at 13,000 rpm for 2 minutes at 4 °C. After centrifugation, the 70% ethanol was removed without disturbing the pellet. Leaving the pellet on ice with the lid open for ~5 minutes allowed any remaining ethanol to evaporate before resuspending the pellet in 20 µl DNA/RNA-free water. The sample was stored at -80 °C in the freezer before DNAase treatment.

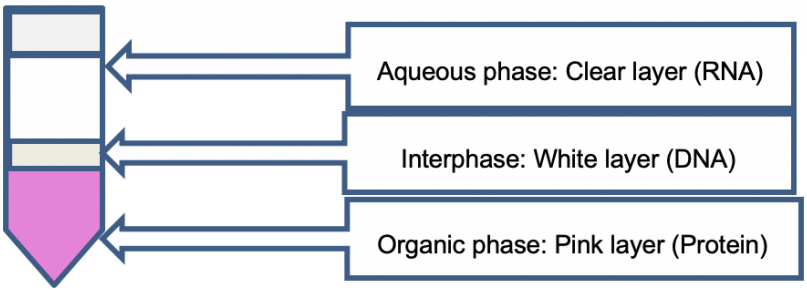

Figure 11: Phase separation process

4.4.2 DNase treatment

The Precision DNase kit from Primer Design was used to purify RNA by removing genomic DNA (gDNA). We prepared the Mastermix and added 2 µl of 10x Precision DNase reaction buffer and 0.2 µl of Precision DNase enzyme to each sample. For DNase treatment, we vortexed and wrapped the samples in cling film to prevent contamination before placing them in an incubator at 30 °C for 10 minutes. We then incubated the samples at 55 °C for 5 minutes for DNase inactivation. The samples were centrifuged at 10,000 rpm for 2 minutes and the supernatant RNA was transferred to another Eppendorf tube. The sample was either stored at -80 °C in a freezer or used in the next step of RNA measurement.

4.4.3 RNA measurement

RNA was quantified from 1.6 µl of each sample and analysed using a NanoDrop ND-1000 spectrophotometer (Thermo Scientific, Loughborough, UK), using the manufacturer's instructions to determine the concentration and purity of RNA: 260/280 (the purity should be in the range of 1.9–2.1, with a lower ratio indicating protein or phenol contamination) and 260/230 (the purity should be in the range of 2.0–2.2, with a lower ratio indicating protein, phenol, or carbohydrate contamination).

4.4.4 Reverse transcription of RNA

The Precision nanoScriptTM 2 reverse transcription kit (Primer design) was used to reverse transcribe 1,000 ng RNA into cDNA. For the annealing step, 1 μl of random nonamer primer was added to the 1,000-ng sample, according to the manufacturer's guidelines. The sample was then vortexed and centrifuged in pulse mode. We heated the sample at 65 °C for 5 minutes, then immediately cooled it in an ice water bath. For the extension step, we prepared a mixture according to the protocol outlined in Table 2, adding 10 μl of this mixture to each of the samples on ice. We vortexed the sample briefly, followed by a pulse centrifugation, and incubated it at 25 °C for 5 minutes. We then heated the sample at 42 °C for 20 minutes and the reaction was heat inactivated at 75 °C for 10 minutes. The cDNA sample was stored at -20 °C in a freezer or used in the next step of real-time PCR.

Table 2: Components of the mixture for one reaction of the extension step.

Components for one reaction	**Volume (μl)**
nanoScript2 4X Buffer (BLACK)	5.0
dNTP mix 10mM (ORANGE)	1.0
RNAse/DNAse free water (WHITE)	3.0
nanoScript2 enzyme (WHITE)*	1.0
Final volume	**10**

4.4.5 Real-time quantitative PCR

The cDNA samples were diluted with de-ionised water to a final cDNA concentration of 10 ng/μl. The components of one reaction (10 μl) of 384-well plate include the cDNA sample, 2x iTaq SYBR Green mastermix, and primer (specific to the gene), and are outlined in Table 3. The sequences for each primer are listed in Table 4. We used working stocks of forward and reverse primers at a concentration of 5 μM. To ensure accuracy, the real-time quantitative PCR was performed in duplicate with each sample on a LightCycler 480 Real-Time PCR System. The difference in Ct value

between the target gene and the housekeeping gene GAPDH (ΔCt) was then used to calculate the relative quantity (RQ) using the following formula:

$$RQ = 2^{-\Delta Ct} \times 100$$

GAPDH is commonly used as a housekeeping gene because it is a well-known, highly conserved and ubiquitous protein involved in glycolysis. Moreover, GAPDH is expressed in many types of cells and tissues under a wide range of physiological conditions, and its expression level is relatively stable under different treatments and experimental conditions.

Table 3: Components of the mixture for real-time quantitative PCR.

Components for one reaction	**Volume (µl)**
2x iTaq SYBR Green mastermix	5.0
Forward primer (specific to the gene)	0.5
Reverse primer (specific to the gene)	0.5
RNA/DNA free water	2.0
cDNA sample	2.0
Final volume	**10**

Table 4: Sequence of each target gene.

Target gene	Forward primer	Reverse primer
hGAPDH	5'-GGA AGG ACT CAT GAC CAC AGT-3'	5'-GGA TGA TGT TCT GGA GAG CCC-3'
hIR	5'-GTC ATC AAC GGG CAG TTT G-3'	5'-GGT GCA GCC GTG TGA CTT AC-3'
hIGF1R	5'-CCA GGC CAA AAC AGG AAC TGA A-3'	5'-TCT CTT TCT ATG GAA GAC GTA CAG CAT-3'
hNOS	5'-CTC GAG CAC CCC ACG CT-3'	5'-AGC GGT GAG GGT CAC ACA G-3'
hAkt1	5'-AGC GAC GTG GCT ATT GTG AAG-3'	5'-GCC ATC ATT CTT GAG GAG GAA GT-3'
hAkt2	5'-ACC ACA GTC ATC GAG AGG ACC-3'	5'-GGA GCC ACA CTT GTA GTC CA-3'
hAkt3	5'-TGT GGA TTT ACC TTA TCC CCT CA-3'	5'-GTT TGG CTT TGG TCG TTC TGT-3'
hNOX2	5'-CTG GAC AGG AAT CTC ACC TTT CAT-3'	5'-AAT TTA TCT ACA CGT TAC CAC ACT TAG-3'
hNOX4	5'-CAC CAG ATG TTG GGG CTA GG-3'	5'-TGA TCC TCG GAG GTA AGC CA-3'
hSOD1	5'-CTA GCG AGT TAT GGC GAC GA-3'	5'-TGG TCC ATT ACT TTC CTT CTG CT-3'
hSOD2	5'-GCT CCC CGC GCT TTC TTA-3'	5'-GCT GGT GCC GCA CAC T-3'
hSOD3	5'-AGG CCT CCA TTT GTA CCG AA-3'	5'-AGT CTC AGG GCT TAT GGG GT-3'
hCat	5'-TTG CCA CAG GAA AGT ACC CC-3'	5'-TGA GGC CAA ACC TTG GTG AG-3'

Real-time PCR investigations of the NOX2 and SOD3 genes were difficult despite attempts to use several NOX2 primer sequences, as shown in Table 5.

Table 5: Sequences of NOX2 primers.

Target gene	Forward primer	Reverse primer
hNOX2 a	5'-TCA TCA CCA AGG TGG TCA CTC-3'	5'-ACA CCT TTG GGC ACT TGA CA-3'
hNOX2 b	5'-CTG TGA ATG AGG GGC TCT CC-3'	5'-CCA GTG CTG ACC CAA GAA GTT-3'
hNOX2 c	5'-CCT AAG ATA GCG GTT GAT GG-3'	5'-GAC TTG AGA ATG GAT GCG AA-3'
hNOX2 d	5'-GTC ACA CCC TTC GCA TCC ATT CTC AAG TCA GT-3'	5'-CTG AGA CTC ATC CCA GCC AGT GAG GTA G-3'
hNOX2 e	5'-ACC GGG TTT ATG ATA TTC CAC CT-3'	5'-GAT TTC GAC AGA CTG GCA AGA-3'
hNOX2 f	5'-AAC GAA TTG TAC GTG GGC AGA-3'	5'-GAG GGT TTC CAG CAA ACT GAG-3'
hNOX2 g	5'-AAG ATC TAC TTC TAC TGG CTG-3'	5'-AGA TGT TGT AGC TGA GGA AG-3'
hNOX2 h	5'-ATA AAG AAC CCT GAA GGA GG-3'	5'-AAT TAA TAT GAG GCA CAG CG-3'
hNOX2 i	5'-CTT CTT TAG TAT CCA TAT CCG C-3'	5'-TAT CTT AGG TAG TTT CCA CGC-3'
hNOX2 j	5'-CTG GAC AGG AAT CTC ACC TTT CAT-3'	5'-AAT TTA TCT ACA CGT TAC CAC ACT TAG-3'
hNOX2 KO	5'-ACT TCT TGG GTC AGC ACT GG-3'	5'-ATT CCT GTC CAG TTG TCT TCG-3'

4.5 Insulin signalling by Western blot technique

4.5.1 Preparing endothelial cell samples

The Western blot technique was used to investigate insulin signalling in the endothelial cells. Cell samples were grown to confluence in a six-well plate, with one well for basal, one for control, and one for each insulin concentration of 25, 50, 100, and 150 nM. We changed the media 1 day prior to harvesting the samples. The control and insulin wells used 2 ml of serum starvation media (SSM; prepare using 50 ml of endothelial growth media MV and 0.2% foetal bovine serum), and the basal well used 2 ml of endothelial growth media MV containing antibiotics and supplement. In the morning, 2 µl of 25-, 50-, and 100-µM stock insulin were added to the 25, 50, 100 nM insulin wells, respectively, and 3 µl of 100-µM stock insulin were added to the 150 nM insulin well. The samples were mixed well and incubated at 37 °C for 10 minutes. After removing the media, we added 2 ml of cold PBS and mixed thoroughly to eliminate the PBS. We filled each well with 100 µl of cell extraction buffer (with protease inhibitor) and collected the cell sample using a cell scraper. The samples were stored at -80 °C in the freezer before protein measurement.

4.5.2 Protein measurement

Harvested samples were kept on ice for 30 minutes, with occasional vortexing, then centrifuged at 13,000 rpm at 4 °C for 15 minutes. We then transferred the supernatant to new Eppendorf tubes and stored them on ice. The protein concentrations of the samples were determined using a bicinchoninic acid (BCA) protein assay kit and spectrophotometer. The samples were calculated to the volume required for the experiment, which was 40 µg of protein.

4.5.3 Gel electrophoresis

Prior to electrophoresis, protein samples were boiled to denature the proteins for 5 minutes at 95 °C. We prepared a tank and NuPAGE™ 4–12% Bis-Tris gel, then added 25 ml MES buffer and diluted to 500 ml with distilled water. We added 5 µl of Precision Plus Protein™ WesternC™ Blotting Standards and 40 µg of each sample

into separate wells. We ran the gel with a power pack machine at 180 V for one gel or 160 V for two gels for ~90 minutes. We then turned off the power, pulled out the electrodes, and carefully removed the gels.

4.5.4 Membrane transfer

Prior to transferring to the PVDF membrane, we prepared 10x transfer buffers (58.15 g of Tris base, 29.28 g of glycine, and 18.5 ml of 20% SDS topped up with 1,000 ml water) and 1x transfer buffers (100 ml of 10x transfer buffer, 200 ml of methanol, and 700 ml of distilled water). We sequentially soaked the PVDF membrane in 100% methanol, distilled water, and 1x transfer buffer. We then prepared a transfer stack on the black side of a cassette, as illustrated in Figure 12. We placed the cassette, magnetic stirrer, and 1x transfer buffer in the tank. We then ran the stirrer and power pack machine at 100 V for 1 hour.

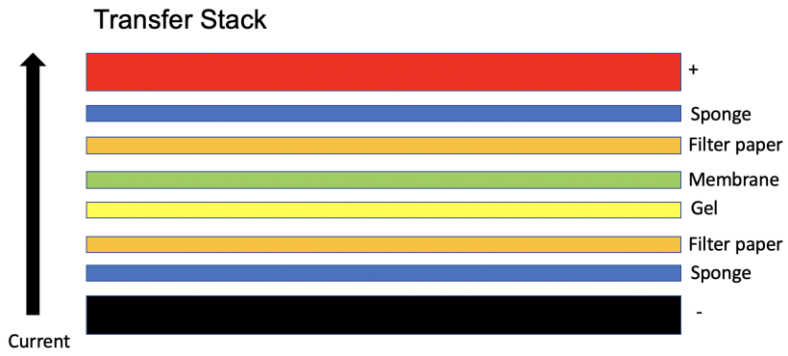

Figure 12: Stack preparation for the protein from SDS-PAGE gel transfer to PVDF membrane.

4.5.5 Immunostaining

After the protein transfer, the membrane was detached from the transfer sandwich. Then, a clean scalpel was used to cut the membrane at the levels corresponding to 50 kDa and 75 kDa from the reference ladder, making it possible to perform simultaneous immunostaining for eNOS, Akt, and β actin as a control. To prepare PBST 0.05% Tween or wash buffer, dissolve 5 tablets of PBS in 500 μl of Tween-20 and 1,000 ml of water. The three membranes were then incubated for 20

minutes at room temperature in 10 mL of a 5% BSA buffer, which was prepared by mixing 20 mL of PBST 0.05% Tween and 1 gm of BSA powder, to block non-specific binding.

During these 20 minutes period, the primary antibodies (both phosphoprotein and total protein antibodies) were prepared in a 5% BSA buffer at a final dilution of 1:1,000. After removing 10 ml of 5% BSA buffer, the membranes were incubated overnight with their respective primary antibody solutions for 16-20 hours at 4°C. The following morning, the membranes were washed three times for 15 minutes each in PBST 0.05% Tween. At this stage, the appropriate Ig/HRP secondary antibody was prepared in a 10 mL solution of 5% milk buffer. This buffer was made by mixing 20 mL of PBST 0.05% Tween with 1 gm of milk powder, resulting in a final dilution of 1:5,000. The membrane was then incubated in this solution for one hour at room temperature. Afterwards, a 1:25,000 dilution of anti-Western C marker (Streptactin) in PBST 0.05% Tween was prepared and the membrane was incubated in this solution for 15 minutes. Finally, the membranes were washed twice with PBST 0.05% Tween for 15 minutes each.

4.5.6 Densitometry (band quantification)

This present study focused on signalling in the IR/Akt/eNOS pathway. Proteins of interest were visualised and detected by a chemiluminescent detection methods (Genesys). We prepared a peroxide mixture in a new Eppendorf tube by combining 600 µl Immobilon Western HRP substrate luminol reagent with 600 µl peroxide reagent. We then stored the peroxide solution in the dark environment. Before imaging, we poured the peroxide mixture to completely submerge the blot. Protein band images were analysed using densitometry (gene tool program) to evaluate the relative amount of protein staining present in each image.

4.6 Superoxide measurement

Cell samples were grown to confluence in two wells of a six-well plate, with one well as the control and the other containing 100 nM insulin. The cell media was changed 1 day before sample harvesting by adding 2 ml of SSM to the insulin well. In the morning, we filled the insulin well with 2 µl of 100-µM stock insulin, then mixed and

incubated it at 37 °C for 30 minutes. After removing the media, we added 2 ml of PBS and mixed thoroughly to completely eradicate the PBS. We trypsinised and pelleted the cells in the centrifuge, and then resuspend the pellet in 400 µl of SBS to obtain a final suspension. For cell counting purposes, 20 µL of each sample was removed and mixed with an equal volume of trypan blue solution. The mixture was injected into a haemocytometer and the cells were counted under a microscope. Extrapolation of the count estimated the number of cells present in the solution (approximately 50,000 cells per well). We filled each tube with 1:1,000 of NADPH and prepared 15 µM lucigenin in 300 µM NADPH-containing SBS for the luminol reaction, with superoxide in the cell samples. We aliquoted 50,000 cells of the cell suspension into each well of a Corning 96-Well Solid White Polystyrene Microplate. For accuracy purpose, the superoxide measurement was carried out using a CLARIOstar® Plus Luminescence Plate Reader, with each sample analysed in triplicate. We recorded the luminescence every 96 seconds for 35 minutes until reaching a luminescence plateau.

4.7 Angiogenesis assay

Subcutaneous white adipose tissue from the pectoral region was harvested and placed in EC growth media. Surface blood vessels were dissected from the adipose tissue sample, which was then cut into pieces no larger than 1 mm^3 under sterile cell culture conditions. To prepare each sample, a minimum of 20 pieces were embedded in a fibrin matrix in each well of a 24-well cell culture plate. We prepared the fibrin matrix by adding 12.5 µl of thrombin to the centre of each well and mixing thoroughly. We then added 500 µl/well of 4 U/ml aprotinin and 2 mg/ml fibrinogen type 1 to the mixture. We placed a piece of adipose tissue into the well before the matrix had completely set up. The plates were incubated at room temperature for 20 minutes before being heated to 37 ^oC for another 20 minutes to ensure that the matrix had completely formed around the piece of adipose tissue. We carefully pipetted 1 ml of EC media onto the top of each well and plates were cultured for up to 7 days at 37 ^oC with 5% CO_2. During the culture period, the media were discarded and replaced every second day. Throughout the experiment, the samples were imaged at 4x magnification using an Olympus fluorescence microscope CKX41, and the number and length of endothelial sprouts emerging from each piece of fat were measured.

4.8 Statistical analysis

Data sets are reported as mean with a standard error of the mean (SEM). For statistical analysis, the Fisher's exact test, two-tailed unpaired Student's t-test, and ANOVA (Analysis of Variance) test were used. Fisher's exact test is a statistical test used for comparing proportions between two groups. The main benefit of Fisher's exact test is that it provides an accurate statistical test for small sample sizes and can be used for testing independence in a 2x2 contingency table, whereas many other tests, such as the chi-square test, have restrictions. The two-tailed unpaired Student's t-test is used to compare the means of two independent groups, regardless of whether the difference is positive or negative, making it a useful test for a wide range of applications. This test is particularly useful when the sample size is small. ANOVA is a statistical test used to compare the means of more than two groups. The main benefit of ANOVA is that it provides a powerful way to test the equality of means across multiple groups, taking into account the variability within each group. In this study, differences with a p-value of < 0.05 were considered statistically significant. Graphs and statistical analyses were produced using Origin Pro 2019b.

Chapter 5: **Results**

5 Results

Thirty-nine patients were included in this study and the clinical characteristics are shown in table 7 with comparison between normal, DM, HF, and DM/HF. Clear differences between the groups can be seen in terms of NYHA class I ($p < 0.001$) and II ($p = 0.018$), history of IHD ($p = 0.035$), history of DCM ($p = 0.009$), renal function ($p = 0.002$), HbA1c ($p < 0.001$), and LV systolic function ($p < 0.001$).

Table 6: Demographic and clinical characteristics of the patients, with comparison between normal, DM, HF, and DM/HF patients.

	Normal (n=10)	DM (n=4)	HF (n=15)	DM/HF (n=10)	P value
Age, y	73 ± 11	68 ± 13.3	71 ± 10.9	69 ± 10.3	0.816
Male gender, %	90	50	67	80	0.338
BMI, kg/m2	28.1 ± 3.6	34.1 ± 11.0	30.5 ± 5.5	33.3 ± 6.3	0.198
NYHA class, %					
I	90	75	7	10	**<0.001**
II	0	25	60	50	**0.018**
III	10	0	33	40	0.240
Past history, %					
IHD	0	50	47	50	**0.035**
DCM	0	0	40	60	**0.009**
AF	40	25	47	40	0.965
CABG	10	0	7	20	0.872
HTN	30	25	27	30	1.000
COPD	0	0	13	20	0.635
Blood test					
Hb (g/L)	135 ± 18.9	116.3 ± 27.6	129.9 ± 16.3	130 ± 17.5	0.416
Na (mmol/L)	137.1 ± 3.7	139.3 ± 2.4	137.5 ± 4.3	140.3 ± 1.9	0.183
K (mmol/L)	4.54 ± 0.62	4.7 ± 0.53	4.45 ± 0.47	4.8 ± 0.36	0.400
Cr (mmol/L)	80.7 ± 18.5	62.5 ± 7.4	109.7 ± 34.6	105.7 ± 37.5	**0.019**
eGFR (ml/min/1.73^2)	78.3 ± 12.7	89 ± 2.7	57.1 ± 18.3	62.2 ± 19.7	**0.002**
NT-pro BNP (ng/L)	1068.7 ± 1154.9	920.7 ± 1089.3	5235.8 ± 5840.2	7668.6 ± 8993.1	0.202
HbA1c (mmol/mol)	38.4 ± 4.3	52.3 ± 2.9	40.2 ± 3.4	54.3 ± 10.8	**<0.001**
Echocardiography					
LVEF (%)	54.9 ± 2.4	55 ± 0	24.7 ± 10.2	30.9 ± 12.1	**<0.001**
PASP (mmHg)	36.5 ± 13.4	35	30.1 ± 14.4	38 ± 7.5	0.930
LVIDs (mm)	35	32 ± 2.8	49.8 ± 11.3	47.3 ± 5.0	0.160
LVIDd (mm)	51.1 ± 6.0	48 ± 1.4	60.9 ± 8.2	61.4 ± 7.7	**0.004**

Data are presented as mean ± SD or percentages of patients. NYHA = New York Heart Association; IHD = ischemic heart disease; DCM = dilated cardiomyopathy; AF = atrial fibrillation; CABG = coronary artery bypass graft; HTN = hypertension; COPD = chronic obstructive pulmonary disease; LVEF = left ventricular ejection fraction; PASP = pulmonary arterial systolic pressure; LVIDs = left ventricular end-systolic internal diameter; LVIDd = left ventricular end-diastolic internal diameter. Fisher's exact test was used for categorical variables, and ANOVA was used for continuous variables.

Table 8 compares the characteristics of the non-diabetic and diabetic patients. Significant differences were only observed in HbA1c (p <0.001) and blood Na (p = 0.01) between these patient cohorts.

Table 7: Demographic and clinical characteristics of non-diabetic and diabetic patients.

	Non-DM (n=25)	DM (n=14)	P value
Age, y	72 ± 10.7	68 ± 10.7	0.350
Male gender, %	76	71	1.000
BMI, kg/m2	29.5 ± 4.9	33.6 ± 7.6	0.1
NYHA class, %			
I	40	29	0.48
II	36	42	0.67
III	24	29	0.75
Past history, %			
IHD	28	50	0.482
DCM	24	43	0.287
AF	44	36	0.740
CABG	8	14	0.609
HTN	28	29	1.000
COPD	8	14	0.609
Blood test			
Hb (g/L)	132.0 ± 17.2	125.8 ± 21.0	0.37
Na (mmol/L)	137.3 ± 4.0	140.0 ± 2.0	**0.01**
K (mmol/L)	4.49 ± 0.52	4.77 ± 0.40	0.07
Cr (mmol/L)	98.0 ± 32.2	92.4 ± 37.2	0.64
eGFR (ml/min/1.73^2)	64.5 ± 18.8	70.5 ± 20.6	0.48
NT-pro BNP (ng/L)	3568.9 ± 4942.9	5644.2 ± 8050.2	0.48
HbA1c (mmol/mol)	39.5 ± 3.8	53.7 ± 9.0	**<0.001**
Echocardiography			
LVEF (%)	36.2 ± 17.0	38.3 ± 15.2	0.71
PASP (mmHg)	33.7 ± 13.6	37.4 ± 6.7	0.48
LVIDs (mm)	47.3 ± 11.8	41.2 ± 9.2	0.36
LVIDd (mm)	57.3 ± 8.8	56.5 ± 9.1	0.82

Data are presented as mean ± SD or percentages of patients. NYHA = New York Heart Association; IHD = ischemic heart disease; DCM = dilated cardiomyopathy; AF = atrial fibrillation; CABG = coronary artery bypass graft; HTN = hypertension; COPD = chronic obstructive pulmonary disease; LVEF = left ventricular ejection fraction; PASP = pulmonary arterial systolic pressure; LVIDs = left ventricular end-systolic internal diameter; LVIDd = left ventricular end-diastolic internal diameter. Fisher's exact test was used for categorical variables, and the t-test was used for continuous variables.

When patients were classified as non-HF or HF, significant differences were observed in the proportions of patients with NYHA class I (p <0.001), II (p =0.003), III (p = 0.048), history of IHD (p = 0.013), history of DCM (p = 0.003), renal function (p <0.001), NT-proBNP (p = 0.011), and LV systolic function (p <0.001, Table 9).

Table 8: Demographic and clinical characteristics of the patients with and without heart failure.

	Non-HF (n=14)	HF (n=25)	P value
Age, y	71 ± 11.4	70 ± 10.5	0.84
Male gender, %	79	72	0.721
BMI, kg/m2	29.8 ± 6.7	31.6 ± 5.8	0.41
NYHA class, %			
I	86	8	**<0.001**
II	7	56	**0.003**
III	7	36	**0.048**
Past history, %			
IHD	14	48	**0.013**
DCM	0	48	**0.003**
AF	36	44	0.740
CABG	7	12	1.000
HTN	29	28	1.000
COPD	0	16	0.277
Blood test			
Hb (g/L)	129.6 ± 22.4	130.0 ± 16.4	0.96
Na (mmol/L)	137.7 ± 3.5	138.5 ± 3.8	0.5
K (mmol/L)	4.59 ± 0.58	4.58 ± 0.46	0.99
Cr (mmol/L)	75.5 ± 17.9	108.2 ± 34.9	**<0.001**
eGFR (ml/min/1.73^2)	81.4 ± 11.8	59 ± 18.6	**<0.001**
NT-pro BNP (ng/L)	1019.3 ± 1065.7	6300.1 ± 7217.7	**0.011**
HbA1c (mmol/mol)	42.7 ± 7.7	46.0 ± 10.1	0.28
Echocardiography			
LVEF (%)	54.9 ± 1.9	27.2 ± 11.2	**<0.001**
PASP (mmHg)	36 ± 9.5	34.6 ± 12.6	0.84
LVIDs (mm)	33 ± 2.6	48.9 ± 9.0	**0.002**
LVIDd (mm)	50 ± 5.0	61.1 ± 7.8	**<0.001**

Data are presented as mean ± SD or percentages of patients. NYHA = New York Heart Association; IHD = ischemic heart disease; DCM = dilated cardiomyopathy; AF = atrial fibrillation; CABG = coronary artery bypass graft; HTN = hypertension; COPD = chronic obstructive pulmonary disease; LVEF = left ventricular ejection fraction; PASP = pulmonary arterial systolic pressure; LVIDs = left ventricular end-systolic internal diameter; LVIDd = left ventricular end-diastolic internal diameter. Fisher's exact test was used for categorical variables, and the t-test was used for continuous variables.

The medications taken by each cohort of patients are shown in Table 10.

Table 9: Medications taken by each cohort of patients: Normal, DM, HF, and DM/HF.

	Normal (n=10)	DM (n=4)	HF (n=15)	DM/HF (n=10)	P value
Medication, %					
ACEI	30	50	47	60	0.6
Beta blocker	30	50	100	100	**<0.001**
Entresto	0	0	13	10	0.59
Loop diuretic	10	25	67	60	**0.026**
ARB/AIIR	10	25	33	30	0.6
MRA	10	0	67	50	**0.011**
Statin	70	100	67	60	0.53
ASA	0	50	27	20	0.17
Metformin	0	100	0	60	**<0.001**
Insulin	0	0	0	20	0.11
Sulfonylurea	0	25	0	10	0.17
DDP-4 inhibitor	0	0	0	10	0.39
SGLT-2 inhibitor	0	0	0	20	0.11
P2Y12 receptor antagonist					
Clopidogrel	20	0	7	10	0.64
Prasugrel	0	0	0	0	
Ticagrelor	0	25	13	0	0.26
Anticoagulant	40	50	60	60	0.76
Digoxin	10	0	0	20	0.28
Ivabradine	0	0	0	20	0.11

Data are presented as percentages of patients. ACEI = angiotensin-converting enzyme inhibitor; ARB = angiotensin receptor blocker; AIIR = angiotensin II receptor antagonist; MRA = mineralocorticoid receptor antagonist; DPP-4 inhibitor = dipeptidyl peptidase-4 inhibitor; SGLT-2 inhibitor = sodium-glucose cotransporter-2 inhibitor. Fisher's exact test was used for categorical variables.

5.1 Endothelial cell isolation

In the first steps of our protocol for endothelial cell isolation, we discovered that cells from two wells of a 24-well plate (P0) grew slowly to confluence in 4–6 weeks and were contaminated with RBCs. The protocol was then changed to remove dead cells and RBCs using the Dead Cell Removal Kit (Miltenyi Biotec) and RBC lysis buffer, respectively. For the new protocol, cells were grown to confluence from P0 in 3 weeks (average time to confluence = 21.5 days), with lower RBC contamination. Cells from each well were then plated into a single well of a six-well plate (P1), and cells were grown to confluence in 1 week (average time to confluence = 7.5 days). When comparing normal, DM, HF, and DM/HF patients, we found no difference in time to confluence from P0–P1 and P1–P2 in each cohort (Figure 13).

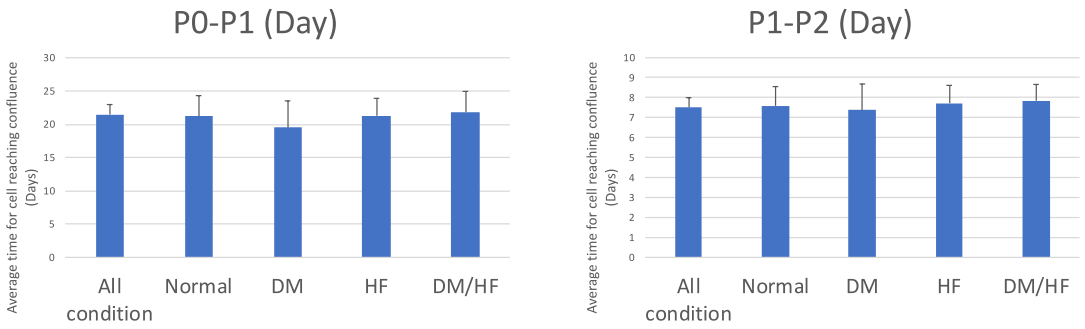

Figure 13: Average time to confluence of the isolated cells in each group from P0–P1 and P1–P2.

Images of the morphology of isolated cells obtained from skeletal muscle and adipose tissue are shown in Figure 14A and B, respectively. These cells showed a typical ‘cobblestone’ monolayer pattern, which is compatible with endothelial cells.

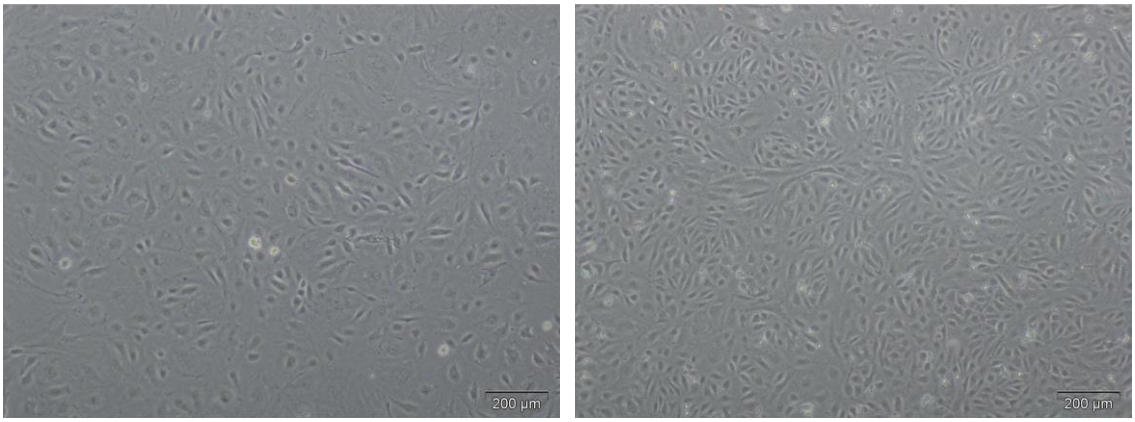

A B

Figure 14: Morphology of the isolated cells showed a ‘cobblestone’ monolayer pattern, which is compatible with endothelial cells. A. Cells isolated from skeletal muscle. B. Cells isolated from adipose tissue.

Additional examination is necessary to determine the identity and purity of these isolated cells, as certain skeletal muscle tissue samples were contaminated with skeletal muscle cells, as illustrated in Figure 15.

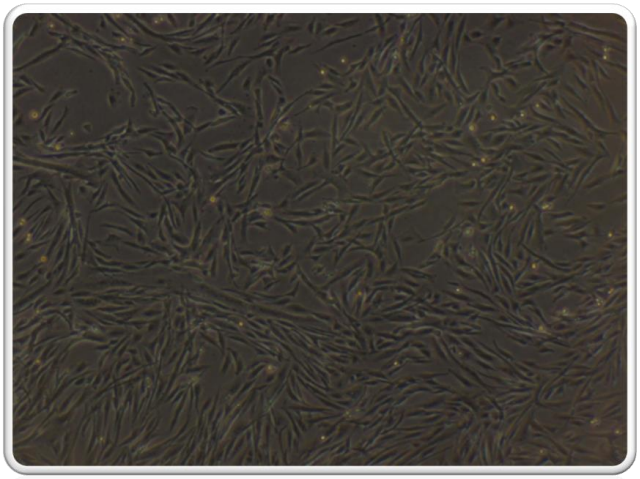

Figure 15: Cells isolated from a skeletal muscle sample that had been contaminated with skeletal muscle cells.

5.2 Confirmation of the identity of endothelial cells

5.2.1 Intracellular calcium measurement induced by VEGF

A fluorescence-based method for calcium measurement was used to validate the cells from endothelial cell isolation. These cells were confirmed by using intracellular calcium influx in response to VEGF stimulation. As shown in Figure 16, the cells reacted favourably to VEGF, indicating that they were representative of a large proportion of endothelial cells. This finding, however, did not confirm the purity of these endothelial cells; flow cytometry was used for this purpose.

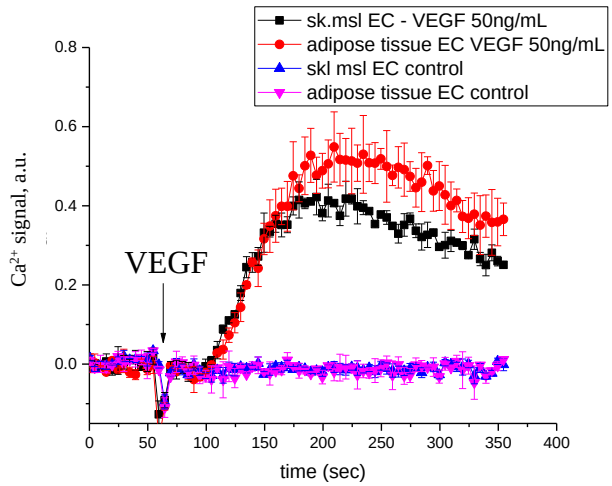

Figure 16: Intracellular calcium flux of isolated cells from skeletal muscle (sk.msl EC) and adipose tissue (adipose tissue EC) increased significantly in response to 50 ng/ml VEGF stimulation.

5.2.2 Flow cytometric analysis of isolated endothelial cells

To determine the purity of the endothelial cells, flow cytometry was used to investigate the binding of three different fluorochrome-labelled antibodies to endothelial cell surface antigens. These antibodies were CD45-FITC, CD144-PE, and CD31-PerCP-Vio700. Flow cytometric data were analysed in a dot plot and histogram using different parameters, such as forward-scattered light (FSC) and side-scattered light (SSC). In addition, gating was used to restrict the analysis to endothelial cells (dot plot in the lower panel of Figure 17 and 18), which revealed that 98.0 ± 1.0% (mean ± SEM, n = 4) and 98.0 ± 0.7% (mean ± SEM, n = 12) of the cells in skeletal muscle and adipose tissue, respectively, were endothelial cells (CD31-PerCP positive and CD144-PE positive).

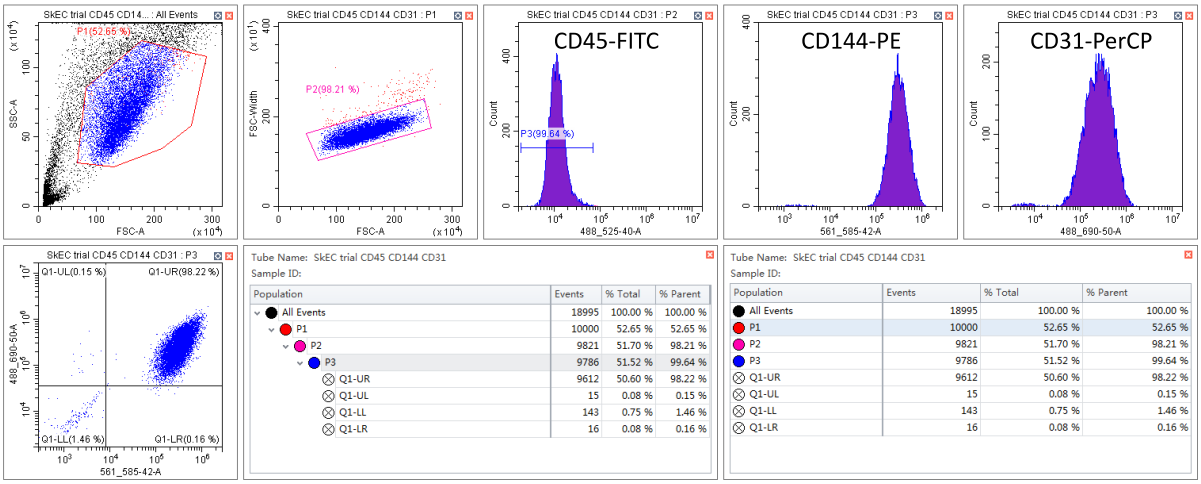

Figure 17: Flow cytometry of human skeletal muscle endothelial cells fully stained with CD31+ and CD144+ demonstrated a high-purity population of endothelial cells (98.22%). The axes in the lower panel dot plot depict both the fluorescence intensity and the fluorescence channel wavelength of CD144-PE (x-axis) and CD31-PerCP (y-axis).

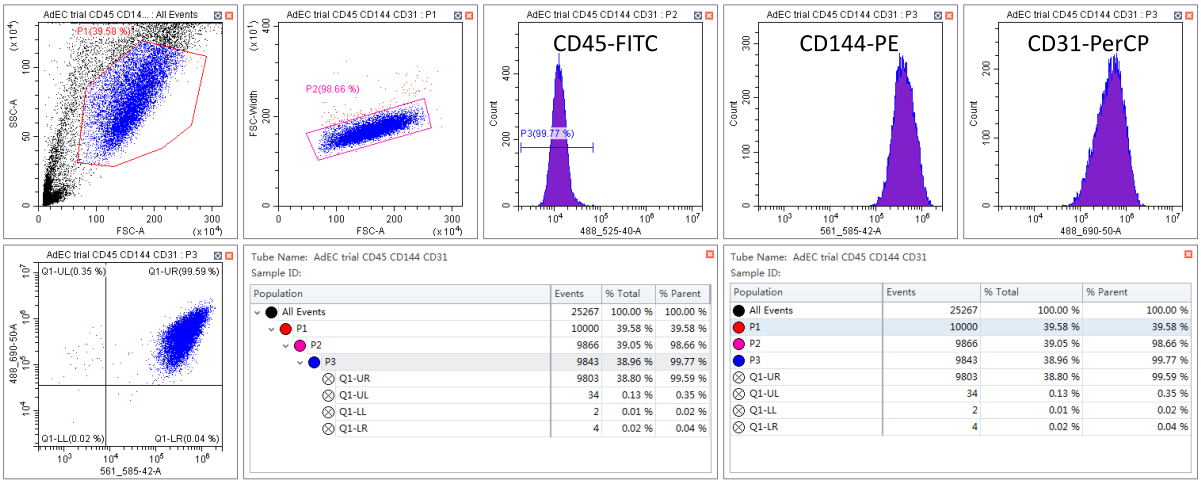

Figure 18: Flow cytometry of human adipose tissue endothelial cells fully stained with CD31+ and CD144+ demonstrated a high-purity population of endothelial cells (99.59%). The axes in the lower panel dot plot depict both the fluorescence intensity and the fluorescence channel-wavelength of CD144-PE (x-axis) and CD31-PerCP (y-axis).

5.3 Gene expression analysis

We examined gene expression in confirmed and purified endothelial cells. Following cDNA preparation and storage at -20 ºC, frequent freeze/thaw cycles were avoided to prevent degradation of cDNA samples. Moreover, cDNA samples are prone to degradation over time, which can result in a loss of quality and accuracy in experiments. When cDNA samples are stored at 4°C, the temperature is higher than the recommended storage temperature of -20°C, which is optimal for preserving the stability of the cDNA samples. As shown in Table 11, cDNA samples of GAPDH degraded after being stored at 4 ºC for more than 8 weeks. As a result, all real-time PCR experiments were conducted within 1 week of the cDNA sample preparation.

Table 10: Gene expression of GAPDH was compared between the first (real-time PCR performed 1 week after cDNA samples were prepared) and second (real-time PCR performed >8 weeks after the cDNA samples were prepared and stored in 4 ^{o}C) results.

First result

Sample	GAPDH		
	Ct1	Ct2	Avg Ct
181	20.86	20.43	20.645
183	22	21.48	21.74
189	19.91	20.06	19.985
191	21.79	22.07	21.93
192	23.25	23.47	23.36
193	21.49	21.54	21.515
196	22.94	23.52	23.23
198	19.13	20.75	19.94
200	19.82	19.85	19.835
201	20.64	21.14	20.89
202	22.29		22.29
205	21.14	21.73	21.435
209	22.3	21.09	21.695
210	24.52	24.23	24.375
218	22.22	21.51	21.865
232	22.87	23	22.935
233	22.32	22.53	22.425

Second result

Sample	GAPDH		
	Ct1	Ct2	Avg Ct
181	21.98	22.47	22.225
183	23.59	23.49	23.54
189	21.77	21.9	21.835
191	23.39	23.58	23.485
192	24.84	24.91	24.875
193	22.83	22.95	22.89
196	25.56	25.39	25.475
198	21.82	21.36	21.59
200	21.65	21.56	21.605
201	22.12	22	22.06
202	24.77	24.76	24.765
205	23.82	23.73	23.775
209	24.12	23.99	24.055
210	28.58	28.62	28.6
218	23.56	23.58	23.57
232	24.63	23.88	24.255
233	24.58	24.78	24.68

Numerous genes were investigated for their expression in ATECs, including IR, IGF1R, Akt1, Akt2, Akt3, eNOS, NOX2, NOX4, SOD1, SOD2, SOD3, and catalase. The housekeeping gene GAPDH was used as a control.

Figure 19 compares the relative expression of genes in normal, DM, HF, and DM/HF patients. While a significant decrease in eNOS mRNA expression was observed in DM compared to normal conditions (0.00084±0.00005 vs 0.0014±0.0002, $p = 0.040$), Akt3 expression was increased in both DM and DM/HF compared to normal conditions. Catalase expression was significantly higher in DM/HF compared to just HF conditions (0.038±0.006 vs 0.023±0.003, $p = 0.045$). This result remains significant when patients are classified as non-DM or DM, as illustrated in Figure 20.

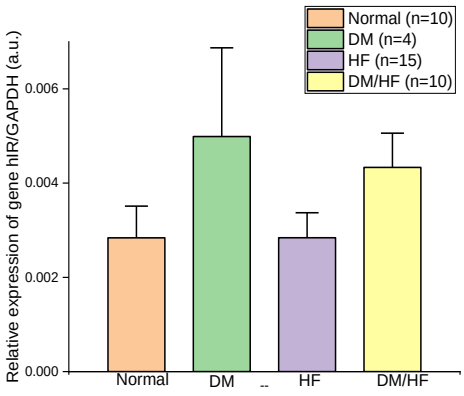

IR/GAPDH

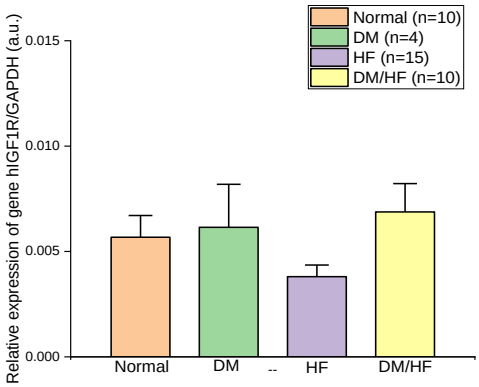

IGF1R/GAPDH

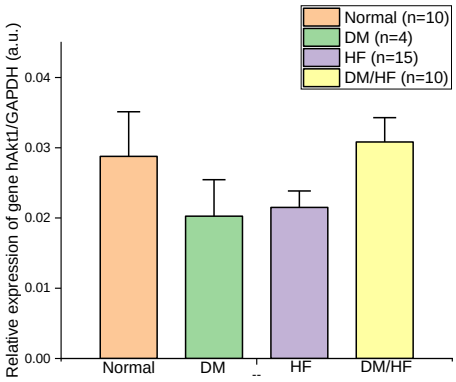

Akt1/GAPDH

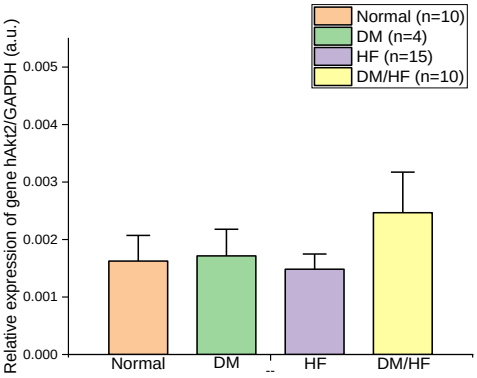

Akt2/GAPDH

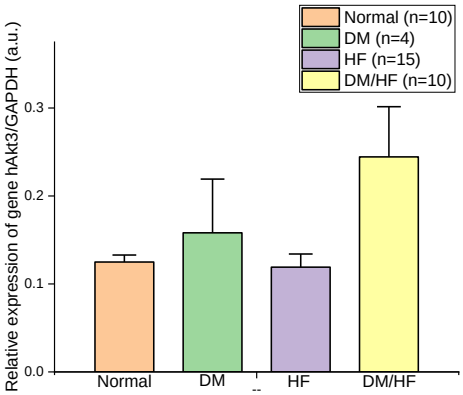

Akt3/GAPDH

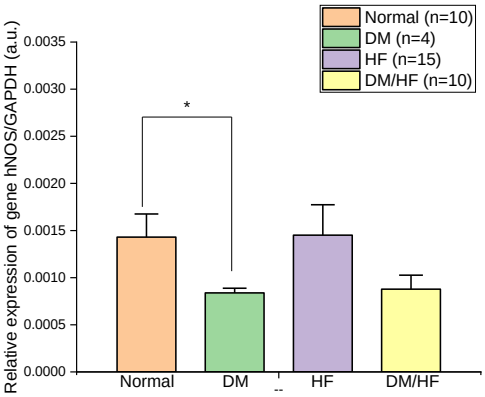

eNOS/GAPDH

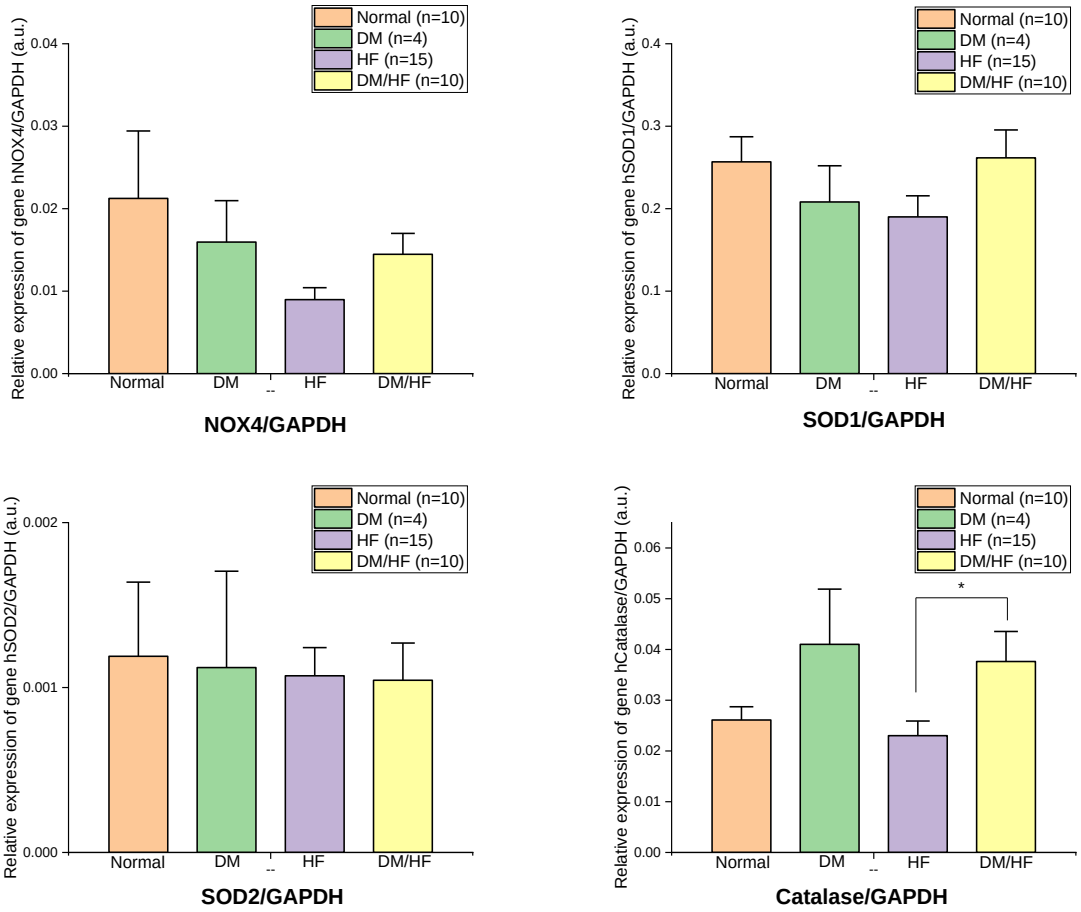

Figure 19: Relative gene expression of IR, IGF1R, Akt1, Akt2, Akt3, eNOS, NOX4, SOD1, SOD2, and catalase between the normal, DM, HF, and DM/HF groups (asterisks denote statistical significance with p-value less than 0.05).

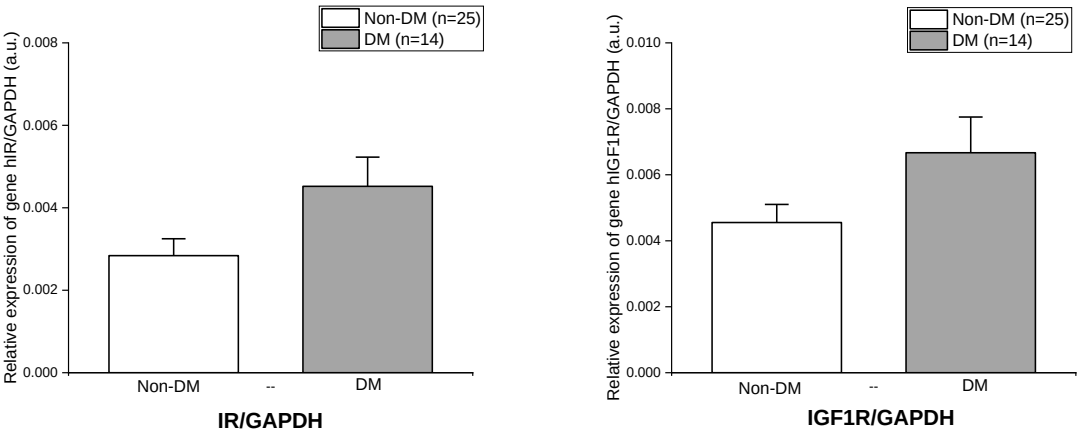

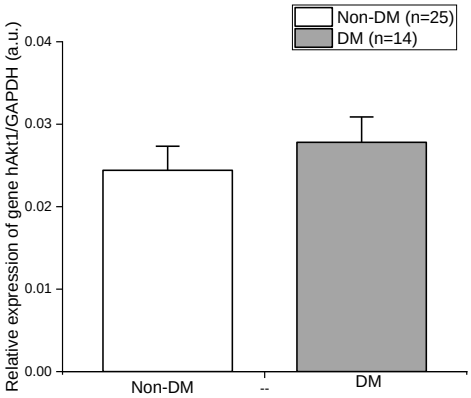

Akt1/GAPDH

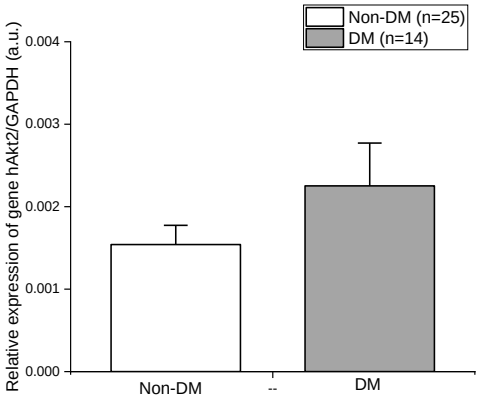

Akt2/GAPDH

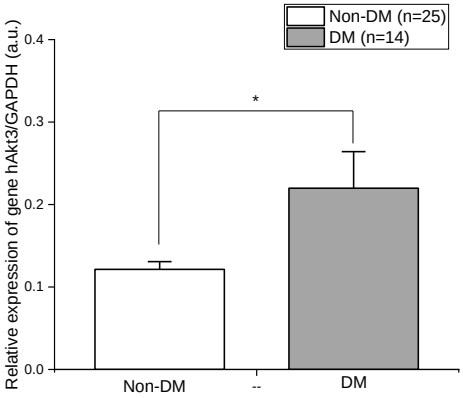

Akt3/GAPDH

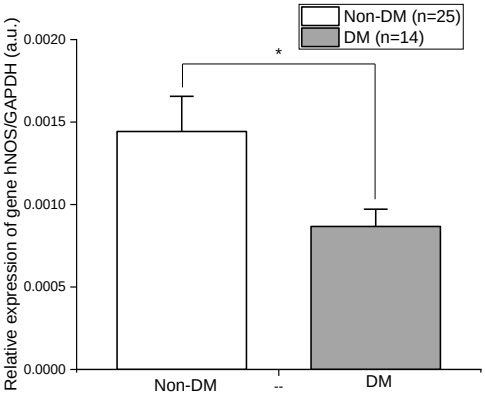

eNOS/GAPDH

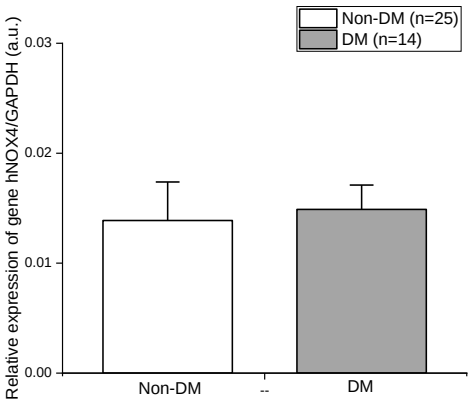

NOX4/GAPDH

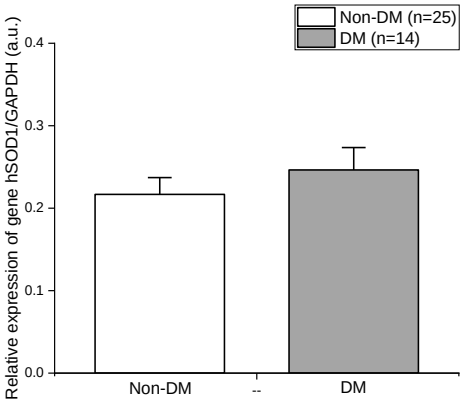

SOD1/GAPDH

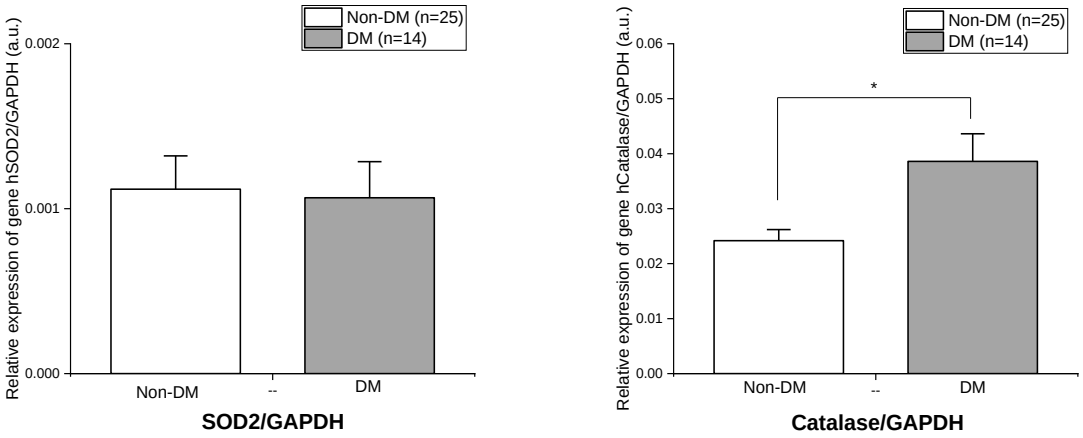

Figure 20: Relative gene expression of IR, IGF1R, Akt1, Akt2, Akt3, eNOS, NOX4, SOD1, SOD2, and catalase between the non-DM and DM groups (asterisks denote statistical significance with p-value less than 0.05).

When patients were classified as non-HF or HF, there were no significant differences between the groups. However, NOX4 mRNA expression showed a trend towards being lower in the HF condition, as illustrated in Figure 21.

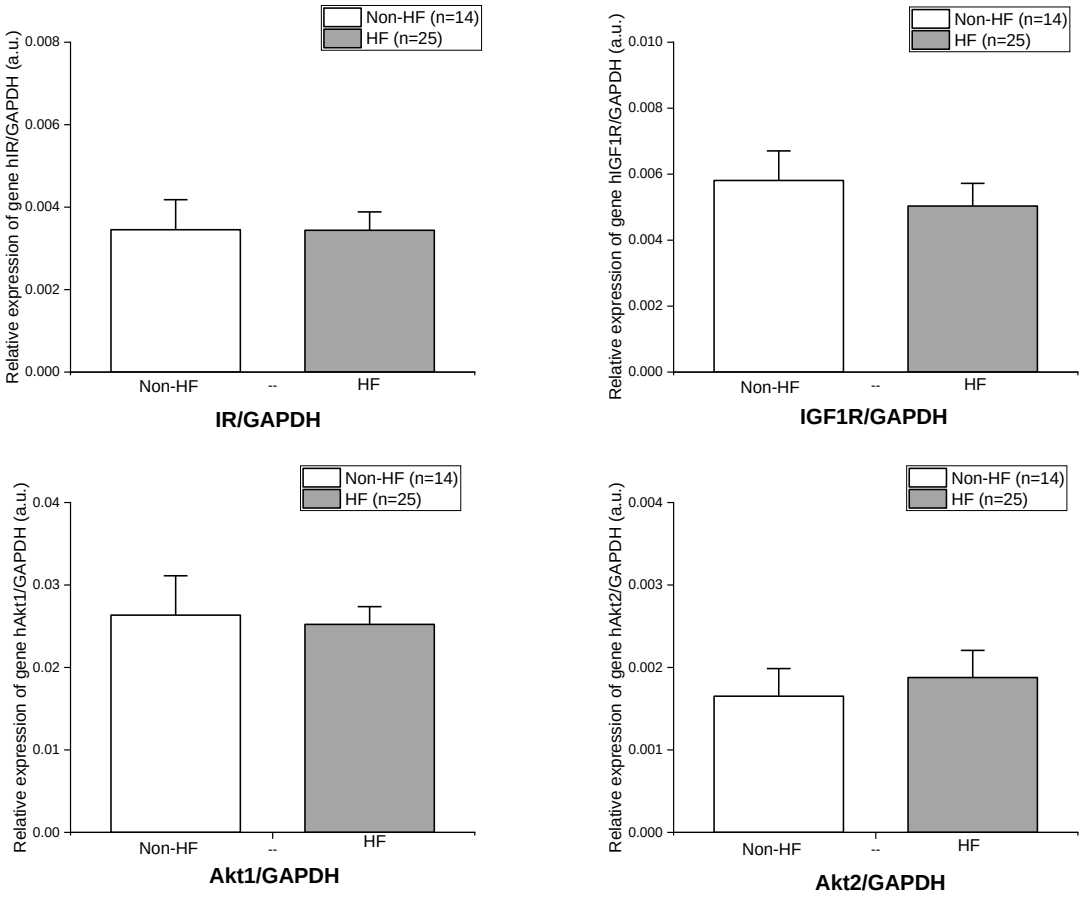

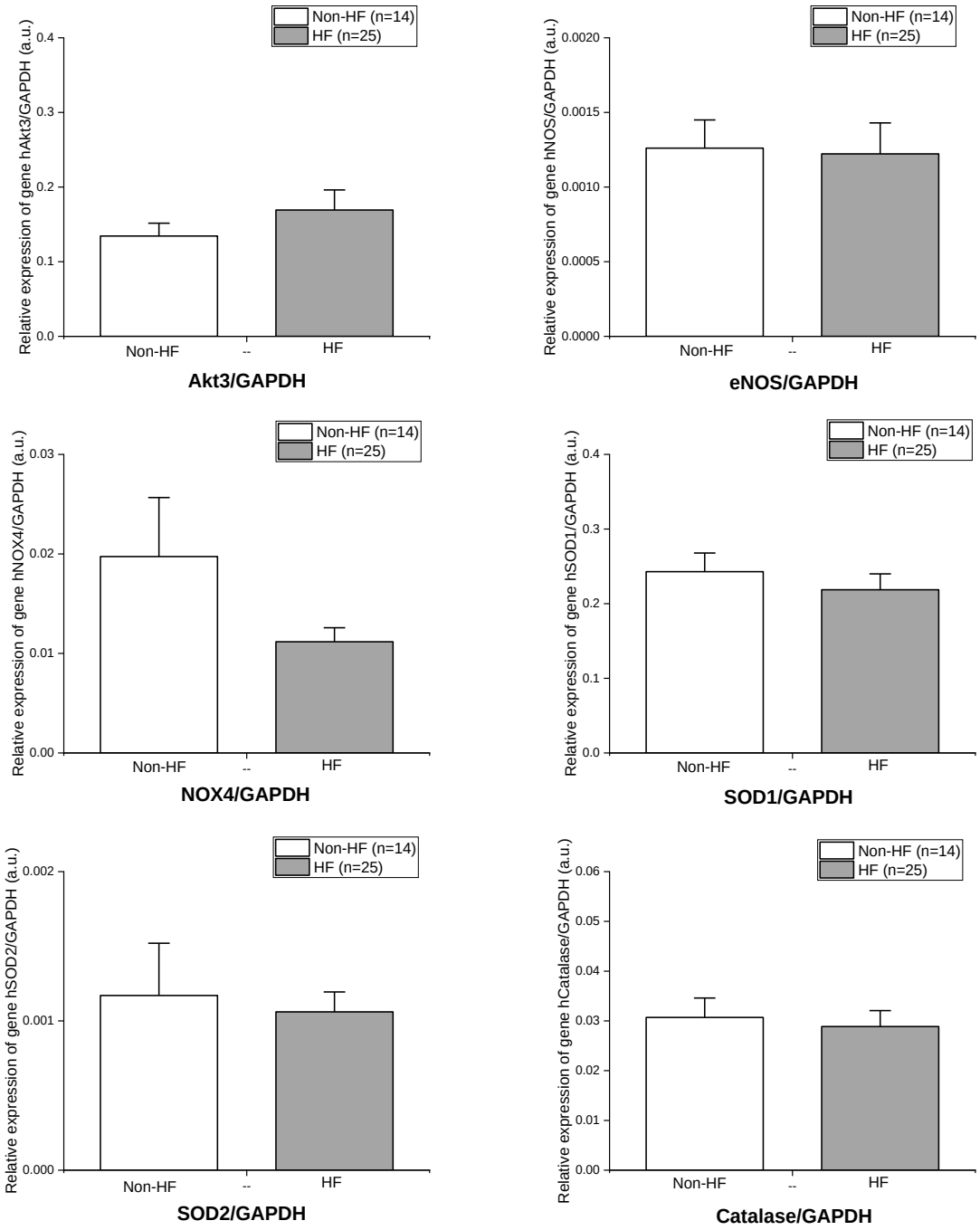

Figure 21: Relative gene expression of IR, IGF1R, Akt1, Akt2, Akt3, eNOS, NOX4, SOD1, SOD2, and catalase between the non-HF and HF groups.

5.4 Protein expression analysis

By using the Western blot technique, the ATECs from HF and DM patients were used to investigate proteins involved in the insulin signalling pathway and ROS production, including IR, IGF1R, Akt, eNOS, p47phox, NOX2, and NOX4. For both phosphorylated and total protein expression, actin (structural or housekeeping protein) was used as a loading control.

Between the non-DM and DM groups, there were no significant differences in basal phosphorylation of IR, Akt, eNOS, p47phox and total expression of IGF1R, NOX2 and NOX4 (Figure 22). While insulin had a minimal effect on stimulating Akt phosphorylation in the DM group, insulin had a significant effect on phosphorylation of IR and Akt in the non-diabetic group ($p = 0.048$ and $p = 0.025$, respectively). Furthermore, we found that insulin stimulation had no effect on the phosphorylation of eNOS and p47phox in both the non-DM and DM groups (Figure 23).

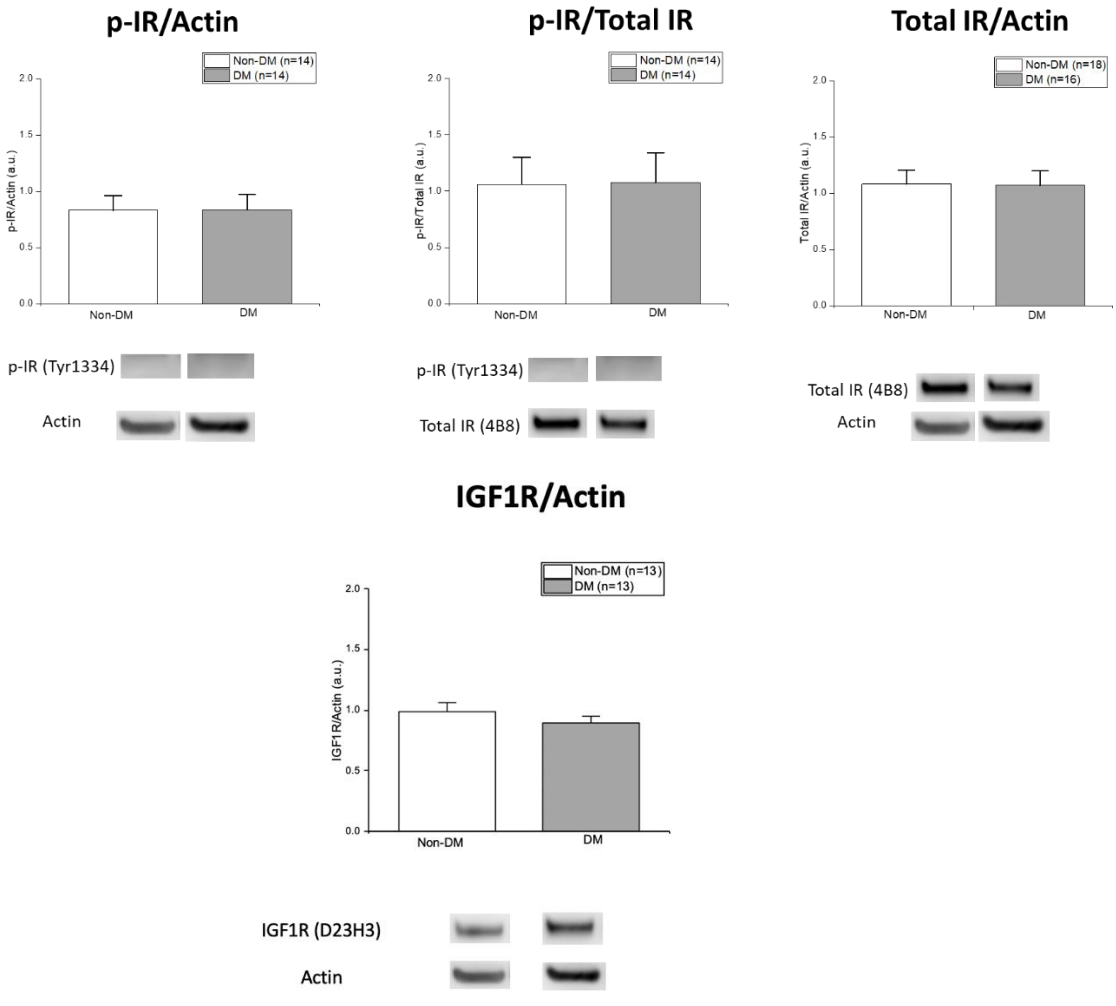

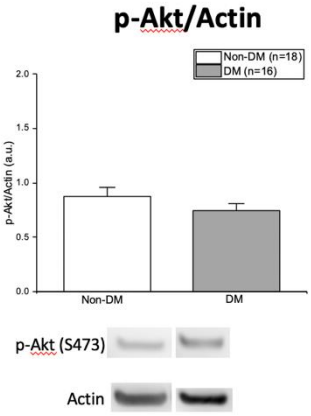
p-Akt/Actin
Non-DM (n=18)
DM (n=16)
p-Akt/Actin (a.u.)
2.0
1.5
1.0
0.5
0.0
Non-DM
DM
p-Akt (S473)
Actin

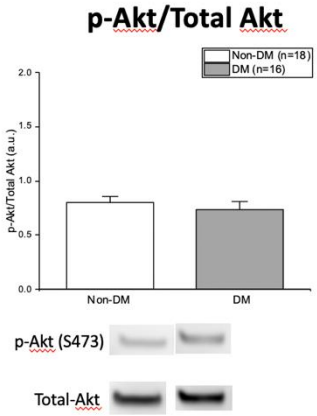
p-Akt/Total Akt
Non-DM (n=18)
DM (n=16)
p-Akt/Total Akt (a.u.)
2.0
1.5
1.0
0.5
0.0
Non-DM
DM
p-Akt (S473)
Total-Akt

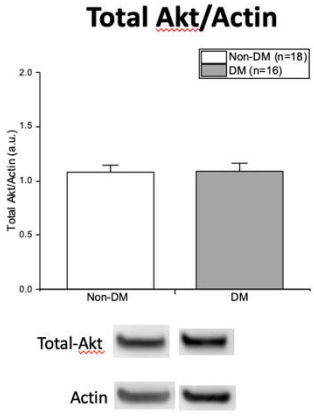
Total Akt/Actin
Non-DM (n=18)
DM (n=16)
Total Akt/Actin (a.u.)
2.0
1.5
1.0
0.5
0.0
Non-DM
DM
Total-Akt
Actin

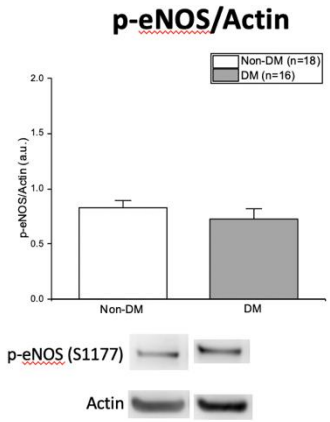
p-eNOS/Actin
Non-DM (n=18)
DM (n=16)
p-eNOS/Actin (a.u.)
2.0
1.5
1.0
0.5
0.0
Non-DM
DM
p-eNOS (S1177)
Actin

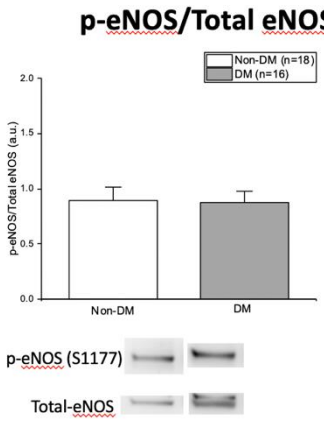
p-eNOS/Total eNOS
Non-DM (n=18)
DM (n=16)
p-eNOS/Total eNOS (a.u.)
2.0
1.5
1.0
0.5
0.0
Non-DM
DM
p-eNOS (S1177)
Total-eNOS

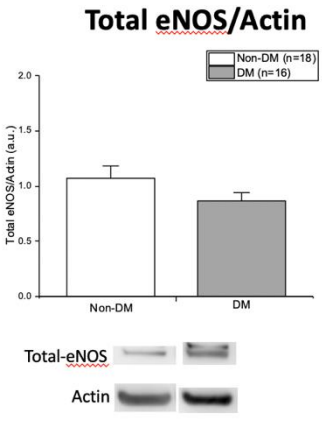
Total eNOS/Actin
Non-DM (n=18)
DM (n=16)
Total eNOS/Actin (a.u.)
2.0
1.5
1.0
0.5
0.0
Non-DM
DM
Total-eNOS
Actin

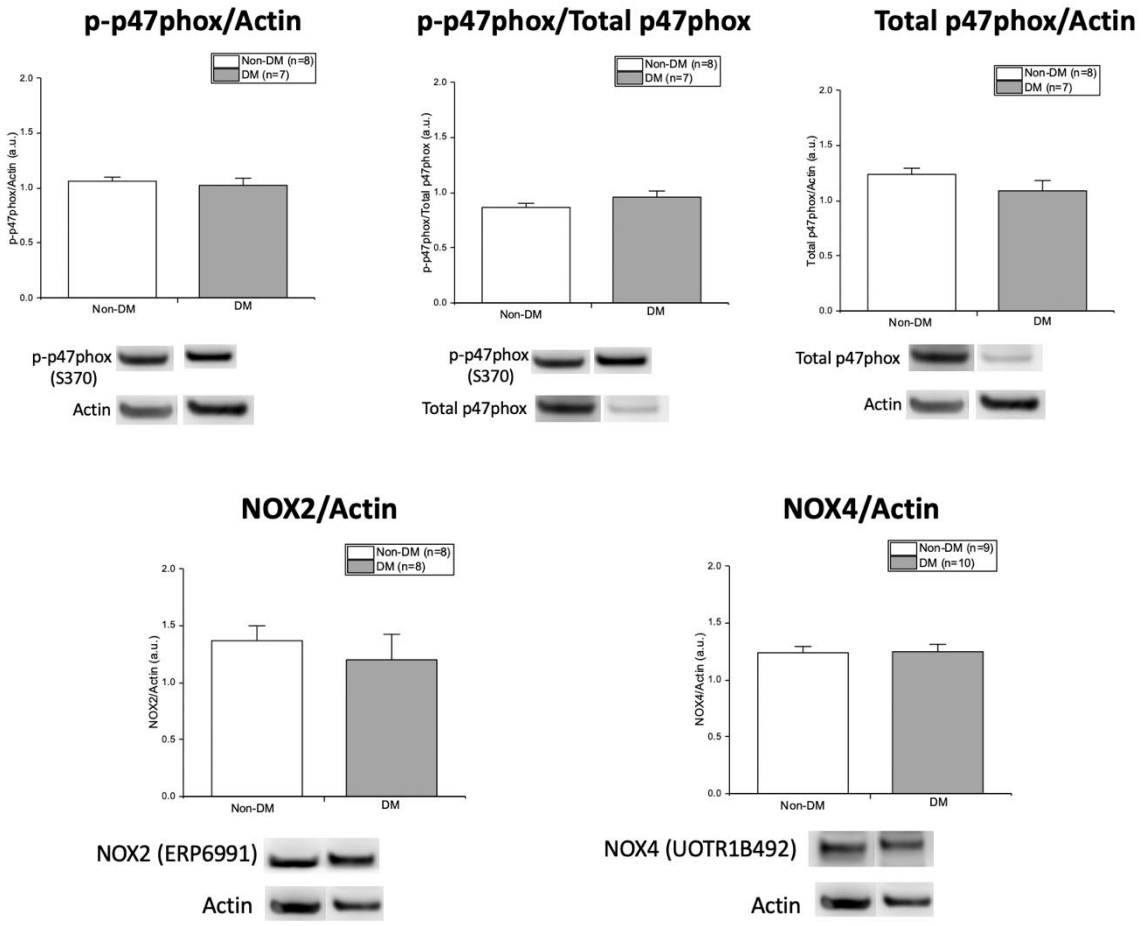

Figure 22: Protein expression of basal phospho-IR, total IR, IGF1R, phospho-Akt, total Akt, phospho-eNOS, total eNOS, phospho-p47phox, total p47phox, NOX2, and NOX4 from human ATECs between the non-diabetic and diabetic groups.

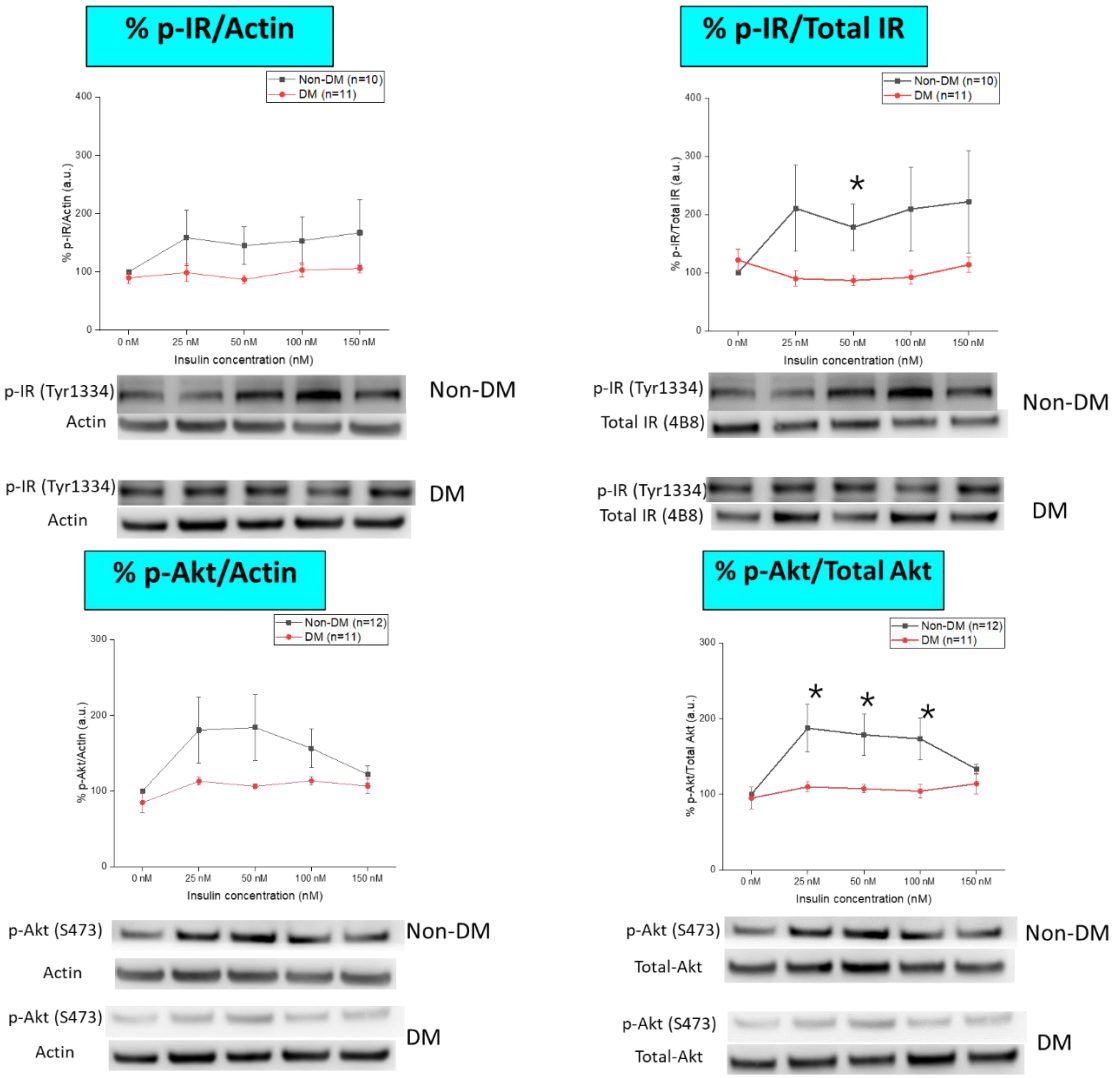
% p-IR/Actin
Non-DM (n=10)
DM (n=11)
% p-IR/Actin (a.u.)
Insulin concentration (nM)
0 nM
25 nM
50 nM
100 nM
150 nM
p-IR (Tyr1334)
Actin
Non-DM
DM
% p-IR/Total IR
% p-IR/Total IR (a.u.)
Total IR (4B8)
*
% p-Akt/Actin
Non-DM (n=12)
DM (n=11)
% p-Akt/Actin (a.u.)
p-Akt (S473)
% p-Akt/Total Akt
% p-Akt/Total Akt (a.u.)
Total-Akt

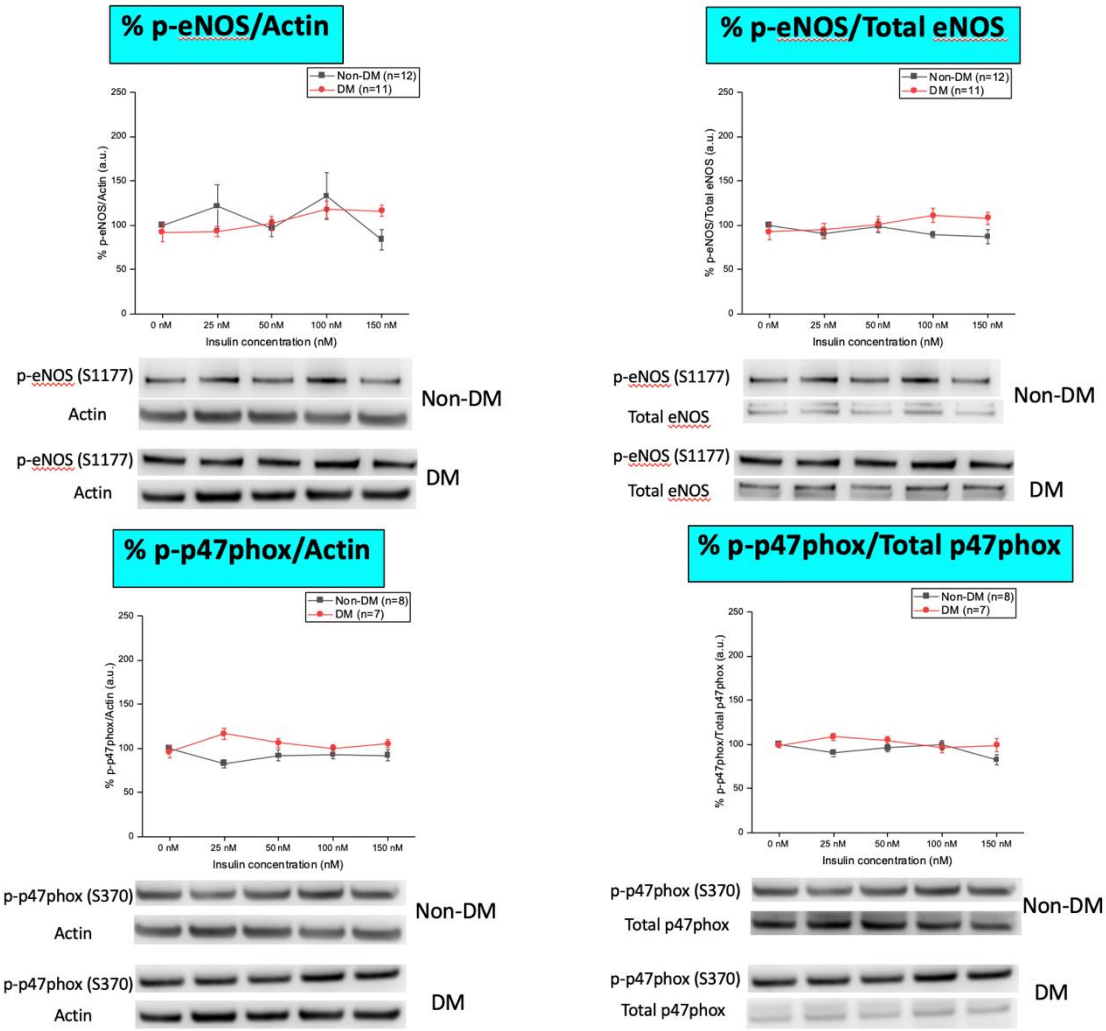

Figure 23: Insulin-stimulated phosphorylation of IR, Akt, eNOS, and p47phox from human ATECs between the non-diabetic and diabetic groups. Values (means ± SE) are expressed relative to no insulin (asterisks denote statistical significance with p-value less than 0.05).

Regarding protein expression in the non-HF and HF groups, there were no significant differences in basal phosphorylation of IR, Akt, eNOS, p47phox and total expression of IGF1R, NOX2, and NOX4 (Figure 24). In terms of insulin-stimulated phosphorylation, insulin had a significant effect in stimulating IR phosphorylation ($p = 0.031$) and showed a trend towards increasing Akt phosphorylation in the non-HF group, whereas it had only a minimal effect on the HF group. We also observed that insulin stimulation had no effect on eNOS and p47phox phosphorylation in both the non-HF and HF groups (Figure 25).

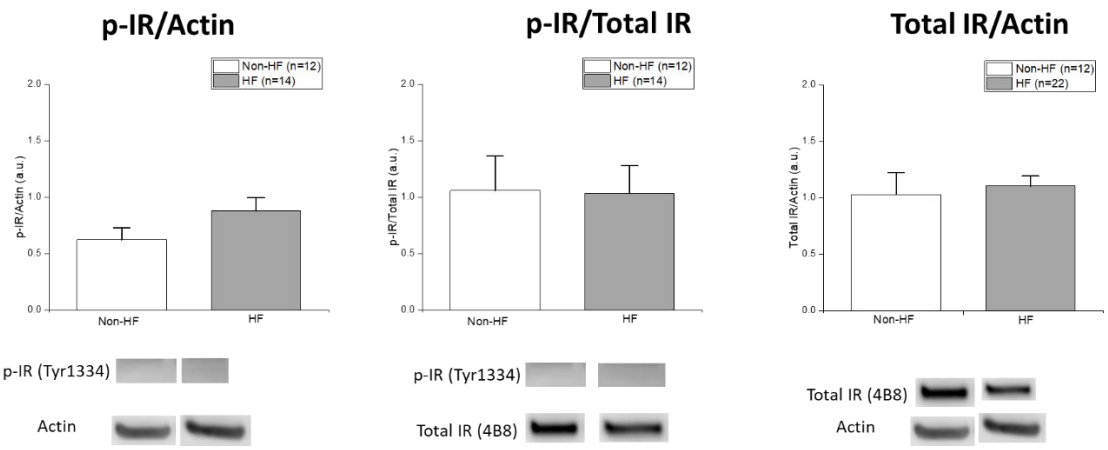
p-IR/Actin
Non-HF (n=12)
HF (n=14)
p-IR/Actin (a.u.)
Non-HF
HF
p-IR (Tyr1334)
Actin
p-IR/Total IR
Non-HF (n=12)
HF (n=14)
p-IR/Total IR (a.u.)
Non-HF
HF
p-IR (Tyr1334)
Total IR (4B8)
Total IR/Actin
Non-HF (n=12)
HF (n=22)
Total IR/Actin (a.u.)
Non-HF
HF
Total IR (4B8)
Actin

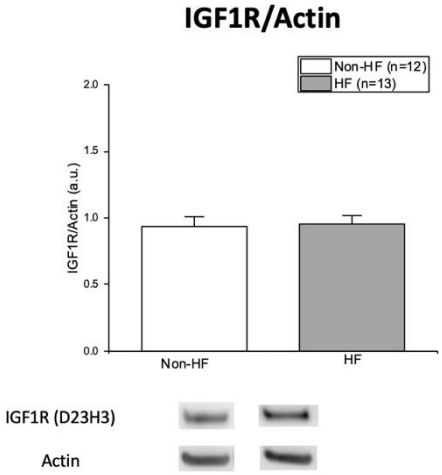
IGF1R/Actin
Non-HF (n=12)
HF (n=13)
IGF1R/Actin (a.u.)
Non-HF
HF
IGF1R (D23H3)
Actin

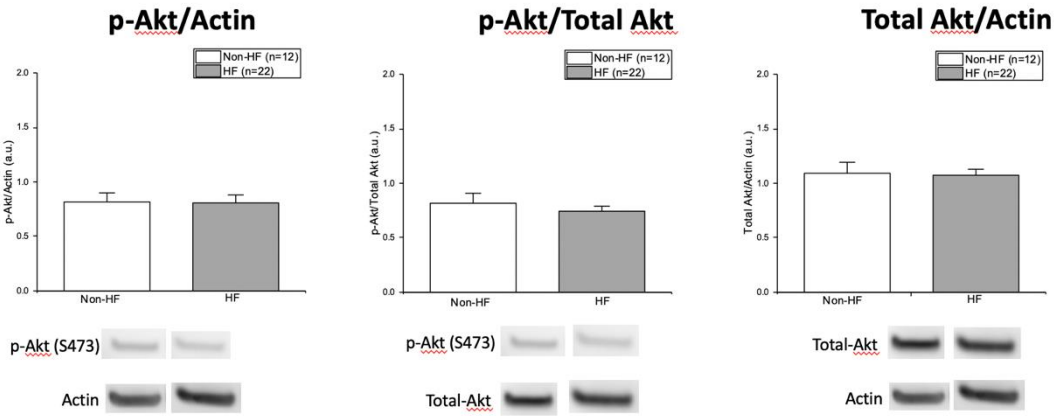
p-Akt/Actin
Non-HF (n=12)
HF (n=22)
p-Akt/Actin (a.u.)
Non-HF
HF
p-Akt (S473)
Actin
p-Akt/Total Akt
Non-HF (n=12)
HF (n=22)
p-Akt/Total Akt (a.u.)
Non-HF
HF
p-Akt (S473)
Total-Akt
Total Akt/Actin
Non-HF (n=12)
HF (n=22)
Total Akt/Actin (a.u.)
Non-HF
HF
Total-Akt
Actin

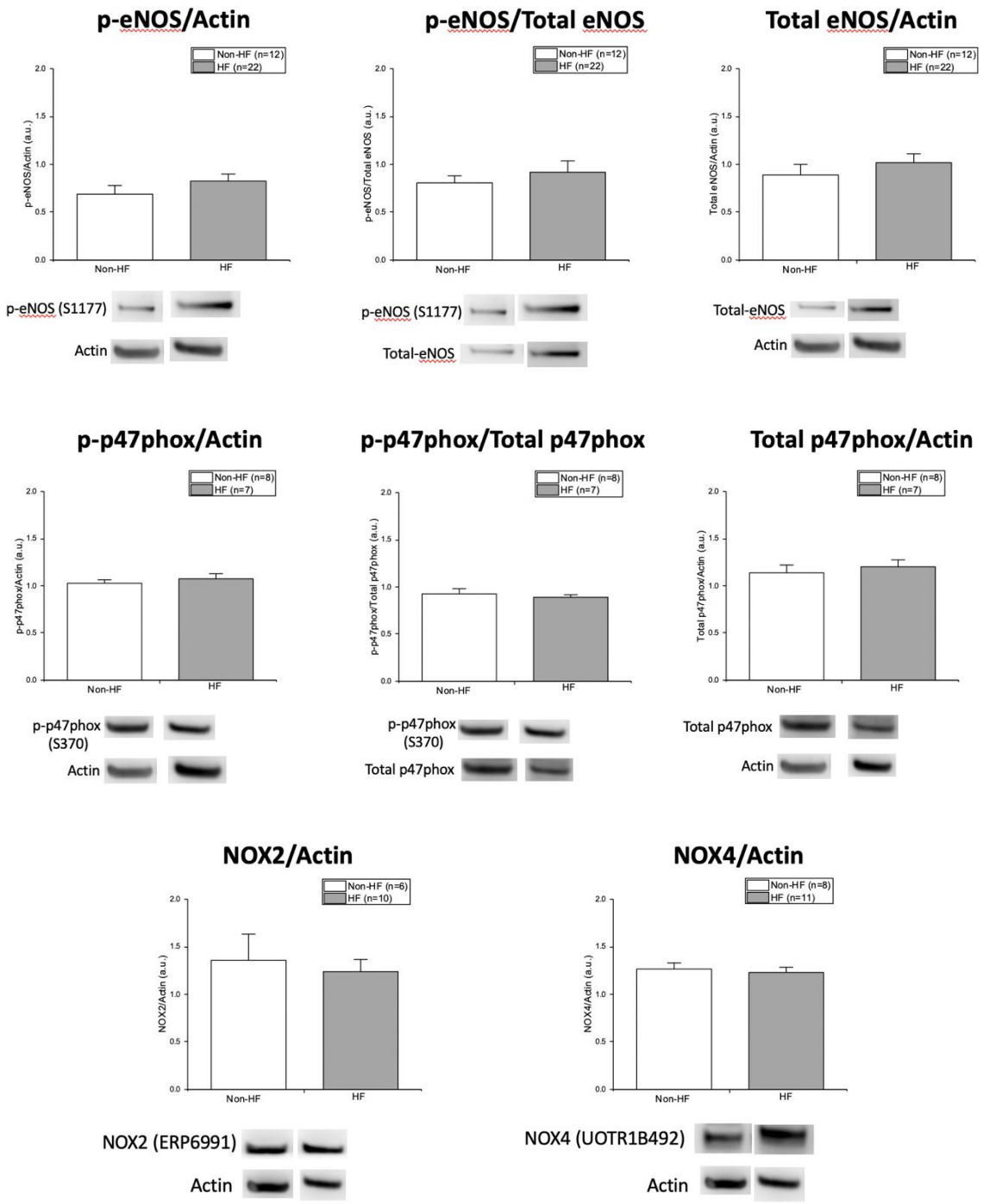

Figure 24: Protein expression of basal phospho-IR, total IR, IGF1R, phospho-Akt, total Akt, phospho-eNOS, total eNOS, phospho-p47phox, total p47phox, NOX2, and NOX4 from human ATECs between the non-HF and HF groups.

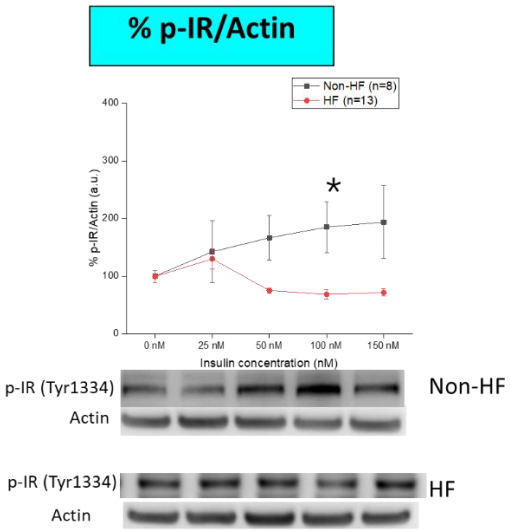
% p-IR/Actin
Non-HF (n=8)
HF (n=13)
% p-IR/Actin (a.u.)
Insulin concentration (nM)
0 nM
25 nM
50 nM
100 nM
150 nM
*
p-IR (Tyr1334)
Actin
Non-HF
p-IR (Tyr1334)
Actin
HF

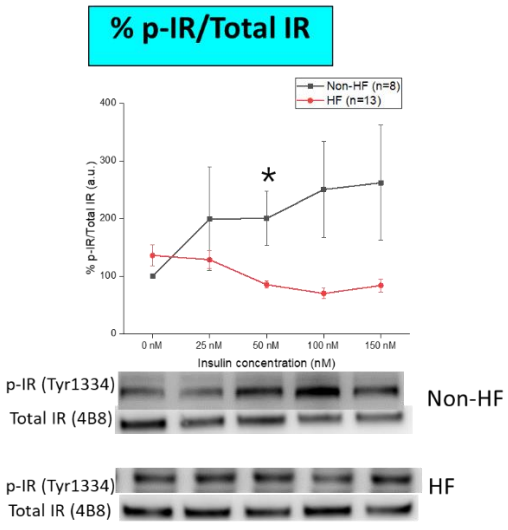
% p-IR/Total IR
Non-HF (n=8)
HF (n=13)
% p-IR/Total IR (a.u.)
Insulin concentration (nM)
0 nM
25 nM
50 nM
100 nM
150 nM
*
p-IR (Tyr1334)
Total IR (4B8)
Non-HF
p-IR (Tyr1334)
Total IR (4B8)
HF

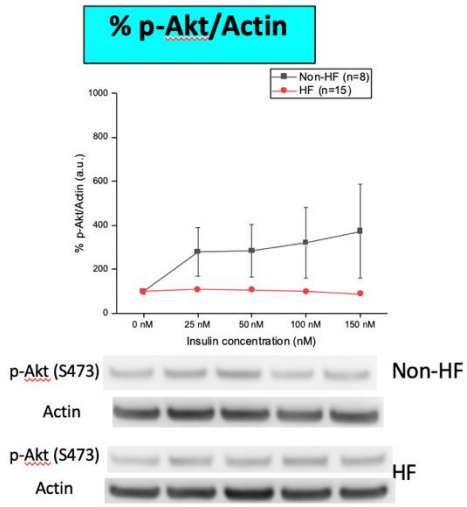
% p-Akt/Actin
Non-HF (n=8)
HF (n=15)
% p-Akt/Actin (a.u.)
Insulin concentration (nM)
0 nM
25 nM
50 nM
100 nM
150 nM
p-Akt (S473)
Actin
Non-HF
p-Akt (S473)
Actin
HF

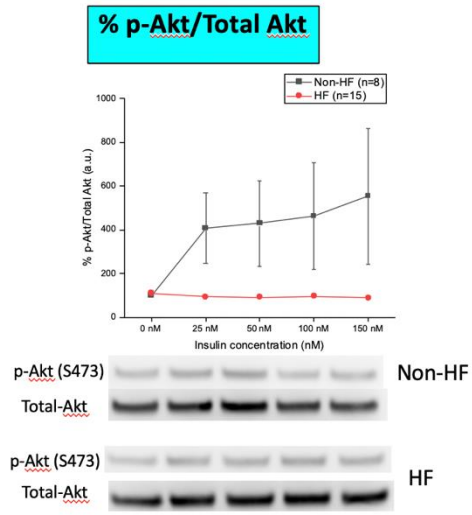
% p-Akt/Total Akt
Non-HF (n=8)
HF (n=15)
% p-Akt/Total Akt (a.u.)
Insulin concentration (nM)
0 nM
25 nM
50 nM
100 nM
150 nM
p-Akt (S473)
Total-Akt
Non-HF
p-Akt (S473)
Total-Akt
HF

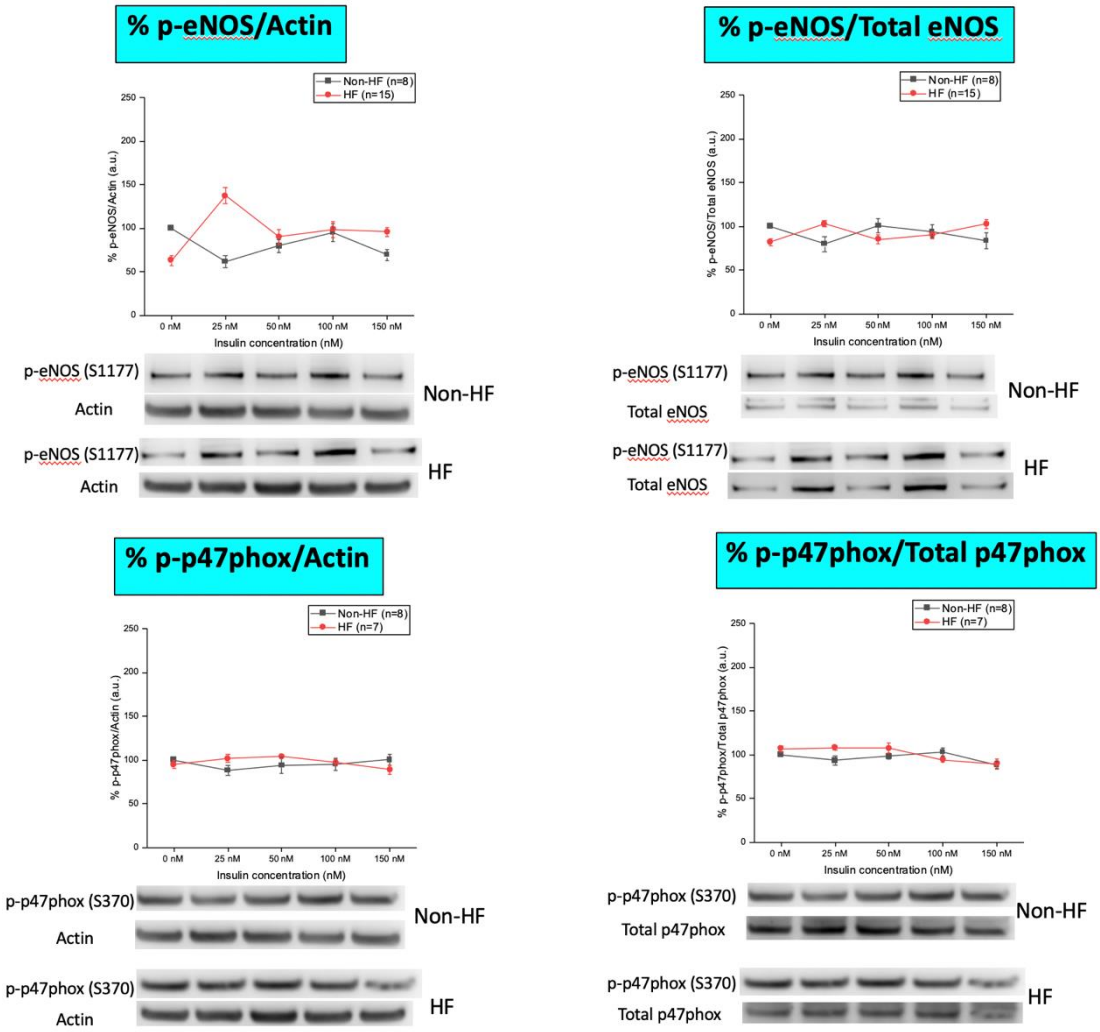

Figure 25: Insulin-stimulated phosphorylation of IR, Akt, eNOS, and p47phox from human ATECs between the non-HF and HF groups. Values (means ± SE) are expressed relative to no insulin (asterisks denote statistical significance with p-value less than 0.05).

5.5 Superoxide production in endothelial cells

We used lucigenin-enhanced chemiluminescence (100 µM) to quantify NADPH-dependent superoxide production. At the start of this experiment, human coronary artery endothelial cells (HCAECs, Lonza cells) were used to compare the normal and DM groups. As shown in Figure 26, superoxide production was higher in the DM group than in the normal group.

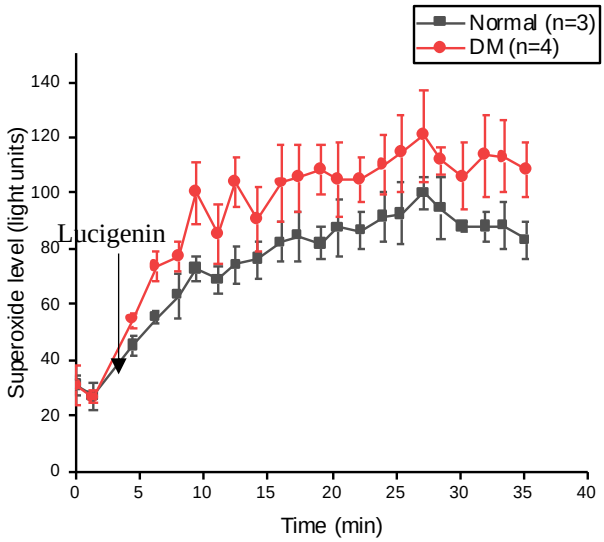

Figure 26: Lucigenin-enhanced chemiluminescence of HCAECs (Lonza cells) between the normal (n = 3) and DM (n = 4) groups.

For ATECs, data indicated that superoxide production was higher in the HF and DM/HF groups compared to DM conditions (153.3 vs 121.2, $p = 0.018$ and 173.7 vs 121.2, $p < 0.001$, respectively), implying that HF was a major contributor to increased superoxide production when compared with diabetes (Figure 27).

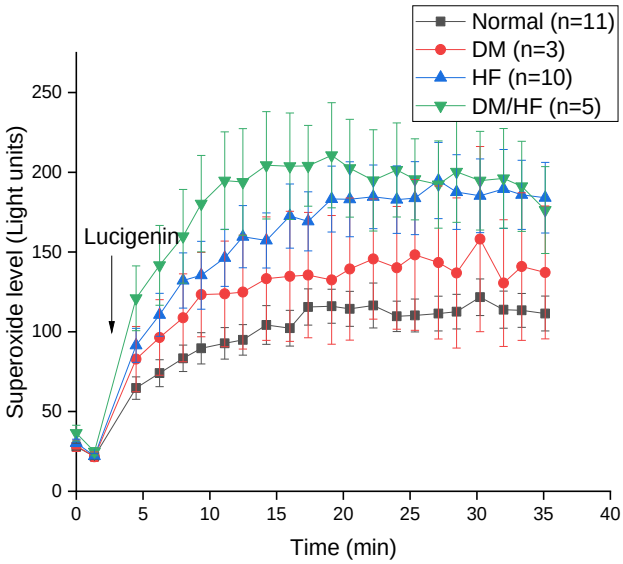

Figure 27: Lucigenin-enhanced chemiluminescence of ATECs between the normal (n = 11), DM (n = 3), HF (n = 10), and DM/HF (n = 5) groups.

When superoxide production in ATECs was observed in the non-DM and DM groups, the data revealed that the DM group tended to produce higher levels of superoxide than the non-DM group (Figure 28). Between the non-HF and HF ATECs,

the HF condition produced significantly more superoxide compared to the non-HF condition (160.1 vs 101.8, $p < 0.001$), as shown in Figure 29.

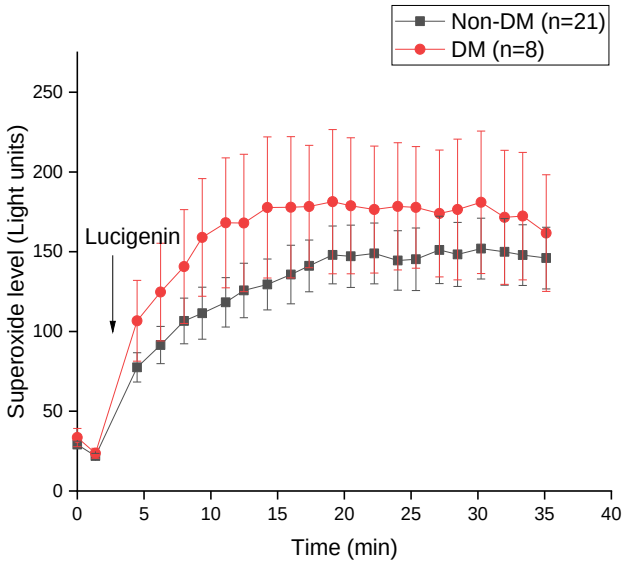

Figure 28: Lucigenin-enhanced chemiluminescence of ATECs between the non-DM (n = 21) and DM (n = 8) groups.

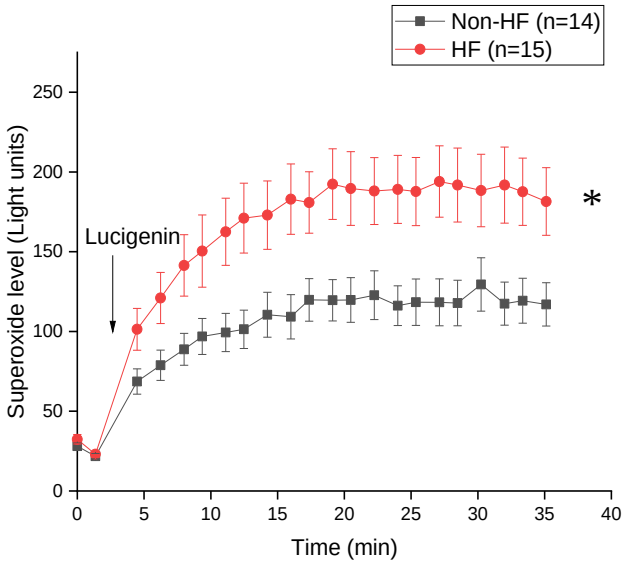

Figure 29: Lucigenin-enhanced chemiluminescence of ATECs between the non-HF (n = 14) and HF (n = 15) groups.

Superoxide production was quantified in ATECs following 100 nM insulin stimulation. The normal group showed higher production of superoxide ($p = 0.011$), whereas the HF and DM/HF groups had lower production of superoxide ($p = 0.027$ and < 0.001, respectively) (Figure 30).

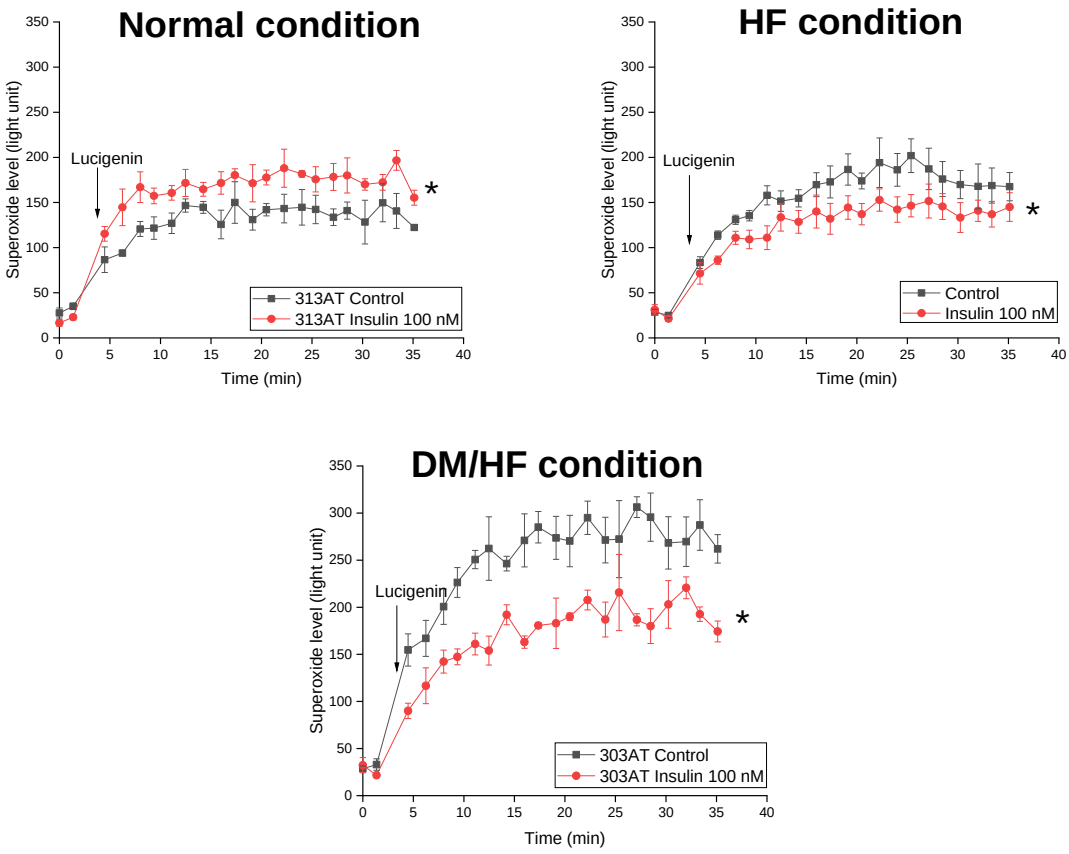

Figure 30: Insulin stimulated the production of superoxide in ATECs under normal, HF, and DM/HF conditions.

5.6 Angiogenic capacity of adipose tissue

The angiogenesis assay was performed on subcutaneous white adipose tissue. On day 7, when the adipose tissue was assessed, the number of sprouts was difficult to count (Figure 31). As a result, the present study evaluated angiogenesis function on day 4.

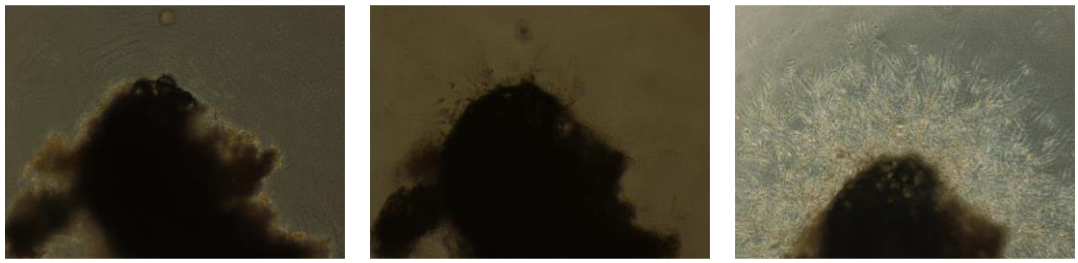

Figure 31: Angiogenesis assay of human white adipose tissue. On day 7, when adipose tissue was assessed, the number of sprouts was difficult to count.

For the first time, the experiment utilised fresh adipose tissue. Table 12 shows the patient characteristics and preliminary angiogenesis results. If fresh adipose tissue is used, the experiment must be conducted late in the day. As a result, the tissue was stored overnight in a tissue storage solution (Miltenyi Biotec) to allow us to perform the angiogenesis assay on the following morning. However, storing tissue overnight did not yield favourable results, as evidenced by the absence of sprout formation on day 4 in all samples (Table 13). As a result, all samples were assayed for angiogenesis on the same day as the tissue samples were collected.

Table 11: Patient characteristics and results of the angiogenesis assay on fresh adipose tissue.

Characteristic	Sample 189	Sample 190	Sample 191	Sample 192	Sample 193
Gender	Male	Male	Male	Male	Male
Age	71	79	67	61	81
BMI (kg/m^2)	41.08	27.16	28.96		24.16
Medical condition					
Diabetes mellitus	No	No	**Yes**	**Yes**	No
Hypertension	No	No	Yes	No	Yes
Hyperlipidemia	Yes	No	Yes	Yes	Yes
Congestive heart failure	**Yes**	**Yes**	No	**Yes**	No
Coronary artery disease	**Yes**	**Yes**	**Yes**	No	No
Type of tissue	**Fresh**	**Fresh**	**Fresh**	**Fresh**	**Fresh**
Average number of sprouts (10 wells per sample) Day 4	32	33	0	39	24
Average length of sprouts (10 wells per sample) Day 4 (µm)	N/A	327.03	0	187.47	179.56

Table 12: Patient characteristics and results of the angiogenesis assay on adipose tissue stored overnight in tissue storage solution (preserved).

Characteristic	Sample 194	Sample 195	Sample 196	Sample 197	Sample 198	Sample 200	Sample 201	Sample 202	Sample 203	Sample 204
Gender	Male	Female	Male	Male	Male	N/A	Male	Female	Female	Male
Age	82	81	84	32	67	N/A	67	77	94	79
BMI (kg/m^2)	27.68	22.49	28.38	25.08	N/A	N/A	20.89		25.5	30.6
Medical condition										
Diabetes mellitus	Yes	No	No	No	Yes	N/A	No	Yes	No	Yes
Hypertension	No	Yes	Yes	No	No	N/A	No	No	No	Yes
Hyperlipidemia	N0	No	No	No	No	N/A	No	No	No	No
Congestive heart failure	Yes	Yes	No	No	Yes	N/A	No	No	Yes	No
Coronary artery disease	Yes	No	No	No	Yes	N/A	No	No	No	No
Type of tissue	Preserved	Preserved	Preserved	Preserved	Preserved	Preserved	Preserved	Preserved	Fresh	Fresh
Average number of sprouts (10 wells per sample) Day 4	0	0	0	0	0	0	0	0	**23**	**0**
Average length of sprouts (10 wells per sample) Day 4 (µm)	0	0	0	0	0	0	0	0	**255**	**0**

For angiogenesis results, Figure 32 and 33 show that the diabetes condition resulted in a lower number of sprouts and a significantly lower length of sprout on day 4. However, there was no significant difference in the number and length of sprouts on day 4 between samples that were classified as non-HF or HF (Figure 34).

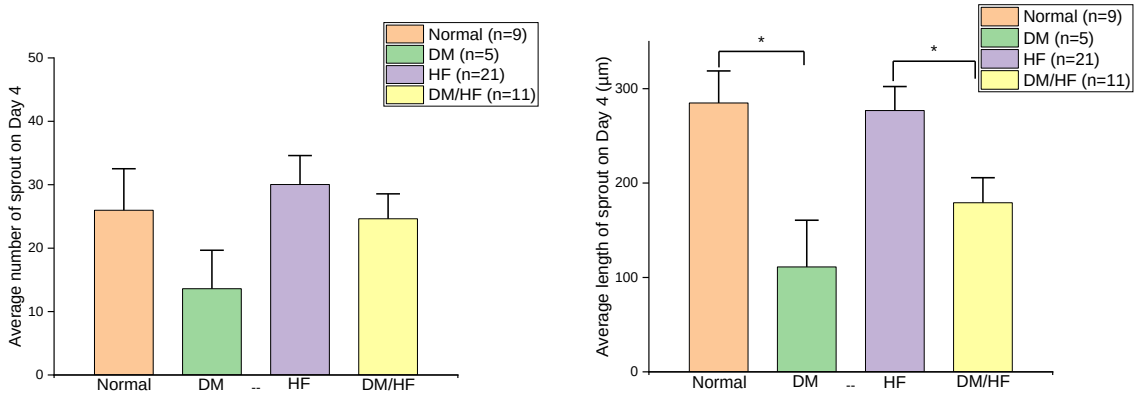

Figure 32: Average sprout number and length on day 4 in human white adipose tissue between the normal (n = 9), DM (n = 5), HF (n = 21), and DM/HF (n = 11) groups.

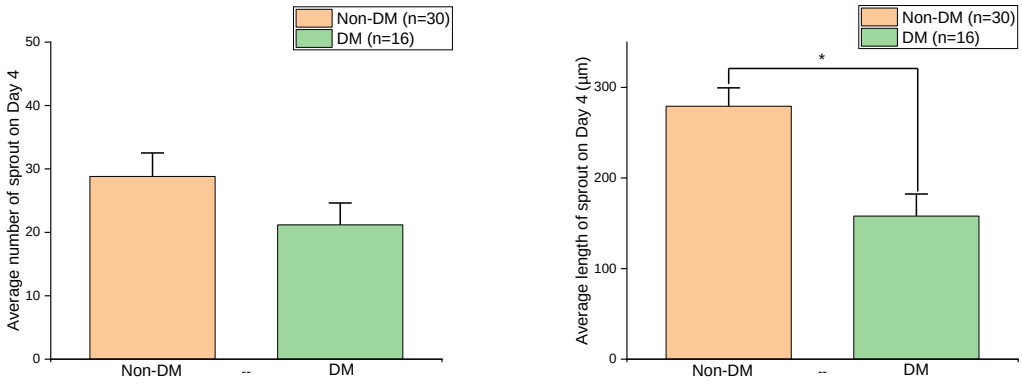

Figure 33: Average sprout number and length on day 4 in human white adipose tissue between the non-DM (n = 30) and DM (n = 16) groups.

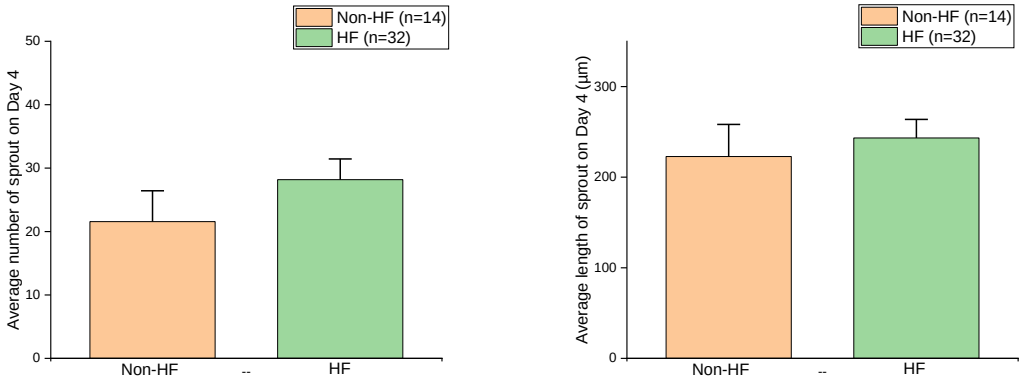

Figure 34: Average sprout number and length on day 4 in human white adipose tissue between the non-HF (n = 14) and HF (n = 32) groups.

Chapter 6: **Discussion**

6 Discussion

HF and diabetes, which both involve insulin resistance and have a significant association with endothelial dysfunction, are common high-morbidity and high-mortality diseases whose prevalence continues to increase. In order to explore their possible overlapping pathophysiologies at a cellular level with a view to novel therapies, endothelial cells have been extensively studied. It is now known that endothelial cells demonstrate a high degree of heterogeneity, not only between macro- and microvascular endothelial cells, but also between microvascular endothelial cells from different organs. Previously, the most common source of endothelial cells for research was from human umbilical veins; however, the HUVECs derived from neonatal tissue had differing physiology and did not constitute an ideal model for studying most physiological and pathological conditions. While the lack of a human microvascular endothelial cell model represents a gap in the research, our own laboratory group proposed a novel method of isolating adipose tissue- and skeletal muscle-derived endothelial cells from patients undergoing CIED implantation. This novel method helps to improve the quality and the translational value of HMVEC research in our laboratory. Understanding the functional characteristics of HMVECs from the perspective of a specific real-life patient is valuable and could lead to the future development of specialised therapeutics.

The present study aimed to investigate insulin signalling and functional characteristics of HMVECs in HF and diabetes patients. Several interesting findings were generated from this work. First, after HMVEC isolation, we demonstrated the feasibility of isolating HSkMECs and HATECs, and that they were pure enough to be used in the experiment. The isolated cells from skeletal muscle and adipose tissue showed significant calcium influx in response to VEGF, confirming a high population of endothelial cells. The purity of the isolated HSkMECs and HATECs was represented by their CD31-PerCP and CD144-PE positivity and CD45-FITC negativity on fluorescent staining (98.0 ± 1.0% and 98.0 ± 0.7%, respectively).

Insulin signalling in endothelial cells was investigated by comparing gene and protein expression between normal, DM, HF, and DM/HF conditions. In terms of gene expression, it was apparent that Akt3 and catalase mRNA expression was increased in the diabetic group; however, eNOS mRNA expression was significantly decreased in the diabetic group as compared with the non-diabetic group. In terms of protein expression, there were no significant differences between the diabetic and non-diabetic groups regarding basal phosphorylation of IR, Akt, eNOS, p47phox, total IGF1R, NOX2, and NOX4. Regarding insulin-stimulated phosphorylation, while IR and Akt phosphorylation showed a blunted response to insulin in the diabetic group, there was no significant difference in eNOS and p47phox phosphorylation between the non-diabetic and diabetic groups.

The present study investigated the angiogenic function of endothelial cells, and the results revealed that sprout length on day 4 was considerably shorter in the diabetic group when compared with the non-diabetic group, whereas HF did not significantly reduce angiogenesis. Among the various essential functions of HMVECs, angiogenesis is a vital process for generating new blood vessels to reperfuse tissues following an ischemic vascular occlusion. HMVECs play a critical role in angiogenesis research as angiogenesis does not occur in large blood vessels. Furthermore, angiogenesis also associated with insulin resistance, which is a condition that leads to excessive ROS generation.

Overproduction of ROS interferes with vascular regeneration, repair, and causes vascular injury. Additional work from our laboratory demonstrated that insulin resistance was characterised by increased NOX2-derived vascular superoxide. However, complete removal of NOX2 in mice with endothelial cell insulin resistance worsened vascular damage, whereas partial pharmacological NOX2 inhibition protected from vascular injury (207). This research suggests that NOX2-derived ROS has a dual effect: it is beneficial at low-to-normal concentrations but harmful at high, pathological concentrations.

Finally, lucigenin-enhanced chemiluminescence was used to study the superoxide production of endothelial cells in each condition. The data showed that

superoxide production was trending towards being higher in the diabetic group compared to the non-diabetic group. However, when comparing the diabetes and heart failure groups, it was discovered that superoxide production was significantly higher in the heart failure group. Furthermore, we found that insulin activated superoxide production under normal conditions, but inhibited superoxide production in insulin resistance.

Each of these findings will be discussed in additional detail in the following section.

6.1 Summary of key findings

6.1.1 Isolation and confirmation of identity of the endothelial cells

While most of the research on endothelial cells has been derived from the study of large vessels, such as HUVECs, the study of HMVECs remains under-investigated. In this study, our laboratory group described a novel method for isolating HMVECs from patients undergoing CIED implantation. This method allows for the simple acquisition of fresh skeletal muscle from the pectoralis major and subcutaneous white adipose tissue with minimal risk of haemorrhage, similar to that seen in regular CIED implantation, approximately 0.58–2.81% (208). As stated in section 4.1.2, isolating HMVECs is a time-consuming process that takes approximately 5–6 hours. After transporting the tissue biopsy from the operating room to the laboratory in the afternoon, the experiment to isolate endothelial cells was completed in the late evening. As a result, the tissue storage solution was used to store the fresh tissue overnight so that the endothelial cells could be isolated the next morning.

For the beginning step of isolation, the immuno-magnetic separation technique of MACS (magnetically-activated cell sorting) technology was used with CD31-coated magnetic beads as the primary antibody. CD31, also known as platelet endothelial cell adhesion molecule-1 (PECAM-1), is expressed in large amounts on mature endothelial cells at intercellular junctions, platelets, and on some white blood cells, such as monocytes, NK cells, granulocytes, B cells, and T cells. However, we discovered that the isolated cells were contaminated by RBCs, which have magnetic

properties due to their iron content. Therefore, the protocol for isolating endothelial cells was modified by adding additional steps to eliminate RBCs. Furthermore, isolated cells grew slowly in cell culture during the first step. We hypothesised that the sudden and severe environmental stress from the endothelial cell isolation process led to cell swelling and eventual lysis. Because dead cells impair viability and may induce apoptosis in endothelial cell cultures, this study attempted to remove the dead cells during the isolation process. After removing the dead cells, microscopy revealed that the cells grew rapidly in the first week and reached confluence in 1 month in a 24-well plate.

Isolating cells using MACS technology is advantageous because it is a highly selective and rapid method for isolating target populations or removing undesirable cells with a high degree of specificity. However, one of the disadvantages of magnet separators is the inefficient drainage of unbound cells, which results in many unbound cells remaining with the bound cells. Therefore, isolating cells from skeletal muscle can occasionally lead to contamination of the sample with skeletal muscle or fibroblastic cells. If the morphology showed clearly contamination, further confirmation methods were not necessary to be conducted. In contrast, isolating cells from adipose tissue yields superior outcomes with less contamination.

The morphology of isolated cells was a cobblestone monolayer pattern that was compatible with endothelial cells and a cell diameter of 17–20 μm. However, the cobblestone morphology can be found in other cell types, such as mesothelial and epithelial cells. As a result, analysing the morphology of isolated cells is not reliable and is insufficient to confirm the presence of endothelial cells.

Confirmation of endothelial cells can be achieved using a variety of classic endothelial cells markers, such as CD31 (PECAM-1), CD54 (ICAM-1), von Willebrand factor (vWF), Weibel-Palade bodies (WPB), angiotensin-converting enzyme (ACE, CD143), and CD144 (VE-cadherin) (209). Endothelial cells can also be confirmed using functional assays, such as VEGF stimulation, NO production, uptake of a fluorescent, labelled, acetylated LDL, or the presence of the endothelial surface layer (ESL) (including glycocalyx) by using a fluorescent labelled lectin (e.g., wheat germ agglutin). In this study, the fluorescence method for calcium measurement was used.

The purpose of this method is to demonstrate the intracellular calcium flux of the endothelial cells stimulated by VEGF. This technique established that the isolated cells were endothelial cells by their induction of a significant calcium influx in response to VEGF. However, this method cannot demonstrate the purity of the endothelial cells. Therefore, before proceeding with further aspects of the experiment, the purity of the isolated endothelial cells had to be determined.

Flow cytometry with specific markers was used to confirm the purity of the endothelial cells. The fluorochrome-labelled antibodies used in this method are CD31-PerCP, CD144-PE, and CD45-FITC. CD144, also known as vascular endothelial (VE)-cadherin, is express in all types of endothelia. CD45, also known as leucocyte common antigen, is a transmembrane protein tyrosine phosphatase located on most haematopoietic cells. Therefore, CD45-FITC-positive cells were gated out to exclude haematopoietic cells, whereas CD31-PerCP-positive and CD144-PE-positive cells were gated to be compatible with endothelial cells. This study found that isolated cells from skeletal muscle (HSkMECs) and adipose tissue (HATECs) were positive for CD31-PerCP and CD144-PE and negative for CD45-FITC on fluorescent staining (98.0 ± 1.0% and 98.0 ± 0.7%, respectively). This finding indicated that the isolated endothelial cells had a high purity and were pure enough to be used in the experiments. Furthermore, this method produced higher yields than previous methods for isolating endothelial cells (purity of 91.0 ± 1.0%, n = 6) (210), and the cells exhibited typical endothelial morphological and phenotypic characteristics.

6.1.2 Insulin signalling in human microvascular endothelial cells

In general, insulin signalling gene and protein expression varies by tissue and in response to environmental signals, and our research investigated this critical pathway in HMVECs between normal, DM, HF, and DM/HF conditions.

6.1.2.1 Gene expression

In terms of gene expression, cDNA samples were stored at -20 °C to prevent degradation and frequent freeze/thaw cycles were avoided. However, cDNA is a highly

unstable single-stranded DNA and should be used as soon as possible due to the scarcity of stability data at 4 °C. All data for the real-time PCR analysis in this study were obtained from cDNA samples that were prepared in less than 1 week because, as shown in Table 9, we discovered that cDNA had a higher CT value when stored at 4 °C for longer than 8 weeks. The findings of the present study are consistent with the findings of Wilkening and Bader (211), who demonstrated that cDNA degrades 50% after 3 weeks of storage at 4 °C.

Insulin resistance and hyperinsulinaemia produced several changes in the mRNA levels of the investigated genes. Our study discovered that, while Akt3 and catalase mRNA expression increased significantly in the diabetic group, eNOS mRNA expression decreased significantly in the diabetic group compared with the non-diabetic group. Contrary to our expectations, previous research using HUVEC cells from patients with gestational diabetes revealed modest reductions in transcript levels, specifically affecting the IR-A isoform (212). However, these findings were consistent with those of Qin and colleagues (77), who found that, while high glucose increased Akt3 mRNA expression, it had no effect on the other isoforms of Akt genes and proteins Akt1, Akt2, p-Akt (Ser 473), and p-Akt (Thr 308). Furthermore, our findings on SOD1 and catalase mRNA expression corroborate those of Limaye and colleagues, who reported that diabetic mice had higher levels of both SOD1 and catalase gene expression (213). Our findings regarding eNOS mRNA were consistent with those of Srinivasan and colleagues, who reported that diabetic mice had decreased eNOS mRNA expression (214).

We discovered that NOX2 genes were difficult to demonstrate in real-time PCR, despite using several NOX2 primer sequences (Table 10). This challenge may be due to low NOX2 mRNA expression in subcutaneous adipose tissue endothelial cells (SATECs). According to previous data, van Buul et al. discovered that NOX4 mRNA was expressed at 100-fold higher levels than NOX2 mRNA in HUVECs (115). Gray et al. found that NOX4 levels were inversely correlated with NOX2 gene and protein levels (121). Therefore, some of the protective effects of NOX4 may be mediated through downregulation of NOX2, and disruption of physiological endothelial NOX4

signalling is thought to be a precursor to metabolic disease pathology via upregulation of other NOX isoforms.

NOX2 may play a minor role in SATECs. If we compare subcutaneous adipose tissue (SAT) and visceral adipose tissue (VAT) in the human body, VAT expansion is significantly associated with increased cardiometabolic risks (215) and more associated with systemic endothelial dysfunction than SAT (216). Due to the difficulty of real-time PCR expression in our study, NOX2 mRNA expression may be low in SATECs. This finding may also be attributed to the fact that NOX2 is an important source of superoxide anion (107), and that it plays a vital role in insulin resistance. Therefore, the location of adipose tissue endothelial cells is an important factor in superoxide production, and future studies on specific cell types will contribute to a more complete understanding of the oxidative stress produced by SATECs and visceral adipose tissue endothelial cells (VATECs).

Our findings for NOX4 mRNA indicated that there was no significant difference between expression in the diabetic and non-diabetic groups. Jiao and colleagues discovered that high glucose levels significantly increased NOX4 mRNA expression in HRECs, whereas NOX1, NOX2, NOX3, and NOX5 mRNA expression levels remained unaffected (217). Endothelial NOX4 is important in high glucose-induced pathological signalling because it alters ROS production, resulting in increased inflammation and fibrosis, which appears to be more severe in the microvasculature. This inconsistency could be explained by the fact that our P3 HATECs were cultured in media without added glucose; as a result, NOX4 mRNA expression was consistent across all HATEC conditions.

Our study discovered that there was no significant difference in the expression of IR, IGF1R, Akt1, Akt2, Akt3, eNOS, SOD1, SOD2, and catalase mRNA between the HF and non-HF groups, whereas NOX4 mRNA expression showed a trend towards being lower in the HF group. This finding could be explained by the fact that the protective effect of NOX4 was diminished in HF (121, 218). However, some contrasting findings have been published that demonstrated that NOX4 expression was significantly upregulated in HF patients and had a detrimental effect (219).

Therefore, to increase the reliability of the experimental results, the number of samples must be increased in future experiments.

6.1.2.2 Protein expression

Regarding protein expression, one must consider that mRNA levels do not always correspond to protein expression levels. There were no significant differences in basal phosphorylation of IR, Akt Ser473, eNOS Ser1177, p47phox, total IGF1R, NOX2, and NOX4 between the non-diabetic and diabetic groups, or between the non-HF and HF groups. This finding could be explained by the fact that HATECs were cultured in media without the addition of glucose or shear stress. As a result, the downstream insulin signalling proteins in the different conditions were unaffected.

6.1.2.3 Insulin-stimulated phosphorylation

We demonstrated phosphorylation of the target protein after 10 minutes of various insulin dosing: 0, 25, 50, 100, and 150 nM (dose response experiments). We intend to use supraphysiological insulin concentrations for stimulating and detecting phosphorylation of proteins. Physiological insulin levels between meals range from 57 to 79 pmol/L; during digestion 1–2 hours following the meal, insulin levels oscillate every 3–6 minutes, fluctuating between >800 pmol/L and <100 pmol/L (220). Therefore, insulin concentrations of 25, 50, 100, and 150 nM were suitable for stimulating phosphorylation of proteins of insulin signalling pathway.

Typically, following insulin stimulation, Akt phosphorylation at Thr308 and Ser473 peaks around 2–5 minutes and is sustained for at least 2–3 hours post-stimulation (221). Kong and colleagues discovered that 5 minutes of low shear stress increased eNOS Ser1177 phosphorylation in HUVECs (222). Furthermore, Salt and colleagues discovered that after 1–2 minutes, insulin stimulated NO production in HAECs (223). Therefore, detecting phosphorylated proteins at a time interval of 10 minutes was considered appropriate for our study. As a result of the design of this experiment, data were analysed at a single interval rather than over a specific period, as in a time-course experiments; therefore, this experiment examined the effect of insulin at various concentrations. While time-course experiments are frequently used

to establish the duration of insulin effects observed at various insulin doses over a specific period, we intended to conduct this experiment in the following step.

While insulin had a minimal effect on stimulating IR and Akt phosphorylation in the diabetic and HF groups, insulin had a significant effect on stimulating IR and Akt phosphorylation in the non-diabetic and non-HF groups. Furthermore, we found that phosphorylation of eNOS and p47phox did not respond to insulin stimulation, which was observed in all groups. Surprisingly, while insulin increased Akt phosphorylation, it had no effect on eNOS phosphorylation in the non-diabetic and non-HF groups. This finding was unexpected and implied that phosphorylation of Akt did not result in the activation of eNOS phosphorylation at Ser1177. This result could be explained by a variety of factors, including increased PKC signalling or decreased VEGF levels during this experiment, both of which resulted in dephosphorylation of eNOS at Ser1177 (83).

6.1.3 Functional characterisation of human microvascular endothelial cells

6.1.3.1 Adipose tissue angiogenesis

Our research revealed that adipose tissue cannot be stored in a tissue storage solution overnight for angiogenesis. As shown in Table 12, no sprout formation was observed on day 4 in any of the preserved samples. The findings of this study are consistent with those of Rojas-Rodriguez and colleagues, who recommended that the time between removing adipose tissue from a human subject and embedding it in Matrigel should be kept to a minimum, preferably under 3 hours (224). Therefore, while we currently have a tissue storage solution that can preserve skeletal muscle and adipose tissue for endothelial isolation, we cannot use this solution to preserve tissue samples for angiogenesis assays. As a result, all samples were tested for angiogenesis within 3 hours of tissue collection.

Our findings are consistent with those of Inoue and colleagues (225), who discovered that diabetes impaired adipose tissue angiogenesis. As previously mentioned, diabetes causes poor angiogenesis through a variety of mechanisms, including decreased proangiogenic factors and signal transduction issues (203). However, we discovered that HF had no effect on adipose tissue angiogenesis (Figure

34), in contrast to Cunningham and Gotlieb's earlier finding that decreased shear stress impaired endothelial function and angiogenesis in HFrEF (198). Shear stress is known to play a significant role in the formation of blood vessels, specifically in angiogenesis. One hypothesis is that adipose tissue from the non-HF and HF conditions was cultured in vitro in a similar environment, free from shear stress; therefore, there was no significant difference in adipose tissue angiogenesis between the non-HF and HF conditions.

6.1.3.2 Superoxide production

Our findings indicated that HF conditions produced the most superoxide when compared with diabetes and normal conditions. Our findings were consistent with the findings of Dworakowski and colleagues, who reported that HF conditions generated over twofold more NADPH-dependent superoxide than non-HF conditions (226). Furthermore, Sukumar and colleagues demonstrated that the pulmonary endothelial cells (PECs) of insulin-resistant mice generated approximately 1.6-fold more superoxide than wild-type PECs (108). Our findings thus support that oxidative stress is an important mechanism in the development of insulin resistance in HF.

Oxidative stress is caused not only by an increase in ROS production, but also by impaired antioxidant defence systems. A previous study reported that targeted antioxidant therapy can partially restore abnormal insulin signalling and improve cardiac structure and function (227). Furthermore, various antioxidants have been investigated. However, clinical trials on the cardioprotective potential of antioxidants in the treatment of cardiac dysfunction remain inconclusive. Therefore, there remains a gap in our understanding of antioxidants and their use in cardiometabolic diseases.

6.2 Limitations

6.2.1 Factors affecting insulin sensitivity and insulin signalling

The results of this investigation of insulin signalling may not be as straightforward as those obtained from cell lines or animal models in which variables

affecting downstream protein expression levels can be controlled. In human studies, a variety of factors, such as obesity, hypertension, and medications all influence insulin signalling.

From patient characteristics in our study, mean BMI of normal group was 28.1 ± 3.6 kg/m^2, which was defined as ‘overweight’ and possibly associated with insulin resistance. Obesity, particularly central abdominal obesity, has been shown to have a detrimental effect on insulin sensitivity (228). In the diabetic group in our study, 71% of patients received metformin, which previous studies found that metformin improve insulin sensitivity in the liver, muscle, and adipose tissue via both AMPK-dependent and AMPK-independent mechanisms (229). Metformin also reduces hyperinsulinemia and hyperglycaemia, both of which have the effect of lowering the levels of ROS (230). Additionally, other conditions characterized by insulin resistance, including sepsis, cancer cachexia, starvation, acromegaly, burn trauma, metabolic syndrome, and increased levels of ROS (231). All these conditions can also affect the downstream proteins of the insulin signaling pathway.

Overexpression of Akt has been observed in breast cancer, colorectal cancer, and a variety of other cancers. For phospho-eNOS Ser1177, several factors can increase their activity, such as shear stress, VEGF, IGF1, oestrogen, adiponectin, leptin, and statins. Furthermore, other diseases have been observed to decrease phospho-eNOS Ser1177, including atherosclerosis, hyperhomocysteinaemia, hypoxia, Alzheimer's disease, and cancer (232). Therefore, other factors affecting the insulin signalling pathway should be thoroughly investigated and evaluated for more explicitly.

6.2.2 Contamination of HSkMECs

This research focused on HMVECs isolated from skeletal muscle and adipose tissue. During the process of isolating endothelium cells from skeletal muscle, a significant proportion of the sample was contaminated with skeletal muscle cells (Figure 15). Due to this contamination, the sample of HSkMECs was insufficient for subsequent tests. As a result, the current study focused exclusively on HATECs. The endothelial cells from skeletal muscle remain an interesting model for studying insulin

signalling. Therefore, future research on HSkMECs will contribute to the establishment of a more comprehensive understanding of HMVECs.

6.2.3 Small sample size

One of the limitations of the current study was the relatively small sample size for the experiments. The COVID-19 pandemic limited access to collect the fresh tissue since the laboratories were closed in response to the ‘stay at home’ order. However, the sample size used in this study was intended to be exploratory, rather than to provide definitive conclusions. Taking this into consideration, we believe that the sample sizes reflected a reasonable compromise that enabled the generation of data that could serve as the basis for future research.

6.2.4 Model of angiogenesis

The model of angiogenesis used in this study was a simplification of the human disease process. Because angiogenesis in humans is highly complex and involves several different pathways, experiments on model adipose tissue angiogenesis are approximations rather than true representations of clinical pathology. Furthermore, the number of sprouts observed may be somewhat limited in our angiogenesis assay, as we could not quantify sprouts above and below the adipose tissue using a microscope. However, the mean number of sprouts that grew on the side of the adipose tissue could be approximated.

6.3 Future directions

6.3.1 Insulin signalling in HMVECs

This thesis focused on the different molecular and cellular genes and proteins involved in insulin signalling in insulin-resistant states of HMVECs. However, other important proteins are also worth studying, including IRS, PI3K, FOXO transcription factors, AMPK, mTOR, and GLUT4. It is important to assess the duration of insulin effects on the proteins of interest by administering 100 nM insulin and harvesting the cells at various periods in a time-course experiment of insulin-stimulated protein

phosphorylation. However, the differences in basal levels of proteins and phosphoproteins in the insulin signaling pathway in freshly isolated endothelial cells are more important. This is because freshly isolated cells are more closely resemble the in vivo environment and therefore provide a more accurate representation of the physiological state.

It would also be beneficial to investigate insulin signalling in other insulin-sensitive human tissues, such as muscle and liver tissue. Moreover, future research comparing SATECs and VATECs in adipose tissue would aid in the development of a more complete understanding of insulin signalling and oxidative stress between those tissues, particularly in epicardial adipose tissue.

It would be interesting to compare gene expression between normal and abnormal endothelial cells in HF and diabetes using RNA sequencing. This technique is more effective for identifying genes of interest. However, RNA sequencing is limited in part by financial and time constraints, and specialist analysis is required to adequately examine the large amount of data generated by this process.

6.3.2 HMVECs in other functional assays

Another important issue concerns experiments on adipose tissue angiogenesis. Although this experiment is more real-world setting because it conducted on whole tissue, the results may not reflect the true function of endothelial cells. Endothelial cell angiogenesis is thus a promising area of future research.

Additional functional assays of interest include determining the effects of insulin resistance and oxidative stress on migration and proliferation of HMVECs, in addition to the production of other ROS, such as hydrogen peroxide, by NOX4 in HMVECs. The previous study demonstrated that NOX4-derived ROS have a protective effect within the vasculature (121). However, it is important to establish better connections between the molecular and cellular phenotyping of the experiments and the patient phenotype to gain a more complete understanding in human health and disease.

6.3.3 The translational value of HMVEC research

As mentioned previously, increased superoxide production by a variety of cells in the vascular system contributes to oxidative stress in the vessel wall and the insulin-resistant state, which disrupts metabolic activity and cell structure. As a result, antioxidants were deemed the obvious solution, but have routinely failed in clinical trials and have occasionally caused harm (233). Prior research on antioxidants has shown that they are non-selective, interfering with both physiological and pathological ROS. As a result, future research on selective NOX inhibitors that are relevant to disease is worth studying.

6.4 Conclusion

The present study provides novel findings about insulin signalling in microvascular endothelial cells in patients with either HF or diabetes. To begin, we developed a novel method for isolating endothelial cells generated from adipose tissue and skeletal muscle from patients undergoing CIED implantation. The isolated cells were confirmed to have high-purity endothelial cells (>98%) and were deemed suitable for use in the experiment. We examined insulin signalling gene and protein expression in confirmed and purified endothelial cells under normal, DM, HF, and DM/HF conditions. We observed a decrease in eNOS mRNA expression in patients with diabetes. Furthermore, we discovered that NOX4 mRNA was expressed at a higher level than NOX2 mRNA in ATECs, despite the fact that NOX2 mRNA cannot be detected by PCR. Regarding protein expression, there were no significant differences in basal phosphorylation of IR, Akt Ser473, eNOS Ser1177, p47phox, total IGF1R, NOX2, and NOX4 between the non-diabetes and diabetes groups, and the non-HF and HF groups. Regarding insulin-stimulated phosphorylation in both the diabetic and HF groups, supraphysiological insulin concentration had a minor effect on the stimulated downstream insulin signalling pathway in the insulin-resistant states.

Regarding functional characterisation of HMVECs, we discovered that diabetic conditions impaired adipose tissue angiogenesis, whereas HF conditions had no effect on adipose tissue angiogenesis. These data must be interpreted with caution as the effect of shear stress was not observed in vitro. In terms of oxidative stress, we

discovered that ATECs under HF conditions produced significantly more superoxide than ATECs under diabetic conditions.

We hope that better understanding the functional characteristics of HMVECs from the perspective of a specific real-life patient will aid in the development of novel drugs and the improvement of existing ones. We believe that improved understanding insulin signalling has the potential to yield significant returns on investments in the near future.

7 References

1. Saeedi P, Petersohn I, Salpea P, Malanda B, Karuranga S, Unwin N, et al. Global and regional diabetes prevalence estimates for 2019 and projections for 2030 and 2045: Results from the International Diabetes Federation Diabetes Atlas, 9(th) edition. Diabetes Res Clin Pract. 2019;157:107843.
2. Saeedi P, Salpea P, Karuranga S, Petersohn I, Malanda B, Gregg EW, et al. Mortality attributable to diabetes in 20-79 years old adults, 2019 estimates: Results from the International Diabetes Federation Diabetes Atlas, 9(th) edition. Diabetes Res Clin Pract. 2020;162:108086.
3. Disease GBD, Injury I, Prevalence C. Global, regional, and national incidence, prevalence, and years lived with disability for 354 diseases and injuries for 195 countries and territories, 1990-2017: a systematic analysis for the Global Burden of Disease Study 2017. Lancet. 2018;392(10159):1789-858.
4. Lippi G, Sanchis-Gomar F. Global epidemiology and future trends of heart failure.
5. Benjamin EJ, Muntner P, Alonso A, Bittencourt MS, Callaway CW, Carson AP, et al. Heart Disease and Stroke Statistics-2019 Update: A Report From the American Heart Association. Circulation. 2019;139(10):e56-e528.
6. Bank IEM, Gijsberts CM, Teng TK, Benson L, Sim D, Yeo PSD, et al. Prevalence and Clinical Significance of Diabetes in Asian Versus White Patients With Heart Failure. JACC Heart Fail. 2017;5(1):14-24.
7. Cubbon RM, Adams B, Rajwani A, Mercer BN, Patel PA, Gherardi G, et al. Diabetes mellitus is associated with adverse prognosis in chronic heart failure of ischaemic and non-ischaemic aetiology. Diabetes & vascular disease research. 2013;10(4):330-6.
8. Russo I, Frangogiannis NG. Diabetes-associated cardiac fibrosis: Cellular effectors, molecular mechanisms and therapeutic opportunities. Journal of molecular and cellular cardiology. 2016;90:84-93.
9. Ponikowski P, Voors AA, Anker SD, Bueno H, Cleland JG, Coats AJ, et al. 2016 ESC Guidelines for the diagnosis and treatment of acute and chronic heart failure: The Task Force for the diagnosis and treatment of acute and chronic heart failure of the European Society of Cardiology (ESC)Developed with the special

contribution of the Heart Failure Association (HFA) of the ESC. European heart journal. 2016;37(27):2129-200.
10. Jia G, Whaley-Connell A, Sowers JR. Diabetic cardiomyopathy: a hyperglycaemia- and insulin-resistance-induced heart disease. Diabetologia. 2018;61(1):21-8.
11. Riehle C, Abel ED. Insulin Signaling and Heart Failure. Circ Res. 2016;118(7):1151-69.
12. Kim JA, Montagnani M, Koh KK, Quon MJ. Reciprocal relationships between insulin resistance and endothelial dysfunction: molecular and pathophysiological mechanisms. Circulation. 2006;113(15):1888-904.
13. Cai H, Harrison DG. Endothelial dysfunction in cardiovascular diseases: the role of oxidant stress. Circ Res. 2000;87(10):840-4.
14. Aird WC. Endothelial cell heterogeneity. Cold Spring Harb Perspect Med. 2012;2(1):a006429.
15. Bierhansl L, Conradi L-C, Treps L, Dewerchin M, Carmeliet P. Central role of metabolism in endothelial cell function and vascular disease. Physiology. 2017;32(2):126-40.
16. Komarova Y, Malik AB. Regulation of endothelial permeability via paracellular and transcellular transport pathways. Annu Rev Physiol. 2010;72:463-93.
17. Chiu JJ, Chien S. Effects of disturbed flow on vascular endothelium: pathophysiological basis and clinical perspectives. Physiol Rev. 2011;91(1):327-87.
18. Shao Y, Saredy J, Yang WY, Sun Y, Lu Y, Saaoud F, et al. Vascular Endothelial Cells and Innate Immunity. Arterioscler Thromb Vasc Biol. 2020;40(6):e138-e52.
19. Pober JS, Sessa WC. Evolving functions of endothelial cells in inflammation. Nat Rev Immunol. 2007;7(10):803-15.
20. Kaperonis EA, Liapis CD, Kakisis JD, Dimitroulis D, Papavassiliou VG. Inflammation and atherosclerosis. Eur J Vasc Endovasc Surg. 2006;31(4):386-93.
21. Wang WY, Lin D, Jarman EH, Polacheck WJ, Baker BM. Functional angiogenesis requires microenvironmental cues balancing endothelial cell migration and proliferation. Lab Chip. 2020;20(6):1153-66.
22. Krock BL, Skuli N, Simon MC. Hypoxia-induced angiogenesis: good and evil. Genes Cancer. 2011;2(12):1117-33.

23. Meza CA, La Favor JD, Kim DH, Hickner RC. Endothelial Dysfunction: Is There a Hyperglycemia-Induced Imbalance of NOX and NOS? Int J Mol Sci. 2019;20(15).
24. Wang M, Hao H, Leeper NJ, Zhu L, Early Career C. Thrombotic Regulation From the Endothelial Cell Perspectives. Arterioscler Thromb Vasc Biol. 2018;38(6):e90-e5.
25. Rajendran P, Rengarajan T, Thangavel J, Nishigaki Y, Sakthisekaran D, Sethi G, et al. The vascular endothelium and human diseases. Int J Biol Sci. 2013;9(10):1057-69.
26. Aird WC. Endothelial cell heterogeneity. Cold Spring Harbor perspectives in medicine. 2012;2(1):a006429.
27. Oikonomou EK, Antoniades C. The role of adipose tissue in cardiovascular health and disease. Nat Rev Cardiol. 2019;16(2):83-99.
28. Corvera S, Gealekman O. Adipose tissue angiogenesis: impact on obesity and type-2 diabetes. Biochim Biophys Acta. 2014;1842(3):463-72.
29. Gogg S, Nerstedt A, Boren J, Smith U. Human adipose tissue microvascular endothelial cells secrete PPARgamma ligands and regulate adipose tissue lipid uptake. JCI Insight. 2019;4(5).
30. Frontini A, Giordano A, Cinti S. Endothelial cells of adipose tissues: a niche of adipogenesis. Cell Cycle. 2012;11(15):2765-6.
31. Velez M, Kohli S, Sabbah HN. Animal models of insulin resistance and heart failure. Heart failure reviews. 2014;19(1):1-13.
32. Riehle C, Abel ED. Insulin signaling and heart failure. Circulation research. 2016;118(7):1151-69.
33. Eelen G, de Zeeuw P, Simons M, Carmeliet P. Endothelial cell metabolism in normal and diseased vasculature. Circulation research. 2015;116(7):1231-44.
34. Tabit CE, Chung WB, Hamburg NM, Vita JA. Endothelial dysfunction in diabetes mellitus: molecular mechanisms and clinical implications. Reviews in endocrine & metabolic disorders. 2010;11(1):61-74.
35. Gimbrone Jr MA, García-Cardeña G. Endothelial cell dysfunction and the pathobiology of atherosclerosis. Circulation research. 2016;118(4):620-36.
36. Franssen C, Chen S, Unger A, Korkmaz HI, De Keulenaer GW, Tschope C, et al. Myocardial Microvascular Inflammatory Endothelial Activation in Heart Failure With Preserved Ejection Fraction. JACC Heart Fail. 2016;4(4):312-24.

37. Greene SJ, Gheorghiade M, Borlaug BA, Pieske B, Vaduganathan M, Burnett JC, Jr., et al. The cGMP signaling pathway as a therapeutic target in heart failure with preserved ejection fraction. J Am Heart Assoc. 2013;2(6):e000536.
38. Heymes C, Vanderheyden M, Bronzwaer JG, Shah AM, Paulus WJ. Endomyocardial nitric oxide synthase and left ventricular preload reserve in dilated cardiomyopathy. Circulation. 1999;99(23):3009-16.
39. Förstermann U, Xia N, Li H. Roles of vascular oxidative stress and nitric oxide in the pathogenesis of atherosclerosis. Circulation research. 2017;120(4):713-35.
40. Bach LA. Endothelial cells and the IGF system. J Mol Endocrinol. 2015;54(1):R1-13.
41. Haeusler RA, McGraw TE, Accili D. Biochemical and cellular properties of insulin receptor signalling. Nat Rev Mol Cell Biol. 2018;19(1):31-44.
42. Song SH, McIntyre SS, Shah H, Veldhuis JD, Hayes PC, Butler PC. Direct measurement of pulsatile insulin secretion from the portal vein in human subjects. J Clin Endocrinol Metab. 2000;85(12):4491-9.
43. Cignarelli A, Genchi VA, Perrini S, Natalicchio A, Laviola L, Giorgino F. Insulin and Insulin Receptors in Adipose Tissue Development. Int J Mol Sci. 2019;20(3).
44. Nagao H, Cai W, Wewer Albrechtsen NJ, Steger M, Batista TM, Pan H, et al. Distinct signaling by insulin and IGF-1 receptors and their extra- and intracellular domains. Proc Natl Acad Sci U S A. 2021;118(17).
45. Pollak M. Insulin-like growth factor physiology and cancer risk. European journal of cancer. 2000;36(10):1224-8.
46. Chisalita SI, Arnqvist HJ. Insulin-like growth factor I receptors are more abundant than insulin receptors in human micro-and macrovascular endothelial cells. American Journal of Physiology-Endocrinology and Metabolism. 2004;286(6):E896-E901.
47. Gao S, Wassler M, Zhang L, Li Y, Wang J, Zhang Y, et al. MicroRNA-133a regulates insulin-like growth factor-1 receptor expression and vascular smooth muscle cell proliferation in murine atherosclerosis. Atherosclerosis. 2014;232(1):171-9.
48. Ardito F, Giuliani M, Perrone D, Troiano G, Lo Muzio L. The crucial role of protein phosphorylation in cell signaling and its use as targeted therapy (Review). Int J Mol Med. 2017;40(2):271-80.

49. Mackenzie RW, Elliott BT. Akt/PKB activation and insulin signaling: a novel insulin signaling pathway in the treatment of type 2 diabetes. Diabetes, metabolic syndrome and obesity: targets and therapy. 2014;7:55.
50. Guo S. Insulin signaling, resistance, and metabolic syndrome: insights from mouse models into disease mechanisms. Journal of Endocrinology. 2014;220(2):T1-T23.
51. Tran N, Garcia T, Aniqa M, Ali S, Ally A, Nauli SM. Endothelial Nitric Oxide Synthase (eNOS) and the Cardiovascular System: in Physiology and in Disease States. Am J Biomed Sci Res. 2022;15(2):153-77.
52. Rahman MS, Hossain KS, Das S, Kundu S, Adegoke EO, Rahman MA, et al. Role of Insulin in Health and Disease: An Update. Int J Mol Sci. 2021;22(12).
53. Malek M, Kielkowska A, Chessa T, Anderson KE, Barneda D, Pir P, et al. PTEN Regulates PI(3,4)P(2) Signaling Downstream of Class I PI3K. Mol Cell. 2017;68(3):566-80 e10.
54. Georgescu MM. PTEN Tumor Suppressor Network in PI3K-Akt Pathway Control. Genes Cancer. 2010;1(12):1170-7.
55. Newton AC, Trotman LC. Turning off AKT: PHLPP as a drug target. Annu Rev Pharmacol Toxicol. 2014;54:537-58.
56. Sasaoka T, Rose DW, Jhun BH, Saltiel AR, Draznin B, Olefsky JM. Evidence for a functional role of Shc proteins in mitogenic signaling induced by insulin, insulin-like growth factor-1, and epidermal growth factor. J Biol Chem. 1994;269(18):13689-94.
57. Boulton TG, Nye SH, Robbins DJ, Ip NY, Radziejewska E, Morgenbesser SD, et al. ERKs: a family of protein-serine/threonine kinases that are activated and tyrosine phosphorylated in response to insulin and NGF. Cell. 1991;65(4):663-75.
58. Davignon J, Ganz P. Role of endothelial dysfunction in atherosclerosis. Circulation. 2004;109(23 Suppl 1):III27-32.
59. Boucher J, Kleinridders A, Kahn CR. Insulin receptor signaling in normal and insulin-resistant states. Cold Spring Harb Perspect Biol. 2014;6(1).
60. Belfiore A, Frasca F, Pandini G, Sciacca L, Vigneri R. Insulin receptor isoforms and insulin receptor/insulin-like growth factor receptor hybrids in physiology and disease. Endocr Rev. 2009;30(6):586-623.

61. Ebina Y, Ellis L, Jarnagin K, Edery M, Graf L, Clauser E, et al. The human insulin receptor cDNA: the structural basis for hormone-activated transmembrane signalling. Cell. 1985;40(4):747-58.
62. Belfiore A, Malaguarnera R, Vella V, Lawrence MC, Sciacca L, Frasca F, et al. Insulin Receptor Isoforms in Physiology and Disease: An Updated View. Endocr Rev. 2017;38(5):379-431.
63. Kaminska D, Hamalainen M, Cederberg H, Kakela P, Venesmaa S, Miettinen P, et al. Adipose tissue INSR splicing in humans associates with fasting insulin level and is regulated by weight loss. Diabetologia. 2014;57(2):347-51.
64. Tornqvist HE, Avruch J. Relationship of site-specific beta subunit tyrosine autophosphorylation to insulin activation of the insulin receptor (tyrosine) protein kinase activity. J Biol Chem. 1988;263(10):4593-601.
65. Jia G, Cheng G, Soundararajan K, Agrawal DK. Insulin-like growth factor-I receptors in atherosclerotic plaques of symptomatic and asymptomatic patients with carotid stenosis: effect of IL-12 and IFN-gamma. Am J Physiol Heart Circ Physiol. 2007;292(2):H1051-7.
66. Gusscott S, Jenkins CE, Lam SH, Giambra V, Pollak M, Weng AP. IGF1R Derived PI3K/AKT Signaling Maintains Growth in a Subset of Human T-Cell Acute Lymphoblastic Leukemias. PLoS One. 2016;11(8):e0161158.
67. Baserga R. The IGF-I receptor in cancer research. Exp Cell Res. 1999;253(1):1-6.
68. Ullrich A, Gray A, Tam AW, Yang-Feng T, Tsubokawa M, Collins C, et al. Insulin-like growth factor I receptor primary structure: comparison with insulin receptor suggests structural determinants that define functional specificity. EMBO J. 1986;5(10):2503-12.
69. Favelyukis S, Till JH, Hubbard SR, Miller WT. Structure and autoregulation of the insulin-like growth factor 1 receptor kinase. Nat Struct Biol. 2001;8(12):1058-63.
70. Araki E, Lipes MA, Patti ME, Bruning JC, Haag B, 3rd, Johnson RS, et al. Alternative pathway of insulin signalling in mice with targeted disruption of the IRS-1 gene. Nature. 1994;372(6502):186-90.
71. Yamauchi T, Tobe K, Tamemoto H, Ueki K, Kaburagi Y, Yamamoto-Honda R, et al. Insulin signalling and insulin actions in the muscles and livers of insulin-resistant, insulin receptor substrate 1-deficient mice. Mol Cell Biol. 1996;16(6):3074-84.

72. Withers DJ, Gutierrez JS, Towery H, Burks DJ, Ren JM, Previs S, et al. Disruption of IRS-2 causes type 2 diabetes in mice. Nature. 1998;391(6670):900-4.
73. Al-Salam A, Irwin DM. Evolution of the vertebrate insulin receptor substrate (Irs) gene family. BMC Evol Biol. 2017;17(1):148.
74. Breitkopf SB, Yang X, Begley MJ, Kulkarni M, Chiu YH, Turke AB, et al. A Cross-Species Study of PI3K Protein-Protein Interactions Reveals the Direct Interaction of P85 and SHP2. Sci Rep. 2016;6:20471.
75. Chalhoub N, Baker SJ. PTEN and the PI3-kinase pathway in cancer. Annu Rev Pathol. 2009;4:127-50.
76. Hanada M, Feng J, Hemmings BA. Structure, regulation and function of PKB/AKT--a major therapeutic target. Biochim Biophys Acta. 2004;1697(1-2):3-16.
77. Qin B, Liu J, Liu S, Li B, Ren J. MiR-20b targets AKT3 and modulates vascular endothelial growth factor-mediated changes in diabetic retinopathy. Acta Biochim Biophys Sin (Shanghai). 2016;48(8):732-40.
78. Ding L, Zhang L, Biswas S, Schugar RC, Brown JM, Byzova T, et al. Akt3 inhibits adipogenesis and protects from diet-induced obesity via WNK1/SGK1 signaling. JCI Insight. 2017;2(22).
79. Stuehr DJ. Structure-function aspects in the nitric oxide synthases. Annu Rev Pharmacol Toxicol. 1997;37:339-59.
80. Fulton D, Ruan L, Sood SG, Li C, Zhang Q, Venema RC. Agonist-stimulated endothelial nitric oxide synthase activation and vascular relaxation. Role of eNOS phosphorylation at Tyr83. Circ Res. 2008;102(4):497-504.
81. Dimmeler S, Fleming I, Fisslthaler B, Hermann C, Busse R, Zeiher AM. Activation of nitric oxide synthase in endothelial cells by Akt-dependent phosphorylation. Nature. 1999;399(6736):601-5.
82. Chen ZP, Mitchelhill KI, Michell BJ, Stapleton D, Rodriguez-Crespo I, Witters LA, et al. AMP-activated protein kinase phosphorylation of endothelial NO synthase. FEBS Lett. 1999;443(3):285-9.
83. Michell BJ, Chen Z, Tiganis T, Stapleton D, Katsis F, Power DA, et al. Coordinated control of endothelial nitric-oxide synthase phosphorylation by protein kinase C and the cAMP-dependent protein kinase. J Biol Chem. 2001;276(21):17625-8.

84. Chen CA, Druhan LJ, Varadharaj S, Chen YR, Zweier JL. Phosphorylation of endothelial nitric-oxide synthase regulates superoxide generation from the enzyme. J Biol Chem. 2008;283(40):27038-47.
85. Van Puyvelde K, Mets T, Njemini R, Beyer I, Bautmans I. Effect of advanced glycation end product intake on inflammation and aging: a systematic review. Nutr Rev. 2014;72(10):638-50.
86. Inoguchi T, Li P, Umeda F, Yu HY, Kakimoto M, Imamura M, et al. High glucose level and free fatty acid stimulate reactive oxygen species production through protein kinase C--dependent activation of NAD(P)H oxidase in cultured vascular cells. Diabetes. 2000;49(11):1939-45.
87. Baker RG, Hayden MS, Ghosh S. NF-kappaB, inflammation, and metabolic disease. Cell Metab. 2011;13(1):11-22.
88. Wright JJ, Kim J, Buchanan J, Boudina S, Sena S, Bakirtzi K, et al. Mechanisms for increased myocardial fatty acid utilization following short-term high-fat feeding. Cardiovascular research. 2009;82(2):351-60.
89. Battiprolu PK, Hojayev B, Jiang N, Wang ZV, Luo X, Iglewski M, et al. Metabolic stress-induced activation of FoxO1 triggers diabetic cardiomyopathy in mice. The Journal of clinical investigation. 2012;122(3):1109-18.
90. Forman HJ, Maiorino M, Ursini F. Signaling functions of reactive oxygen species. Biochemistry. 2010;49(5):835-42.
91. Hajam YA, Rani R, Ganie SY, Sheikh TA, Javaid D, Qadri SS, et al. Oxidative Stress in Human Pathology and Aging: Molecular Mechanisms and Perspectives. Cells. 2022;11(3).
92. Phaniendra A, Jestadi DB, Periyasamy L. Free radicals: properties, sources, targets, and their implication in various diseases. Indian J Clin Biochem. 2015;30(1):11-26.
93. Sies H, Jones DP. Reactive oxygen species (ROS) as pleiotropic physiological signalling agents. Nat Rev Mol Cell Biol. 2020;21(7):363-83.
94. Dubois-Deruy E, Peugnet V, Turkieh A, Pinet F. Oxidative Stress in Cardiovascular Diseases. Antioxidants (Basel). 2020;9(9).
95. Vermot A, Petit-Hartlein I, Smith SME, Fieschi F. NADPH Oxidases (NOX): An Overview from Discovery, Molecular Mechanisms to Physiology and Pathology. Antioxidants (Basel). 2021;10(6).

96. Bedard K, Krause KH. The NOX family of ROS-generating NADPH oxidases: physiology and pathophysiology. Physiol Rev. 2007;87(1):245-313.
97. Drummond GR, Sobey CG. Endothelial NADPH oxidases: which NOX to target in vascular disease? Trends Endocrinol Metab. 2014;25(9):452-63.
98. Brandes RP, Weissmann N, Schroder K. Nox family NADPH oxidases: Molecular mechanisms of activation. Free Radic Biol Med. 2014;76:208-26.
99. Schroder K, Zhang M, Benkhoff S, Mieth A, Pliquett R, Kosowski J, et al. Nox4 is a protective reactive oxygen species generating vascular NADPH oxidase. Circ Res. 2012;110(9):1217-25.
100. Szanto I, Rubbia-Brandt L, Kiss P, Steger K, Banfi B, Kovari E, et al. Expression of NOX1, a superoxide-generating NADPH oxidase, in colon cancer and inflammatory bowel disease. J Pathol. 2005;207(2):164-76.
101. Lu J, Jiang G, Wu Y, Antony S, Meitzler JL, Juhasz A, et al. NADPH oxidase 1 is highly expressed in human large and small bowel cancers. PLoS One. 2020;15(5):e0233208.
102. Thompson JA, Larion S, Mintz JD, Belin de Chantemele EJ, Fulton DJ, Stepp DW. Genetic Deletion of NADPH Oxidase 1 Rescues Microvascular Function in Mice With Metabolic Disease. Circ Res. 2017;121(5):502-11.
103. Frey RS, Ushio-Fukai M, Malik AB. NADPH oxidase-dependent signaling in endothelial cells: role in physiology and pathophysiology. Antioxid Redox Signal. 2009;11(4):791-810.
104. Youn JY, Gao L, Cai H. The p47phox- and NADPH oxidase organiser 1 (NOXO1)-dependent activation of NADPH oxidase 1 (NOX1) mediates endothelial nitric oxide synthase (eNOS) uncoupling and endothelial dysfunction in a streptozotocin-induced murine model of diabetes. Diabetologia. 2012;55(7):2069-79.
105. Zhang Y, Murugesan P, Huang K, Cai H. NADPH oxidases and oxidase crosstalk in cardiovascular diseases: novel therapeutic targets. Nat Rev Cardiol. 2020;17(3):170-94.
106. Aurelius J, Thoren FB, Akhiani AA, Brune M, Palmqvist L, Hansson M, et al. Monocytic AML cells inactivate antileukemic lymphocytes: role of NADPH oxidase/gp91(phox) expression and the PARP-1/PAR pathway of apoptosis. Blood. 2012;119(24):5832-7.
107. Csanyi G, Taylor WR, Pagano PJ. NOX and inflammation in the vascular adventitia. Free Radic Biol Med. 2009;47(9):1254-66.

108. Sukumar P, Viswambharan H, Imrie H, Cubbon RM, Yuldasheva N, Gage M, et al. Nox2 NADPH oxidase has a critical role in insulin resistance-related endothelial cell dysfunction. Diabetes. 2013;62(6):2130-4.
109. Valente AJ, Irimpen AM, Siebenlist U, Chandrasekar B. OxLDL induces endothelial dysfunction and death via TRAF3IP2: inhibition by HDL3 and AMPK activators. Free Radic Biol Med. 2014;70:117-28.
110. Mahmoud AM, Ali MM, Miranda ER, Mey JT, Blackburn BK, Haus JM, et al. Nox2 contributes to hyperinsulinemia-induced redox imbalance and impaired vascular function. Redox Biol. 2017;13:288-300.
111. Du J, Fan LM, Mai A, Li JM. Crucial roles of Nox2-derived oxidative stress in deteriorating the function of insulin receptors and endothelium in dietary obesity of middle-aged mice. Br J Pharmacol. 2013;170(5):1064-77.
112. Murdoch CE, Chaubey S, Zeng L, Yu B, Ivetic A, Walker SJ, et al. Endothelial NADPH oxidase-2 promotes interstitial cardiac fibrosis and diastolic dysfunction through proinflammatory effects and endothelial-mesenchymal transition. J Am Coll Cardiol. 2014;63(24):2734-41.
113. Zhang B, Liu Z, Hu X. Inhibiting cancer metastasis via targeting NAPDH oxidase 4. Biochem Pharmacol. 2013;86(2):253-66.
114. Ago T, Kitazono T, Ooboshi H, Iyama T, Han YH, Takada J, et al. Nox4 as the major catalytic component of an endothelial NAD(P)H oxidase. Circulation. 2004;109(2):227-33.
115. Van Buul JD, Fernandez-Borja M, Anthony EC, Hordijk PL. Expression and localization of NOX2 and NOX4 in primary human endothelial cells. Antioxid Redox Signal. 2005;7(3-4):308-17.
116. Block K, Gorin Y, Abboud HE. Subcellular localization of Nox4 and regulation in diabetes. Proc Natl Acad Sci U S A. 2009;106(34):14385-90.
117. Nisimoto Y, Diebold BA, Cosentino-Gomes D, Lambeth JD. Nox4: a hydrogen peroxide-generating oxygen sensor. Biochemistry. 2014;53(31):5111-20.
118. Datla SR, Peshavariya H, Dusting GJ, Mahadev K, Goldstein BJ, Jiang F. Important role of Nox4 type NADPH oxidase in angiogenic responses in human microvascular endothelial cells in vitro. Arterioscler Thromb Vasc Biol. 2007;27(11):2319-24.
119. Sanchez-Gomez FJ, Calvo E, Breton-Romero R, Fierro-Fernandez M, Anilkumar N, Shah AM, et al. NOX4-dependent Hydrogen peroxide promotes shear

stress-induced SHP2 sulfenylation and eNOS activation. Free Radic Biol Med. 2015;89:419-30.
120. Hu P, Wu X, Khandelwal AR, Yu W, Xu Z, Chen L, et al. Endothelial Nox4-based NADPH oxidase regulates atherosclerosis via soluble epoxide hydrolase. Biochim Biophys Acta Mol Basis Dis. 2017;1863(6):1382-91.
121. Gray SP, Di Marco E, Kennedy K, Chew P, Okabe J, El-Osta A, et al. Reactive Oxygen Species Can Provide Atheroprotection via NOX4-Dependent Inhibition of Inflammation and Vascular Remodeling. Arterioscler Thromb Vasc Biol. 2016;36(2):295-307.
122. Patti ME, Corvera S. The role of mitochondria in the pathogenesis of type 2 diabetes. Endocr Rev. 2010;31(3):364-95.
123. Yan J, Jiang J, He L, Chen L. Mitochondrial superoxide/hydrogen peroxide: An emerging therapeutic target for metabolic diseases. Free Radic Biol Med. 2020;152:33-42.
124. Zhao QD, Viswanadhapalli S, Williams P, Shi Q, Tan C, Yi X, et al. NADPH oxidase 4 induces cardiac fibrosis and hypertrophy through activating Akt/mTOR and NFkappaB signaling pathways. Circulation. 2015;131(7):643-55.
125. Ghanbari H, Keshtgar S, Kazeroni M. Inhibition of the CatSper Channel and NOX5 Enzyme Activity Affects the Functions of the Progesterone-Stimulated Human Sperm. Iran J Med Sci. 2018;43(1):18-25.
126. Brar SS, Corbin Z, Kennedy TP, Hemendinger R, Thornton L, Bommarius B, et al. NOX5 NAD(P)H oxidase regulates growth and apoptosis in DU 145 prostate cancer cells. Am J Physiol Cell Physiol. 2003;285(2):C353-69.
127. Dho SH, Kim JY, Lee KP, Kwon ES, Lim JC, Kim CJ, et al. STAT5A-mediated NOX5-L expression promotes the proliferation and metastasis of breast cancer cells. Exp Cell Res. 2017;351(1):51-8.
128. Hong J, Resnick M, Behar J, Wang LJ, Wands J, DeLellis RA, et al. Acid-induced p16 hypermethylation contributes to development of esophageal adenocarcinoma via activation of NADPH oxidase NOX5-S. Am J Physiol Gastrointest Liver Physiol. 2010;299(3):G697-706.
129. Serrander L, Jaquet V, Bedard K, Plastre O, Hartley O, Arnaudeau S, et al. NOX5 is expressed at the plasma membrane and generates superoxide in response to protein kinase C activation. Biochimie. 2007;89(9):1159-67.

130. Elbatreek MH, Sadegh S, Anastasi E, Guney E, Nogales C, Kacprowski T, et al. NOX5-induced uncoupling of endothelial NO synthase is a causal mechanism and theragnostic target of an age-related hypertension endotype. PLoS Biol. 2020;18(11):e3000885.
131. Jha JC, Dai A, Holterman CE, Cooper ME, Touyz RM, Kennedy CR, et al. Endothelial or vascular smooth muscle cell-specific expression of human NOX5 exacerbates renal inflammation, fibrosis and albuminuria in the Akita mouse. Diabetologia. 2019;62(9):1712-26.
132. Jay DB, Papaharalambus CA, Seidel-Rogol B, Dikalova AE, Lassegue B, Griendling KK. Nox5 mediates PDGF-induced proliferation in human aortic smooth muscle cells. Free Radic Biol Med. 2008;45(3):329-35.
133. Touyz RM. Reactive oxygen species as mediators of calcium signaling by angiotensin II: implications in vascular physiology and pathophysiology. Antioxid Redox Signal. 2005;7(9-10):1302-14.
134. Del Maestro RF. Role of superoxide anion radicals in microvascular permeability and leukocyte behaviour. Can J Physiol Pharmacol. 1982;60(11):1406-14.
135. Di Marco E, Gray SP, Kennedy K, Szyndralewiez C, Lyle AN, Lassegue B, et al. NOX4-derived reactive oxygen species limit fibrosis and inhibit proliferation of vascular smooth muscle cells in diabetic atherosclerosis. Free Radic Biol Med. 2016;97:556-67.
136. Craige SM, Chen K, Pei Y, Li C, Huang X, Chen C, et al. NADPH oxidase 4 promotes endothelial angiogenesis through endothelial nitric oxide synthase activation. Circulation. 2011;124(6):731-40.
137. McCord JM, Fridovich I. Superoxide dismutase. An enzymic function for erythrocuprein (hemocuprein). J Biol Chem. 1969;244(22):6049-55.
138. Fukai T, Ushio-Fukai M. Superoxide dismutases: role in redox signaling, vascular function, and diseases. Antioxid Redox Signal. 2011;15(6):1583-606.
139. Ballinger SW, Patterson C, Knight-Lozano CA, Burow DL, Conklin CA, Hu Z, et al. Mitochondrial integrity and function in atherogenesis. Circulation. 2002;106(5):544-9.
140. Faraci FM, Didion SP. Vascular protection: superoxide dismutase isoforms in the vessel wall. Arterioscler Thromb Vasc Biol. 2004;24(8):1367-73.

141. Stralin P, Karlsson K, Johansson BO, Marklund SL. The interstitium of the human arterial wall contains very large amounts of extracellular superoxide dismutase. Arterioscler Thromb Vasc Biol. 1995;15(11):2032-6.
142. Kobylecki CJ, Afzal S, Nordestgaard BG. Genetically Low Antioxidant Protection and Risk of Cardiovascular Disease and Heart Failure in Diabetic Subjects. EBioMedicine. 2015;2(12):2010-5.
143. Goyal MM, Basak A. Human catalase: looking for complete identity. Protein Cell. 2010;1(10):888-97.
144. Atalay M, Laaksonen DE, Niskanen L, Uusitupa M, Hanninen O, Sen CK. Altered antioxidant enzyme defences in insulin-dependent diabetic men with increased resting and exercise-induced oxidative stress. Acta Physiol Scand. 1997;161(2):195-201.
145. Bhatia S, Shukla R, Venkata Madhu S, Kaur Gambhir J, Madhava Prabhu K. Antioxidant status, lipid peroxidation and nitric oxide end products in patients of type 2 diabetes mellitus with nephropathy. Clin Biochem. 2003;36(7):557-62.
146. Qin F, Lennon-Edwards S, Lancel S, Biolo A, Siwik DA, Pimentel DR, et al. Cardiac-specific overexpression of catalase identifies hydrogen peroxide-dependent and -independent phases of myocardial remodeling and prevents the progression to overt heart failure in G(alpha)q-overexpressing transgenic mice. Circ Heart Fail. 2010;3(2):306-13.
147. Casado A, de la Torre R, Lopez-Fernandez ME, Carrascosa D, Casado MC, Ramirez MV. Superoxide dismutase and catalase blood levels in patients with malignant diseases. Cancer Lett. 1995;93(2):187-92.
148. Arsova-Sarafinovska Z, Eken A, Matevska N, Erdem O, Sayal A, Savaser A, et al. Increased oxidative/nitrosative stress and decreased antioxidant enzyme activities in prostate cancer. Clin Biochem. 2009;42(12):1228-35.
149. Kodydkova J, Vavrova L, Stankova B, Macasek J, Krechler T, Zak A. Antioxidant status and oxidative stress markers in pancreatic cancer and chronic pancreatitis. Pancreas. 2013;42(4):614-21.
150. Tang C, Yin G, Huang C, Wang H, Gao J, Luo J, et al. Peroxiredoxin-1 ameliorates pressure overload-induced cardiac hypertrophy and fibrosis. Biomed Pharmacother. 2020;129:110357.
151. Ibarrola J, Arrieta V, Sadaba R, Martinez-Martinez E, Garcia-Pena A, Alvarez V, et al. Galectin-3 down-regulates antioxidant peroxiredoxin-4 in human cardiac

fibroblasts: a new pathway to induce cardiac damage. Clin Sci (Lond). 2018;132(13):1471-85.
152. Kuzuya K, Ichihara S, Suzuki Y, Inoue C, Ichihara G, Kurimoto S, et al. Proteomics analysis identified peroxiredoxin 2 involved in early-phase left ventricular impairment in hamsters with cardiomyopathy. PLoS One. 2018;13(2):e0192624.
153. Lubos E, Loscalzo J, Handy DE. Glutathione peroxidase-1 in health and disease: from molecular mechanisms to therapeutic opportunities. Antioxid Redox Signal. 2011;15(7):1957-97.
154. Park TJ, Park JH, Lee GS, Lee JY, Shin JH, Kim MW, et al. Quantitative proteomic analyses reveal that GPX4 downregulation during myocardial infarction contributes to ferroptosis in cardiomyocytes. Cell Death Dis. 2019;10(11):835.
155. Mironczuk-Chodakowska I, Witkowska AM, Zujko ME. Endogenous non-enzymatic antioxidants in the human body. Adv Med Sci. 2018;63(1):68-78.
156. Rezk-Hanna M, Seals DR, Rossman MJ, Gupta R, Nettle CO, Means A, et al. Ascorbic Acid Prevents Vascular Endothelial Dysfunction Induced by Electronic Hookah (Waterpipe) Vaping. J Am Heart Assoc. 2021;10(5):e019271.
157. Keaney JF, Jr., Guo Y, Cunningham D, Shwaery GT, Xu A, Vita JA. Vascular incorporation of alpha-tocopherol prevents endothelial dysfunction due to oxidized LDL by inhibiting protein kinase C stimulation. J Clin Invest. 1996;98(2):386-94.
158. Costa TJ, Barros PR, Arce C, Santos JD, da Silva-Neto J, Egea G, et al. The homeostatic role of hydrogen peroxide, superoxide anion and nitric oxide in the vasculature. Free Radic Biol Med. 2021;162:615-35.
159. Thomas SR, Chen K, Keaney JF, Jr. Hydrogen peroxide activates endothelial nitric-oxide synthase through coordinated phosphorylation and dephosphorylation via a phosphoinositide 3-kinase-dependent signaling pathway. J Biol Chem. 2002;277(8):6017-24.
160. Heistad DD. Oxidative stress and vascular disease: 2005 Duff lecture. Arterioscler Thromb Vasc Biol. 2006;26(4):689-95.
161. Montorfano I, Becerra A, Cerro R, Echeverria C, Saez E, Morales MG, et al. Oxidative stress mediates the conversion of endothelial cells into myofibroblasts via a TGF-beta1 and TGF-beta2-dependent pathway. Lab Invest. 2014;94(10):1068-82.
162. Schulz E, Anter E, Keaney JF, Jr. Oxidative stress, antioxidants, and endothelial function. Curr Med Chem. 2004;11(9):1093-104.

163. Laight DW, Carrier MJ, Anggard EE. Antioxidants, diabetes and endothelial dysfunction. Cardiovasc Res. 2000;47(3):457-64.
164. Lund DD, Chu Y, Miller JD, Heistad DD. Protective effect of extracellular superoxide dismutase on endothelial function during aging. Am J Physiol Heart Circ Physiol. 2009;296(6):H1920-5.
165. Ulker S, McMaster D, McKeown PP, Bayraktutan U. Impaired activities of antioxidant enzymes elicit endothelial dysfunction in spontaneous hypertensive rats despite enhanced vascular nitric oxide generation. Cardiovasc Res. 2003;59(2):488-500.
166. Kim DH, Meza CA, Clarke H, Kim JS, Hickner RC. Vitamin D and Endothelial Function. Nutrients. 2020;12(2).
167. Kunisaki M, Fumio U, Nawata H, King GL. Vitamin E normalizes diacylglycerol-protein kinase C activation induced by hyperglycemia in rat vascular tissues. Diabetes. 1996;45 Suppl 3:S117-9.
168. Economides PA, Khaodhiar L, Caselli A, Caballero AE, Keenan H, Bursell SE, et al. The effect of vitamin E on endothelial function of micro- and macrocirculation and left ventricular function in type 1 and type 2 diabetic patients. Diabetes. 2005;54(1):204-11.
169. Gori T, Munzel T. Oxidative stress and endothelial dysfunction: therapeutic implications. Ann Med. 2011;43(4):259-72.
170. Lee IM, Cook NR, Gaziano JM, Gordon D, Ridker PM, Manson JE, et al. Vitamin E in the primary prevention of cardiovascular disease and cancer: the Women's Health Study: a randomized controlled trial. JAMA. 2005;294(1):56-65.
171. Lonn E, Bosch J, Yusuf S, Sheridan P, Pogue J, Arnold JM, et al. Effects of long-term vitamin E supplementation on cardiovascular events and cancer: a randomized controlled trial. JAMA. 2005;293(11):1338-47.
172. Pisoschi AM, Pop A, Iordache F, Stanca L, Predoi G, Serban AI. Oxidative stress mitigation by antioxidants - An overview on their chemistry and influences on health status. Eur J Med Chem. 2021;209:112891.
173. Gutteridge JM. Does redox regulation of cell function explain why antioxidants perform so poorly as therapeutic agents? Redox Rep. 1999;4(3):129-31.
174. Tonnesen MG, Feng X, Clark RA. Angiogenesis in wound healing. J Investig Dermatol Symp Proc. 2000;5(1):40-6.

175. Silvestre JS, Smadja DM, Levy BI. Postischemic revascularization: from cellular and molecular mechanisms to clinical applications. Physiol Rev. 2013;93(4):1743-802.
176. Christiaens V, Lijnen HR. Angiogenesis and development of adipose tissue. Mol Cell Endocrinol. 2010;318(1-2):2-9.
177. Baeriswyl V, Christofori G. The angiogenic switch in carcinogenesis. Semin Cancer Biol. 2009;19(5):329-37.
178. Capitao M, Soares R. Angiogenesis and Inflammation Crosstalk in Diabetic Retinopathy. J Cell Biochem. 2016;117(11):2443-53.
179. Tanabe K, Maeshima Y, Sato Y, Wada J. Antiangiogenic Therapy for Diabetic Nephropathy. Biomed Res Int. 2017;2017:5724069.
180. Chertok VM, Chertok AG, Zenkina VG. Endotelial-Dependent of the Regulation of Angiogenesis. Tsitologiia. 2017;59(4):243-58.
181. Germain S, Monnot C, Muller L, Eichmann A. Hypoxia-driven angiogenesis: role of tip cells and extracellular matrix scaffolding. Curr Opin Hematol. 2010;17(3):245-51.
182. Okonkwo UA, DiPietro LA. Diabetes and Wound Angiogenesis. Int J Mol Sci. 2017;18(7).
183. Michailidou Z, Turban S, Miller E, Zou X, Schrader J, Ratcliffe PJ, et al. Increased angiogenesis protects against adipose hypoxia and fibrosis in metabolic disease-resistant 11beta-hydroxysteroid dehydrogenase type 1 (HSD1)-deficient mice. J Biol Chem. 2012;287(6):4188-97.
184. Cooke JP. NO and angiogenesis. Atheroscler Suppl. 2003;4(4):53-60.
185. Suzuki J. L-arginine supplementation causes additional effects on exercise-induced angiogenesis and VEGF expression in the heart and hind-leg muscles of middle-aged rats. J Physiol Sci. 2006;56(1):39-44.
186. Murohara T, Asahara T, Silver M, Bauters C, Masuda H, Kalka C, et al. Nitric oxide synthase modulates angiogenesis in response to tissue ischemia. J Clin Invest. 1998;101(11):2567-78.
187. Kuwabara M, Kakinuma Y, Ando M, Katare RG, Yamasaki F, Doi Y, et al. Nitric oxide stimulates vascular endothelial growth factor production in cardiomyocytes involved in angiogenesis. J Physiol Sci. 2006;56(1):95-101.

188. Shizukuda Y, Tang S, Yokota R, Ware JA. Vascular endothelial growth factor-induced endothelial cell migration and proliferation depend on a nitric oxide-mediated decrease in protein kinase Cdelta activity. Circ Res. 1999;85(3):247-56.
189. Dulak J, Jozkowicz A, Dembinska-Kiec A, Guevara I, Zdzienicka A, Zmudzinska-Grochot D, et al. Nitric oxide induces the synthesis of vascular endothelial growth factor by rat vascular smooth muscle cells. Arterioscler Thromb Vasc Biol. 2000;20(3):659-66.
190. Ushio-Fukai M. Redox signaling in angiogenesis: role of NADPH oxidase. Cardiovasc Res. 2006;71(2):226-35.
191. Son Y, Kim S, Chung HT, Pae HO. Reactive oxygen species in the activation of MAP kinases. Methods Enzymol. 2013;528:27-48.
192. Xi G, Shen X, Maile LA, Wai C, Gollahon K, Clemmons DR. Hyperglycemia enhances IGF-I-stimulated Src activation via increasing Nox4-derived reactive oxygen species in a PKCzeta-dependent manner in vascular smooth muscle cells. Diabetes. 2012;61(1):104-13.
193. Romero M, Jimenez R, Sanchez M, Lopez-Sepulveda R, Zarzuelo A, Tamargo J, et al. Vascular superoxide production by endothelin-1 requires Src non-receptor protein tyrosine kinase and MAPK activation. Atherosclerosis. 2010;212(1):78-85.
194. Evangelista AM, Thompson MD, Bolotina VM, Tong X, Cohen RA. Nox4- and Nox2-dependent oxidant production is required for VEGF-induced SERCA cysteine-674 S-glutathiolation and endothelial cell migration. Free Radic Biol Med. 2012;53(12):2327-34.
195. Oshikawa J, Urao N, Kim HW, Kaplan N, Razvi M, McKinney R, et al. Extracellular SOD-derived H2O2 promotes VEGF signaling in caveolae/lipid rafts and post-ischemic angiogenesis in mice. PLoS One. 2010;5(4):e10189.
196. Mu P, Liu Q, Zheng R. Biphasic regulation of H2O2 on angiogenesis implicated NADPH oxidase. Cell Biol Int. 2010;34(10):1013-20.
197. Huang SS, Zheng RL. Biphasic regulation of angiogenesis by reactive oxygen species. Pharmazie. 2006;61(3):223-9.
198. Cunningham KS, Gotlieb AI. The role of shear stress in the pathogenesis of atherosclerosis. Lab Invest. 2005;85(1):9-23.
199. Chong AY, Caine GJ, Lip GY. Angiopoietin/tie-2 as mediators of angiogenesis: a role in congestive heart failure? Eur J Clin Invest. 2004;34(1):9-13.

200. Carnicer R, Crabtree MJ, Sivakumaran V, Casadei B, Kass DA. Nitric oxide synthases in heart failure. Antioxid Redox Signal. 2013;18(9):1078-99.
201. Kota SK, Meher LK, Jammula S, Kota SK, Krishna SV, Modi KD. Aberrant angiogenesis: The gateway to diabetic complications. Indian J Endocrinol Metab. 2012;16(6):918-30.
202. Qi W, Yang C, Dai Z, Che D, Feng J, Mao Y, et al. High levels of pigment epithelium-derived factor in diabetes impair wound healing through suppression of Wnt signaling. Diabetes. 2015;64(4):1407-19.
203. Martin A, Komada MR, Sane DC. Abnormal angiogenesis in diabetes mellitus. Med Res Rev. 2003;23(2):117-45.
204. Drela E, Stankowska K, Kulwas A, Rosc D. Endothelial progenitor cells in diabetic foot syndrome. Adv Clin Exp Med. 2012;21(2):249-54.
205. Khanna S, Biswas S, Shang Y, Collard E, Azad A, Kauh C, et al. Macrophage dysfunction impairs resolution of inflammation in the wounds of diabetic mice. PLoS One. 2010;5(3):e9539.
206. Mirza R, Koh TJ. Dysregulation of monocyte/macrophage phenotype in wounds of diabetic mice. Cytokine. 2011;56(2):256-64.
207. Maqbool A, Watt NT, Haywood N, Viswambharan H, Skromna A, Makava N, et al. Divergent effects of genetic and pharmacological inhibition of Nox2 NADPH oxidase on insulin resistance-related vascular damage. Am J Physiol Cell Physiol. 2020;319(1):C64-C74.
208. Nichols CI, Vose JG. Incidence of Bleeding-Related Complications During Primary Implantation and Replacement of Cardiac Implantable Electronic Devices. J Am Heart Assoc. 2017;6(1).
209. Goncharov NV, Nadeev AD, Jenkins RO, Avdonin PV. Markers and Biomarkers of Endothelium: When Something Is Rotten in the State. Oxid Med Cell Longev. 2017;2017:9759735.
210. Arts CH, Heijnen-Snyder GJ, Joosten PP, Verhagen HJ, Eikelboom BC, Sixma JJ, et al. A novel method for isolating pure microvascular endothelial cells from subcutaneous fat tissue ideal for direct cell seeding. Lab Invest. 2001;81(10):1461-5.
211. Wilkening S, Bader A. Quantitative real-time polymerase chain reaction: methodical analysis and mathematical model. J Biomol Tech. 2004;15(2):107-11.

212. Westermeier F, Salomon C, Gonzalez M, Puebla C, Guzman-Gutierrez E, Cifuentes F, et al. Insulin restores gestational diabetes mellitus-reduced adenosine transport involving differential expression of insulin receptor isoforms in human umbilical vein endothelium. Diabetes. 2011;60(6):1677-87.
213. Limaye PV, Raghuram N, Sivakami S. Oxidative stress and gene expression of antioxidant enzymes in the renal cortex of streptozotocin-induced diabetic rats. Mol Cell Biochem. 2003;243(1-2):147-52.
214. Srinivasan S, Hatley ME, Bolick DT, Palmer LA, Edelstein D, Brownlee M, et al. Hyperglycaemia-induced superoxide production decreases eNOS expression via AP-1 activation in aortic endothelial cells. Diabetologia. 2004;47(10):1727-34.
215. Pou KM, Massaro JM, Hoffmann U, Vasan RS, Maurovich-Horvat P, Larson MG, et al. Visceral and subcutaneous adipose tissue volumes are cross-sectionally related to markers of inflammation and oxidative stress: the Framingham Heart Study. Circulation. 2007;116(11):1234-41.
216. Parikh NI, Keyes MJ, Larson MG, Pou KM, Hamburg NM, Vita JA, et al. Visceral and subcutaneous adiposity and brachial artery vasodilator function. Obesity (Silver Spring). 2009;17(11):2054-9.
217. Jiao W, Ji J, Li F, Guo J, Zheng Y, Li S, et al. Activation of the NotchNox4reactive oxygen species signaling pathway induces cell death in high glucosetreated human retinal endothelial cells. Mol Med Rep. 2019;19(1):667-77.
218. Zhang M, Brewer AC, Schroder K, Santos CX, Grieve DJ, Wang M, et al. NADPH oxidase-4 mediates protection against chronic load-induced stress in mouse hearts by enhancing angiogenesis. Proc Natl Acad Sci U S A. 2010;107(42):18121-6.
219. Varga ZV, Pipicz M, Baan JA, Baranyai T, Koncsos G, Leszek P, et al. Alternative Splicing of NOX4 in the Failing Human Heart. Front Physiol. 2017;8:935.
220. Hellman B, Gylfe E, Grapengiesser E, Dansk H, Salehi A. Insulin oscillations--clinically important rhythm. Antidiabetics should increase the pulsative component of the insulin release2007. 2236-9 p.
221. Yudushkin I. Control of Akt activity and substrate phosphorylation in cells. IUBMB Life. 2020;72(6):1115-25.
222. Kong X, Qu X, Li B, Wang Z, Chao Y, Jiang X, et al. Modulation of low shear stressinduced eNOS multisite phosphorylation and nitric oxide production via protein kinase and ERK1/2 signaling. Mol Med Rep. 2017;15(2):908-14.

223. Salt IP, Morrow VA, Brandie FM, Connell JM, Petrie JR. High glucose inhibits insulin-stimulated nitric oxide production without reducing endothelial nitric-oxide synthase Ser1177 phosphorylation in human aortic endothelial cells. J Biol Chem. 2003;278(21):18791-7.
224. Rojas-Rodriguez R, Gealekman O, Kruse ME, Rosenthal B, Rao K, Min S, et al. Adipose tissue angiogenesis assay. Methods Enzymol. 2014;537:75-91.
225. Inoue O, Usui S, Takashima SI, Nomura A, Yamaguchi K, Takeda Y, et al. Diabetes impairs the angiogenic capacity of human adipose-derived stem cells by reducing the CD271(+) subpopulation in adipose tissue. Biochem Biophys Res Commun. 2019;517(2):369-75.
226. Dworakowski R, Walker S, Momin A, Desai J, El-Gamel A, Wendler O, et al. Reduced nicotinamide adenine dinucleotide phosphate oxidase-derived superoxide and vascular endothelial dysfunction in human heart failure. J Am Coll Cardiol. 2008;51(14):1349-56.
227. Ilkun O, Wilde N, Tuinei J, Pires KM, Zhu Y, Bugger H, et al. Antioxidant treatment normalizes mitochondrial energetics and myocardial insulin sensitivity independently of changes in systemic metabolic homeostasis in a mouse model of the metabolic syndrome. J Mol Cell Cardiol. 2015;85:104-16.
228. Mughal RS, Bridge K, Buza I, Slaaby R, Worm J, Klitgaard-Povlsen G, et al. Effects of obesity on insulin: insulin-like growth factor 1 hybrid receptor expression and Akt phosphorylation in conduit and resistance arteries. Diabetes & vascular disease research. 2018:1479164118802550.
229. Rena G, Hardie DG, Pearson ER. The mechanisms of action of metformin. Diabetologia. 2017;60(9):1577-85.
230. Algire C, Moiseeva O, Deschenes-Simard X, Amrein L, Petruccelli L, Birman E, et al. Metformin reduces endogenous reactive oxygen species and associated DNA damage. Cancer Prev Res (Phila). 2012;5(4):536-43.
231. Houstis N, Rosen ED, Lander ES. Reactive oxygen species have a causal role in multiple forms of insulin resistance. Nature. 2006;440(7086):944.
232. Kolluru GK, Siamwala JH, Chatterjee S. eNOS phosphorylation in health and disease. Biochimie. 2010;92(9):1186-98.
233. A MD, A GH. Why antioxidant therapies have failed in clinical trials. J Theor Biol. 2018;457:1-5.